Exploiting genetic vulnerabilities for BAP1 loss by synthetic lethality

Inaugural-Dissertation

zur

Erlangung des Doktorgrades

Dr. rer. nat.

der Fakultät für

Biologie

an der

Universität Duisburg-Essen

vorgelegt von

Anna Bazarna

aus Donezk

am 14.02.2022

Die der vorliegenden Arbeit zugrunde liegenden Experimente wurden am Brückeninstitut für Experimentelle Tumortherapien & Abteilung für Translationale Genomik solider Tumore (DKFZ/DKTK Partnerstandort Essen) der Universität Duisburg-Essen oder an einer anderen gleichwertigen Einrichtung durchgeführt.

1. Gutachter: Prof. Dr. J. Siveke
2. Gutachter: Prof. Dr. V. Jendrossek

Vorsitzender des Prüfungsausschusses: Prof. Dr. R. Küppers

Tag der mündlichen Prüfung: 21.06.2022

DOI: 10.17185/duepublico/76129
URN: urn:nbn:de:hbz:465-20240408-093720-4

Abstract

BRCA1-associated protein 1 (*BAP1*) is a tumor suppressor gene that encodes a nuclear deubiquitinating enzyme with crucial roles in different physiological functions. Therefore, it is not surprising that loss of BAP1 is associated with aggressive tumors, higher incidence of metastasis and poor overall survival in several cancer entities such as renal cell carcinoma (RCC), uveal melanoma (UM) and intrahepatic cholangiocarcinoma (ICC). However, there are no specific treatments for tumors with BAP1 loss. Thus, the aim of this study is to identify potential therapeutic targets for treatments of patients with *BAP1* mutations by performing a large-scale RNA interference screen. Therefore, the BAP1-deficient renal cell carcinoma cell line UMRC-6 reconstituted with wild-type *BAP1* or an empty vector control was used for the shRNA screen. The histone deacetylase *HDAC1* was identified as a possible synthetic lethal interactor of cancer cells with inactive BAP1. As expected for a true synthetic lethal gene in the context of BAP1 loss, *HDAC1* knockdown led to a decrease of cell proliferation and colony formation in different BAP1-deficient cell lines of RCC, ICC and UM, but not in BAP1-expressing ones. In addition, the HDAC1 inhibitor quisinostat decreased the cell viability of BAP1-deficient cell lines more than the cell viability of *BAP1* competent cell lines. Besides, *HDAC1* knockdown showed a stronger effect on the cell proliferation of *BAP1* knockout UM cells than the knockdown of *HDAC4,* which was reported recently to be a key target in *BAP1*-mutant uveal melanoma. By characterizing the role of HDAC1 in BAP1-deficient cancer cells, it was detected that *HDAC1* knockdown had a higher efficiency suppressing the migration of cells with BAP1 loss compared to BAP1-expressed ones. Furthermore, *HDAC1* knockdown showed in cell cycle arrest assays that it is leading to a G1 arrest in *BAP1* knockout cells. However, an association between HDAC1 inhibition and apoptosis of *BAP1* knockout cells could be not uncovered. These findings suggest that HDAC1 regulates the proliferation, cell migration and tumor growth of *BAP1*-mutant tumor entities by regulating the G1 cell cycle arrest independently of apoptosis. In the future, further investigation in the interplay between HDAC1 and BAP1 deficiency can provide higher evidence on the mechanisms behind their synthetic lethality. Notably, *HDAC1* knockdown suppressed tumor growth only in a BAP1-deficient cholangiocarcinoma xenograft mouse model, validating *in vivo* the synthetic lethality interaction of HDAC1 with BAP1 loss. This provides the rationale of treating *BAP1*-mutant cancers with HDAC1 inhibitors.

Zusammenfassung

Das BRCA1-assoziiertes Protein 1 (*BAP1*) Gen ist ein Tumorsuppressorgen, welches eine nuklear-loklaisierte Deubiquitinase mit wichtigen physiologischen Funktionen kodiert. Aus diesem Grunde ist es nicht verwunderlich, dass ein Verlust des BAP1 Proteins mit einem aggressiven Tumor-Phänotyp, Metastasierung, sowie einem schlechten Gesamtüberleben in diversen Tumorentitäten, z.B. im klarzelligem Nierenkrebskarzinom (RCC), im Aderhautmelanom (UM) und im intrahepatischen Gallengangskarzinom, assoziiert ist. Aktuell sind keine spezifischen Therapieansätze für Krebspatienten mit *BAP1* Mutationen vorhanden, weshalb in diesem Projekt ein neuer, potenzieller Therapieansatz für Patienten mit *BAP1*-Mutationen untersucht werden soll. Für die Untersuchungen wurde ein lentiviraler shRNA-Screen mit der BAP1-defizienten Nierenkrebszelllinie UMRC-6 durchgeführt, welche entweder mit einem BAP1-exprimierenden Plasmid oder ein Kontrollplasmid (Leervektor) transduziert wurde. Mit Hilfe des shRNA-Screens konnte *HDAC1* als ein möglicher synthetisch-letaler Interaktionspartner in BAP1-inaktiven Nierenkrebszellen identifiziert werden. Wie es zu erwarten war, führte die Reduktion der HDAC1-Proteinexpression zu einer geringeren Zellproliferation und Zellwachstum in verschiedenen BAP1-defizienten RCC, ICC und UM Zelllinien, wohingegen sie keinen Effekt auf das Zellüberleben von BAP1-exprimierenden Krebszelllinien zeigte. Darüber hinaus hatte der HDAC1-Inhibitor Quisinostat einen höheren Einfluss auf das Überleben von BAP1-defizienten Krebszelllinien als auf das Überleben von BAP1-exprmierenden Krebszelllinien. *Interessanterweise* zeigen die in dieser Arbeit durchgeführten Untersuchungen, dass der Verlust der HDAC1-Proteinexpression das Tumorzellwachstums einer *BAP1*-deletierten Aderhautmelanomzelllinie stärker reduziert als der Expressionsverlust des HDAC4-Proteins, wobei *HDAC4* in einer aktuellen Studie als ein letaler Interaktionspartner in *BAP1*-mutierten Aderhautmelanomen identifiziert werden konnte. Eine weiterführende Charakterisierung der Rolle von HDAC1 in BAP1-defizienten Krebszelllinien konnte darüber hinaus zeigen, dass der Verlust der HDAC1-Proteinexpression die Zellmigration von *BAP1*-deletierten Nierenkrebszelllinien beeinträchtigt und, dass eine reduzierte HDAC1-Proteinexpression den Anteil von *BAP1*-deletierten Tumorzellen in der G1-Phase des Zellzyklus erhöht. Im Gegensatz zum Einfluss von HDAC1 auf den Zellzyklus scheint die HDAC1-Inhibition keinen Einfluss auf die Apoptose in *BAP1*-deletierten Zellen zu nehmen. Diese Ergebnisse deuten darauf hin, dass HDAC1 die

Proliferation, Zellmigration und das Wachstum von Tumoren mit *BAP1*-Mutationen durch eine Regulation des G1-Kontrollpunkts des Zellzyklus Apoptose-unabhängig kontrolliert. Zukünftige Untersuchungen sollten sich auf die Wirkungsmechanismen von HDAC1 in BAP1-defizienten Krebszelllinien fokussieren, um HDAC1 als einen möglichen synthetisch-letalen Interaktionspartner von BAP1-defizienten Tumoren zu verifizieren. Interessanterweise supprimierte der *HDAC1*-Knockdown das Tumorwachstum ausschließlich in einem BAP1-defizienten Cholangiokarzinom-Xenograft Mausmodell, wodurch die synthetisch-letale Interaktion von HDAC1 mit BAP1-defizienten Tumoren *in vivo* validiert werden konnte. Die erhaltenen Ergebnisse weisen auf einen HDAC1-Inhibitor basierte Therapiemöglichkeit für *BAP1*-mutierte Tumorpatienten hin.

Table of Contents

List of Figures

List of Tables

List of Abbreviations

%	percent
°C	Degree Celsius
3p	short arm of chromosome 3
AB	antibody
ANOVA	Analysis of variance
ASXL 1/2	additional sex combs like proteins
ATP	adenosine triphosphate
BAP1	BRCA1-associated protein 1
BARD1	BRCA1-associated RING domain protein 1
BLI	bioluminescence imaging
BSA	bovine serum albumin
Ca^{2+}	calcium
CCA	cholangiocarcinoma
ccRCC	clear cell renal cell carcinoma
chRCC	chromophobe renal cell carcinoma
CO_2	carbone dioxide
COX7c	cytochrome c oxidase subunit 7C
CTD	C-terminal binding domain
CTG	CellTiter-Glo 2.0
dCCA	distal cholangiocarcinoma
ddH_2O	double distelled water
DMSO	dimethyl sulfoxide
DNA	deoxyribonucleic acid
e.g.	Lat. *exempli gratia*
EIF1AX	eukaryotic translation initiation factor 1A X-linked
EV	empty vector
EZH2	enhancer of zeste 2 polycomb repressive complex 2
FBS	fetal bovine serum
FoxK1/K2	forkhead box K1/K2
GNAQ/11	Guanine nucleotide-binding protein G
GTP	guanosintriphosphat
GTPase	guanosintriphosphat hydrolysis
h	hour

H2AK119ub1	mono-ubiquitinated histone H2A at lysine 119
H3K36me3	H3 lysine 36 trimethylating
HATs	histone acetyltransferases
HBM	HCF-1 binding domain
HCF-1	host cell factor C1
HDAC	histone deacetylase
HDACi	histone deacetylase inhibitors
HIF	hypoxia-inducible factor
HT	high-throughput
i. p	intraperitoneally
ICCA	intrahepatic cholangiocarcinoma
LB	Luria broth
LFC	log2 fold change
Luc	Luciferase
min	minute(s)
MM	malignant mesothelioma
mPTP	permeability transition pore
NES	normalized enrichment score
NLS	nuclear localization signals
ns	not significant
PARP	poly-adenosyldiphosphate-ribose polymerase
PBRM1	Polybromo 1
pCCA	perihilar cholangiocarcinoma
PI	propidium iodide
pRCC	papillary renal cell carcinoma
PR-DUB	polycomb group repressive deubiquitinase complex
RCC	renal cell carcinoma
RING finger domain	really Interesting new gene finger domain
s. c.	subcutaneous
sec	seconds
SEM	Standard error of the mean
SETD2	SET domain containing protein 2
SF3B1	splicing factor 3B subunit 1
shRNA	small hairpin ribonucleic acid

SWI/SNF	switch/sucrose non-fermentable
TOP3A	*DNA Topoisomerase III Alpha*
TPDS	tumor predisposition syndrome
UCH	ubiquitin carboxy-terminal hydrolase
UM	uveal melanoma
VHL	Von Hippel-Lindau
wt	wildtype
YFP	yellow fluorescence protein
YY1	Yin Yang 1
α	alpha

1. Introduction

1.1 BRCA-1 associated protein 1

BRCA1-associated protein 1 (BAP1) is an ubiquitin carboxy-terminal hydrolase (UCH) protein of the deubiquitinase family, which is responsible for removing ubiquitin molecules from proteins and histone substrates.

In 1998, BAP1 was first time named and discovered in a lung cancer cell line as a nuclear protein binding to the RING (really Interesting new gene) finger domain of the tumor suppressor protein BRCA1, thereby suppressing BRCA1's tumor suppressor activity (Jensen et al. 1998). Since these initial findings, a plethora of different physiological and pathophysiological functions of BAP1 have been reported.

1.1.1 Structure and function of BAP1

The *BAP1* gene is located on the short (p) arm of chromosome 3 (3p21.1) and encodes a 90 kDa deubiquitinating enzyme (Wang et al. 2016). The BAP1 protein consists of 729 amino acids and three domains (Yu et al. 2010) (Fig. 1).

On the N-terminal side of the BAP1 protein the UCH domain is localized and is accountable for the primary function of removing ubiquitin from ubiquitylated substrates. The second domain contains conserved peptide sequence known as the host cell factor C1 (HCF-1) binding domain (HBM), (Jensen et al. 1998; Machida et al. 2009). The last domain contains a C-terminal binding domain (CTD) and two nuclear localization signals (NLS) (Ventii et al. 2008).

In the past, ubiquitination of proteins was exclusively associated with targeting proteins for proteasomal degradation. However, more recent results indicate that ubiquitination has a more complex role within cells by influencing multifunctional and diverse cellular signaling pathways (Welchman, Gordon, and Mayer 2005). Therefore, by interacting with different proteins such as BRCA1-associated RING domain protein 1 (BARD1), HCF1, BRCA1, forkhead box K1 /K2 (FoxK1/K2), Yin Yang 1 (YY1) and additional sex combs like proteins (ASXL 1/2), BAP1 is involved in many cellular processes, including DNA damage response, replication, cell cycle progression, cell proliferation and histone modification (Ladanyi et al. 2012; White and Harper 2012) (Fig. 1 and Fig. 2).

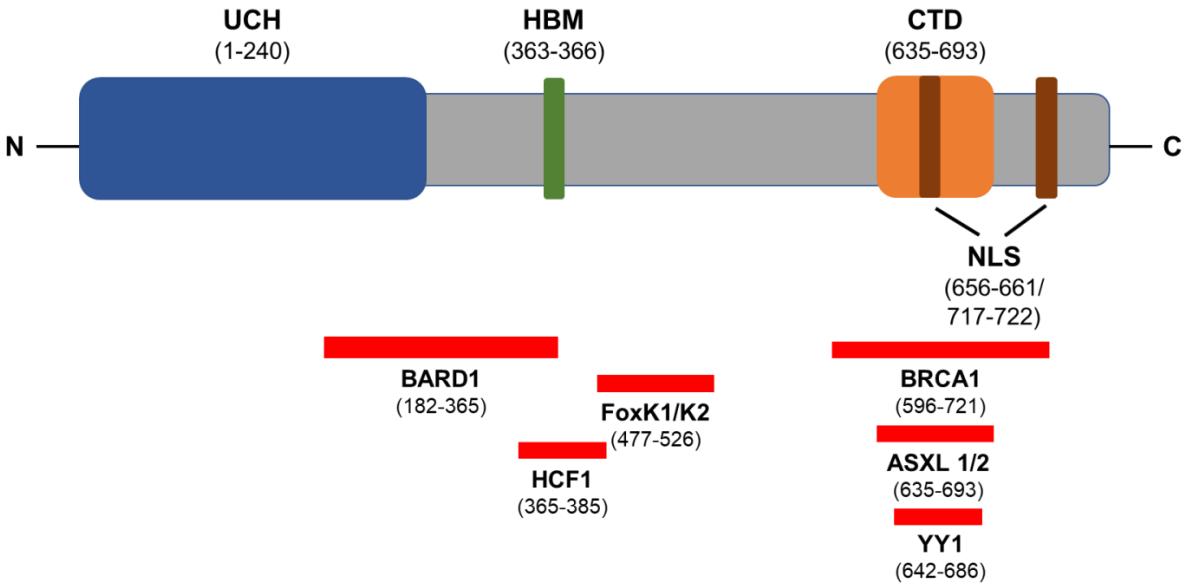

Figure 1: Scheme of functional domains of BRCA1-associated protein 1 (BAP1)
BAP1 consists of 729 amino acid with the 3 different domains: Ubiquitin carboxyl hydrolase (UCH) domain (amino acid 1-240); BARD1-binding region (amino acid 182-365); host cell factor C1 (HCF-1) binding domain (HBM) (amino acid 363-266); HCF-1 binding domain (amino acid 365-385); forkhead box K1/K2 (FoxK1/K2) binding region (amino acid 477-526); BRCA1 binding region (amino acid 596-721), C-terminal binding domain (CTD) (amino acid 635-693); additional sex combs like proteins ASXL 1/2 binding domain (635-693); nuclear localization signals (NSL) (amino acid 656-661 and 717-722) and Ying Yang 1 (YY1) binding domain (amino acid 642-686) (Wang et al. 2016).

BAP1 regulates growth regulation by inhibiting the HCF-1 (Machida et al. 2009) (Fig. 1 and Fig. 2). HCF-1 promotes cell proliferation by activating transcription factors, including proteins of the E2F family, which are involved in cell cycle control during in G1/S phase progression (Tyagi et al. 2007). Therefore, HCF-1 supports the binding of E2F1 transcription factors and H3K4 histone methyltransferase. Thereby, genes needed for S-phase can be transcribed. A loss of BAP1 in mesothelioma cells is leading to an uncontrolled transition of cells from G1 to S phase as BAP1 is responsible for suppressing the HCF-1 activity (Pan et al. 2015).

Furthermore, BAP1 has been shown to interact with HCF-1 and YY1 or FoxK1/K2 respectively in a complex, which controls cell proliferation (Yu et al. 2010). The formed BAP1/HCF-1/YY1 complex binds to the promoter of cytochrome c oxidase subunit 7C (COX7c) that encodes a component of the mitochondrial respiratory chain, which has been shown to enhance cell proliferation. In addition to the abovementioned complex, BAP1 can form a BAP1/HCF-1/FoxK1/K2 complex leading to a downregulation of the expression of FoxK1/K2 targets. The FoxK1/K2 targets are involved in upregulating cell proliferation and cell cycle progression. Therefore, the formed BAP1/HCF-1/FoxK1/K2 complex inhibits these processes (Okino et al. 2015).

Besides the above-mentioned complexes, BAP1 can form a polycomb group repressive deubiquitinase complex (PR-DUB) with the protein ASXL1/2 , which is essential for transcriptional regulation of physiological cell functions associated with embryonic development, stem cell pluripotency, self-renewal and differentiation (Scheuermann et al. 2010; Perez-Garcia et al. 2021) (Fig. 2). Through BAP1's deubiquitinase activity, the PR-DUB complex modulates chromatin by removing a ubiquitin molecule from histone H2A at its lysine 119 residue (H2AK119ub1), therefore regulating the expression of a multitude of genes (Campagne et al. 2019; Peña-Llopis et al. 2012).

Additionally, BAP1 is involved in DNA damage response by interacting with the tumor suppressor BRCA1 (Chen et al. 2002) (Fig. 1 and Fig. 2). The heterodimer complex consisting of BRCA1 and BARD1 functions as an E3 ligase, which activates the homologous DNA damage repair pathway (Wu-Baer et al. 2003). BAP1 is supporting the regulation of the DNA damage mechanisms by binding to the RING finger domain on BARD1 and inhibiting E3 ligase function (Nishikawa et al. 2009).

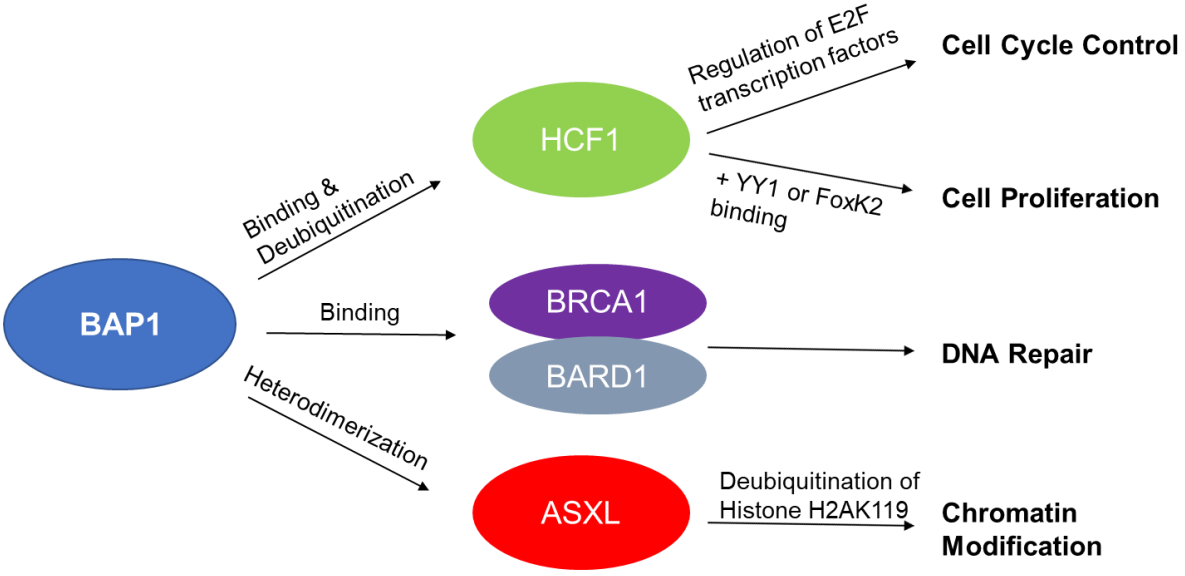

Figure 2: Physiological functions of BAP1
BAP1 is interacting with HCF1, resulting in the recruitment of E2F transcription factors, which control the progression from G1 to S-Phase within the cell cycle. Moreover, BAP1 and HCF1 are forming a complex either with YY1 (BAP1/HCF1/YY1) or with FoxK1/K2 (BAP1/HCF1/FoxK1/K2), which suppress cell proliferation. By binding to the BRCA1/BARD1 complex, BAP1 can regulate the DNA damage repair pathway by promoting double-strand DNA break processes. BAP1 modulates chromatin modulation due to the binding to the ASXL protein to form a polycomb group repressive deubiquitinase complex (PR-DUB) that regulates the Histone H2A deubiquitylation (Nishikawa et al. 2009; Machida et al. 2009; Scheuermann et al. 2010).

Recent studies also showed that BAP1 supports cell death by inducing the activation of a type-3 inositol-1,4,5-triphosphate-receptor, thereby underpinning the release of calcium (Ca^{2+}) from the endoplasmic reticulum to the inter-membrane space of mitochondria (Bononi et al. 2017). The mitochondria overload with Ca^{2+} stimulates the opening of the mitochondrial permeability transition pore (mPTP) and results in the release of pro-apoptotic factors, such as Cytochrome c, which promotes apoptosis (Halestrap 2006).

Taken together, these studies highlight the important physiological role of BAP1 in diverse cellular processes. In addition to the above-mentioned physiological functions, loss of BAP1 is associated with a variety different tumor entities, since BAP1 also functions as a tumor suppressor (Luchini et al. 2016; Murali, Wiesner, and Scolyer 2013; Jensen and Rauscher 1999).

1.1.2 Role of BAP1 in cancer

BAP1 acts as an important tumor suppressor as inactivating mutations lead to the loss of its function, e.g. mutations in the UCH domain, were identified in several human cancers (Carbone et al. 2013; Bhattacharya, Hanpude, and Maiti 2015). In addition to mutations within the UCH domain, other mutations outside the UCH domain are also leading to an inactivation of BAP1 DUB activity (Harbour et al. 2010).

The most frequent mutations occurring in the *BAP1* gene are non-synonymous single nucleotide variations, deletions and insertions (Harbour et al. 2010; Yoshikawa et al. 2012). Furthermore, it was observed that most *BAP1* mutations resulted in protein truncations and the loss of the two BAP1 NLS domains, leading to a loss of nuclear BAP1 translocation in different tumor entities (Ventii et al. 2008). Altogether, different studies identified BAP1 as a key regulator of cancer-associated pathways, showing that its loss can promote cancer development.

In addition, germline mutations of *BAP1* were identified to be predisposing factors for multiple cancers named as BAP1 tumor predisposition syndrome (BAP1-TPDS). Patients with BAP1-TPDS have got a high risk to develop malignant tumors e.g. uveal melanoma (UM), malignant mesothelioma (MM), cutaneous melanoma, renal cell carcinoma (RCC) and intrahepatic cholangiocarcinoma (iCCA) (Gupta et al. 2015; Wang et al. 2016; Farley et al. 2013). In contrast to cancer patients without BAP1-TPDS, BAP1-TPDS cancer patients tend to get cancer already in young age as well their tumors show a more aggressive phenotype (Rai et al. 2016).

However, *BAP1* is frequently mutated in a variety of tumor entities. One of the first cancer types that was found to be associated with *BAP1* mutations, was UM, where 45% of primary UM contain *BAP1* mutations (Harbour et al. 2010). Other cancer types with frequent somatic *BAP1* mutations include e.g. MM, clear cell RCC (ccRCC), CCA as well as other solid tumors (Yoshikawa et al. 2012; Peña-Llopis et al. 2012).

1.2 BAP1-associated tumor entities

1.2.1 Renal cell carcinoma

Kidney cancer accounts for approximately 2% of all cancers worldwide every year, ranked as the 9th most common cancer in men and the 14th most common cancer in women, showing a median age at diagnosis of 64 years (Fitzmaurice et al. 2015; Harrison, Mann, and Pearce 2013; Znaor et al. 2015).

The most common type of kidney cancer is renal cell carcinoma (RCC), which arises from the renal epithelium and accounts for more than 90% of kidney cancer cases (Hsieh et al. 2017). 400.000 patients are diagnosed with RCC every year, hereof 170.000 patients dying from this devastating disease (Motzer et al. 2020). Besides patients' age, race and gender play an important role in the development of RCC, with men being diagnosed almost twice the rate of women between 60 and 70 years of age (Mancini, Righetto, and Baggio 2020).

The most common risk factors include hypertension, obesity and cigarette smoking, however, different diseases, including chronic kidney disease, diabetes mellitus, cystic kidney disease or hemodialysis, have also been shown to promote RCC formation (Hsieh et al. 2017; Denton et al. 2002). The problem is that 25-30% RCC patients have already developed metastasis before their diagnoses. Additionally, around 30% of RCCs will recur after successful resection of the primary tumor (Janzen et al. 2003).

Furthermore, due to a lack of early detection and limited treatment options, in average, advanced RCC patients exhibit a poor survival rate of less than one year, with 25-30% of patients already being present with metastatic disease at the time of diagnosis (Marschner et al. 2017).

Moreover, RCC shows limited clinical response to standard treatment regimens, including chemotherapy and radiotherapy, with nephrectomy being the main curative treatment option for RCC patients (Thorstenson et al. 2015; Chin et al. 2006). Currently, immunotherapies (cytokine-based therapies) are showing the most benefit for patients with an advanced RCC (Amato 2000). Even though these treatments have

shown a clinical response in 10-15% of RCC patients, treatment regimens were also associated with harsh adverse effects, highlighting the unmet clinical need to investigate and identify molecular targets for the development of novel therapeutic strategies for RCC (Motzer and Bukowski 2006).

On the molecular level, RCCs display a heterogenous group of tumors, which consists of more than ten different molecular and histological subtypes with diverse biology, genetics and clinical behavior, appearing either sporadically or as a result of hereditary predisposition (Randall, Millard, and Kurzrock 2014). The most frequent RCC subtypes, which show an incidence rate of more than 5%, are: clear-cell RCC (75%), papillary RCC (10%) (pRCC) and chromophobe RCC (5%) (chRCC) (Linehan 2012), whereby ccRCC accounts for approximately 70% of all deaths associated with kidney cancer (Choueiri and Motzer 2017; Hsieh et al. 2017).

1.2.1.1 Genetic alterations in ccRCC

The development of ccRCC is associated with loss of heterozygosity, which is caused by the partial or entire loss of the short arm of chromosome 3 (loss of 3p). This alteration is observed in approximately 90% of ccRCC cases (Zbar et al. 1987; Chen et al. 2009).

With the chromosome 3p deletion, renal cells can simultaneously lose one copy of the four most frequently mutated tumor suppressor genes in ccRCC, which are localized on the p arm of chromosome 3 as well: Von Hippel-Lindau (*VHL*), Polybromo 1 (*PBRM1*), SET domain containing protein 2 (*SETD2*) and BRCA1 associated protein-1 (*BAP1*) (Fig. 3) (Peña-Llopis et al. 2013).

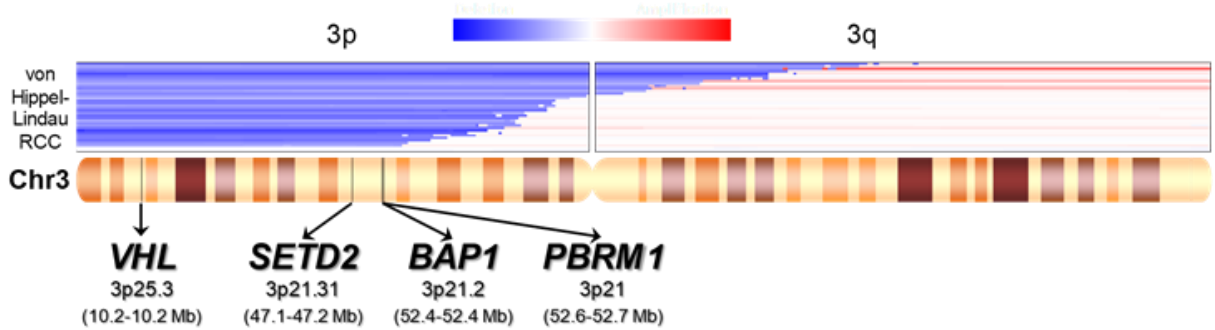

Figure 3: Distribution of tumor suppressor genes on chromosome 3
Schematic representation of the structure of chromosome 3 (region 3p and 3q). Loss or mutation of von Hippel-Lindau (VHL) is seen frequently besides the loss of the 3p part of chromosome 3 during development of RCC. Other tumor suppressors which are located on the 3p region of chromosome 3 are: Polybromo 1 (*PBRM1*), SET domain containing protein 2 (*SETD2*) and BRCA1 associated protein-1 (*BAP1*). (Adapted from Peña-Llopis et al., 2013)

Loss or mutation of the *VHL* gene is one of the decisive steps in the development of ccRCC (Gnarra et al. 1994; Nickerson et al. 2008). Loss of VHL can be found in both sporadic and familiarly ccRCCs and can be caused by somatic mutations or epigenetic inactivation through hypermethylation of the CpG island in the *VHL* promoter.

Under physiological conditions, the VHL protein forms a multiprotein complex, exerts an E3 ubiquitin ligase function that ubiquitinate proteins and, subsequently, leads to degradation of these proteins, mainly hypoxia-inducible factor (HIF) (Kaelin 2007). In ccRCC with biallelic *VHL* inactivation, an accumulation of the HIF protein can be observed, which results in enhanced downstream activation of vascular endothelial growth factor and other genes involved in cell growth, survival and angiogenesis (Forsythe et al. 1996; Masson and Ratcliffe 2014).

Although *VHL* inactivation is an important step during ccRCC development, the loss of VHL function per se is not sufficient to induce renal cell tumorigenesis, as shown in *VHL*-deficient mice (Kapitsinou and Haase 2008). Therefore, the development of ccRCC requires additional genetic events, e.g. the inactivation of additional tumor suppressor genes like *PBRM1.*

Truncating mutations of *PBRM1* are the second most frequent alterations of ccRCC (Varela et al. 2011). *PBRM1* encodes the BAF180 protein, which is a component of the nucleosome remodeling complex switch/sucrose non-fermentable (SWI/SNF), which is repressing the seedling growth by controlling the DNA accessibility. In addition, mutations within the *SETD2* tumor suppressor gene, which encodes a non-redundant histone H3 lysine 36 trimethylating (H3K36me3) enzyme can be observed in 10-15% of ccRCC cases (Edmunds, Mahadevan, and Clayton 2008). Furthermore, *BAP1* mutations occur in 10-15% of ccRCC patients and are associated with an advanced ccRCC phenotype (Guo et al. 2011; Peña-Llopis et al. 2012).

1.2.1.2 Characteristics of mutations associated with ccRCC

Mutations of *BAP1, PBRM1* or *SETD2* can result in a loss of protein function. Depending on their inactivating mutations in *BAP1* and *PBRM1*, patients can be classified with different prognosis (Fig. 4) (Peña-Llopis et al. 2012).

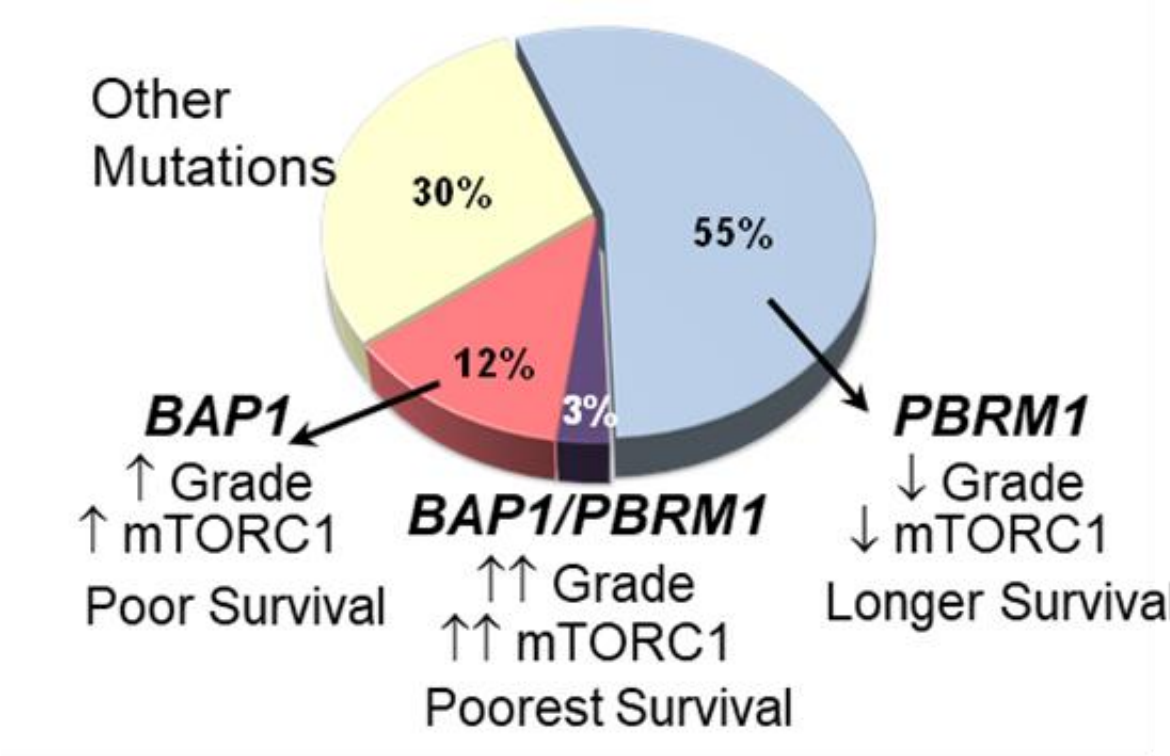

Figure 4: Genetic classification of ccRCC based on the inactivation of BAP1 and PBRM1
Representation of the relative distribution of *BAP1*, *PBRM1* and other mutations in ccRCC. *PBRM1* mutations are the most frequent mutations (55%) in ccRCC and are associated with low tumor grade and a decreased mechanistic target of rapamycin complex 1 (mTORC1) activation. *BAP1* mutations occur in 12% of ccRCC patients and are associated with a high tumor grade, an increased mTORC1 activation and poor survival. ccRCC patients with simultaneous *BAP1* and *PBRM1* mutations (3%) show the poorest survival. 30% of ccRCC patients do not show *BAP1* and *PBRM1* mutations, but mutations independent of the aforementioned genes. (Adapted from Peña-Llopis et al., 2012, courtesy of Samuel Peña-Llopis)

While alterations of *PBRM1* and *SETD2* can be frequently observed, alterations of *BAP1* and *PBRM1* are mutually exclusive (Peña-Llopis et al. 2013). However, 3% of ccRCC patients show a concomitant loss of both tumor suppressor genes, which is associated with highly aggressive tumors and the poorest patient survival (Peña-Llopis et al. 2013; Kapur et al. 2013).

Besides the VHL loss, *PBRM1* mutations also frequently occur in ccRCC patients (55%). Tumors with mutually exclusive *PBRM1* mutations are less aggressive and associated with lower tumor grade and longer overall survival. Furthermore, ccRCC patients with exclusive *PBRM1* mutations can be treated effectively with checkpoint immune inhibitor-based therapy (Hagiwara et al. 2021; Miao et al. 2018).

In contrast, loss or inactivation of BAP1 leads to an aggressive tumor phenotype with high tumor grade, activated mechanistic target of rapamycin complex 1 (mTORC1) and poor survival rates (Peña-Llopis et al. 2012; Kapur et al. 2013).

The *MTOR* gene encodes the mTOR serine/threonine protein kinase, which is involved in the regulation of cell cycle and cell growth (Cuyas et al. 2014). Former investigations showed that a constitutive activation of the mTORC1 pathway can initiate carcinogenesis such as breast, cervical cancer, esophageal squamous cell carcinoma, lung and hepatic cancers, making the mTORC1 pathway a promising therapeutic target in different tumor entities (Tian, Li, and Zhang 2019; Krencz et al. 2018; Lee 2017). However, for ccRCC patients with *BAP1* mutations, there is no effective therapeutic treatment regimen available to date, highlighting the urgent need for identification of novel therapeutic targets in this devastating disease.

1.2.2 Uveal melanoma

1.2.2.1 Uveal melanoma: a rare and aggressive cancer

Uveal melanoma (UM) is the most common primary intraocular malignancy in adults (85%), which develops from melanocytes colonized in the uveal tract. Different histological subtypes of UM can be classified based on the location of cancerous cells in the iris, ciliary body or the choroid (Krantz et al. 2017).

In general, UM is a rare tumor entity (4.3 cases per one million individuals) with predominantly sporadically developing tumors, however, familial uveal melanoma is really rare (approximately 1% of UM patients) (Singh and Topham 2003; Helgadottir and Hoiom 2016).

Since 1971, several publications have described the association between UM and other cancer types, e.g. cutaneous melanoma (CM), breast cancer, and prostate cancer (Johansson et al. 2019; Rednam et al. 1981; Henkind and Roth 1971). Additionally, 11.6% of UM patients have a risk for a hereditary predisposition (Abdel-Rahman et al. 2011). Most likely the second cancer were found in the prostate (2.2%), breast (1.6%), lung (1.2%), genitourinary (1%), gastrointestinal (0.9%), and leukemia/lymphoma (0.8%) (Diener-West et al. 2005).

The five-year survival rate of UM patients discovers with a primary tumor stage is 85% decreasing due to rising of metastasis, whereby up to 50% of UM patients develop metastasis within 5 years after diagnosis (Verma and Mehta 2016; Kujala, Makitie, and Kivela 2003). The median survival after development of metastasis for UM patients is six to twelve months. Distant UM metastasis can frequently be found in liver (89%), lung (29%), and bone (17%) (Diener-West et al. 2005; Carvajal et al. 2017).

While the primary tumor can be treated with potentially curative treatment options, e.g. brachytherapy, local resection, proton beam radiotherapy as well as iodine or ruthenium plaque radiotherapy, no effective therapy regimens are currently available against a metastatic UM disease state (Papastefanou and Cohen 2011).
It is known that the aggressiveness of an UM tumor is associated with the mutational profile of the corresponding cancer cells. Furthermore, the most frequent mutations in UM are reported to be localized within the *Guanine nucleotide-binding protein G* (*GNAQ/11*), *eukaryotic translation initiation factor 1A X-linked* (*EIF1AX*), *splicing factor 3B subunit 1* (*SF3B1*), and *BAP1* genes (Parish et al. 2018; Robertson et al. 2017).

1.2.2.2 Genetic alteration in UM

The most frequently occurring mutations can be detected in 85% of UM patients and are localized in the *GNAQ and GNA11* genes. *GNAQ* and *GNA11* encode for the guanine nucleotide-binding protein alpha (α subunit). The α subunit interacts with the β and γ subunits to form a heterotrimeric G protein, which regulates intracellular signal transduction pathways, e.g. the mitogen-activated protein kinase (MAPK) signaling pathway (Harbour 2012; Harbour and Chao 2014).
The α subunit of the G-protein contains a GTP hydrolysis (GTPase) activity. The activity of a GTPase terminates the normal activity of the G-protein complex. Mutations at amino acid residues glutamine-209 and arginine-183 in *GNAQ/GNA11* occur frequently in UM leading to a disable of the GTPase activity that prevent the inactivation of the G-protein followed by a constitutive activation of the MAPK pathway as well as other growth pathways (Harbour and Chao 2014).
GNAQ/GNA11 mutations themselves are not showing any known prognostic value for UM phenotype. These mutations arise in similar frequency in metastatic and non-metastatic tumors. The diagnosis of other mutations in driver genes, like in *BAP1,* are investigated to be more important for patient outcome (Harbour and Chao 2014; van Essen et al. 2014).

1.2.2.3 Role of *BAP1* mutations in uveal melanoma

BAP1 is mutated in 47% of UM patients and is associated with monosomy 3 and impart poor survival. The relative percentage of *BAP1* mutated patients increases in the metastasized disease state (up to 80%) and *BAP1* mutations are associated with a

dedifferentiated, stem-like and clinically aggressive UM phenotype (Harbour et al. 2010; Karlsson et al. 2020).

BAP1 germline mutations are linked to a 4-fold increased risk of metastasis and poor survival in patients. Thereby, patients with *BAP1* germline mutations show larger tumor diameter and a higher rate of ciliary body involvement (Gupta et al. 2015). It was reported that UM patients with germline mutations of the *BAP1* gene exhibit the mean survival of 4.74 years after diagnosis, while patients without a *BAP1* mutation showed a mean survival of 9.97 years following diagnosis (Kalirai et al. 2014).

In conclusion, both somatic and germline mutations of *BAP1* increase the risk of metastasis development in UM.

1.2.3. Cholangiocarcinoma

Cholangiocarcinoma (CCA) is a relatively rare and highly lethal adenocarcinoma, which arises from the biliary epithelium (cholangiocytes) of the hepatobiliary system, with an incidence rate of approximately seven per one million individuals (Shaib and El-Serag 2004). CCA is the second leading primary hepatobiliary malignancy and accounts for around 3% of all gastrointestinal cancers with a 5-year overall survival rate of less than 5% (Butt et al. 2012; Banales et al. 2020).

Known risk factors for CCA development include liver fluke infestation, bile duct anomalies, primary sclerosing cholangitis, biliary papillomatosis, chemical carcinogens, e.g. thorotrast and nitrosamines, nonalcoholic liver disease, obesity and viral hepatitis (Shaib and El-Serag 2004; Khan, Toledano, and Taylor-Robinson 2008).

CCA can be classified into three different subtypes based on the anatomical location of the tumor, whereby differentiating between intrahepatic (iCCA), perihilar (pCCA) and distal (dCCA) cholangiocarcinoma. Each subtype is related to different genetic aberrations as well as molecular and histological characteristics and therapeutic approaches (Braconi and Patel 2010).

1.2.3.1 Intrahepatic cholangiocarcinoma

iCCA is an aggressive tumor entity that arises from the malignant transformation of cells from the intrahepatic biliary tract and accounts for around 10% of all CCAs worldwide (Esnaola et al. 2016).

Microscopically, iCCA can be divided into a mass forming, a periductal-infiltrating and an intraductal-growing subtype based on the growth pattern, whereby the mass

forming subtype is the most frequent iCCA malignancy with a poor prognosis (Chung et al. 2009; Shaib et al. 2005).

Due to the asymptomatic nature at early stages as well as the lack of specific tumor markers for early tumor detection, 60-70% of iCCA patients are diagnosed at an unresectable or metastatic state (Shaib et al. 2005; Jarnagin et al. 2002). However, the only curative treatment option is surgical resection of the primary tumor, which can be offered to approximately 20-40% of iCCA patients (Bridgewater et al. 2014). Despite successful primary tumor resection, approximately 60% of patients show tumor recurrence with a median survival of 36 months (Hyder et al. 2013). Besides surgery, there are no effective treatments such as chemotherapies or molecular target therapies available (Bridgewater et al. 2014). Therefore, iCCA patients would benefit of a deeper understanding of the molecular mechanisms of this malignancy.

1.2.3.2 *BAP1* as a tumor suppressor in iCCA

Loss of chromosome 3p21 is a frequent event in iCCA patient (50-70%), which results in inactivation of BAP1 reported in up to 25% of iCCA cases associated with a metastatic phenotype and poor prognosis (Mosbeh et al. 2018; Sabbatino et al. 2020). Further, it was investigated that *BAP1* mutations can be used as a predisposition value for iCCA development (Andrici et al. 2016). Another study investigated the value of BAP1 as a marker for iCCA, since BAP1 is frequently lost, thereby resulting in negative nuclear staining for BAP1 in iCCA (Mosbeh et al. 2018).

However, to date, the mechanisms between *BAP1* mutation and the development of an aggressive phenotype of iCCA are barely understood.

1.3 BAP1 and cancer therapy

To date, treatment options for cancer patients with *BAP1* mutations are limited to standard therapies, However, tumors frequently show poor clinical response to the currently available therapeutic regimens, highlighting the urgent need to identify novel therapeutic targets directly associated with *BAP1* mutation (Louie and Kurzrock 2020). One of these therapeutic targets is the enhancer of zeste 2 polycomb repressive complex 2 (EZH2). EZH2 is upregulated in BAP1-deficient tumors and is associated with poor patient survival (LaFave et al. 2015; Sun et al. 2018; Baas and Schunselaar 2018). Recently, it was reported that in a phase ll clinical trial malignant mesothelioma patients with *BAP1* alterations demonstrated a good response to an EZH2 inhibitor

tazemetostat as the majority of malignant mesothelioma patients showed some level of disease control after treatment with tazemetostat (Zauderer et al. 2018).

Other inhibitors that are suggested to treat BAP1-deficient tumors are poly-adenosyldiphosphate-ribose polymerase (PARP) inhibitors, which inhibit the single strand break repair pathway (Baas and Schunselaar 2018; Rouleau et al. 2010). As *BAP1* mutations cause DNA damage repair gene defects, treating BAP1-deficient tumors with PARP-inhibitors to undergo other repair pathways such as the nucleotide or base excision repair mechanism shows a good option that has to be further investigated (Wu, Lu, and Yu 2010; de Koning et al. 2019).

Furthermore, another treatment option for patients with *BAP1* mutated tumors is immunotherapy, which is clinically already in use for the treatment of other aggressive tumor entities. In recent years, the association between *BAP1* alterations and a number of immunological phenotypes in cancer was reported (Figueiredo et al. 2020). A study could demonstrate that mesothelioma patients with *BAP1* mutations showed clinical response (in 20-30% of patients) to immune checkpoint inhibitors (Alley et al. 2017). However, immune checkpoint inhibitors showed no proof of benefit for UM patients (Yang et al. 2018).

Besides immunotherapy, histone deacetylase (HDAC) inhibitors (HDACi) represent another potential therapeutic target for BAP1-deficient tumors (Sacco et al. 2015). Since 2006, HDACi are clinically utilized to treat patients suffering from different tumor types (Duvic and Vu 2007; Landreville et al. 2012).

1.4 Histone deacetylases

1.4.1 Histone deacetylases - Characteristics and functions

HDACs are a class of enzymes that possess epigenetic regulatory functions (Delcuve, Khan, and Davie 2012). These enzymes remove acetyl groups from an amino acid on a histone, thereby supporting the suppression of gene expression, whereas histone acetyltransferases (HATs) have an opposite effect by opening the chromatin due to acetylating histones and allowing gene expression (Fig. 5) (Jenuwein and Allis 2001; Marks, Miller, and Richon 2003; Verdin and Ott 2015).

To date, studies have discovered 18 highly conserved genes, which encode for different HDACs. HDACs are classified into Class I (HDAC1, -2, -3 and -8). Class IIa (HDAC4, -5, -7 and -9), Class IIb (HDAC6 and -10), Class III (sirt1-sirt7) and Class IV (HDAC11) HDACs based on phylogenetic analysis (Varricchio et al. 2014). Class I

HDACs are ubiquitously expressed and are localized in the cellular nucleus (Watamoto et al. 2003; Wada et al. 2009). In contrast, Class II and Class IV HDACs are localized in both the nucleus and cytoplasm (Wang and Yang 2001; Watanabe, Khodosevich, and Monyer 2014). Class III HDACs belong to the sirt family and are functionally unrelated to other HDACs as their deacetylase activity is dependent on nicotinamide adenine dinucleotide, whereas Class I, II and IV are zinc-dependent enzymes (Micelli and Rastelli 2015).

In general, HDACs play a crucial role to regulate the gene expression of several oncogenes, tumor suppressor genes and inflammatory genes (Chen, Zhao, and Zhao 2015).

In addition to histones, HDACs are also involved in deacetylation of many other nonhistone proteins (Choudhary et al. 2009). The hyperexpression of diverse HDACs can impair the downstream gene regulatory network of HDACs targets that can lead to cancer progression. Such abnormalities could be investigated in different cancer entities (Prasad et al. 2014).

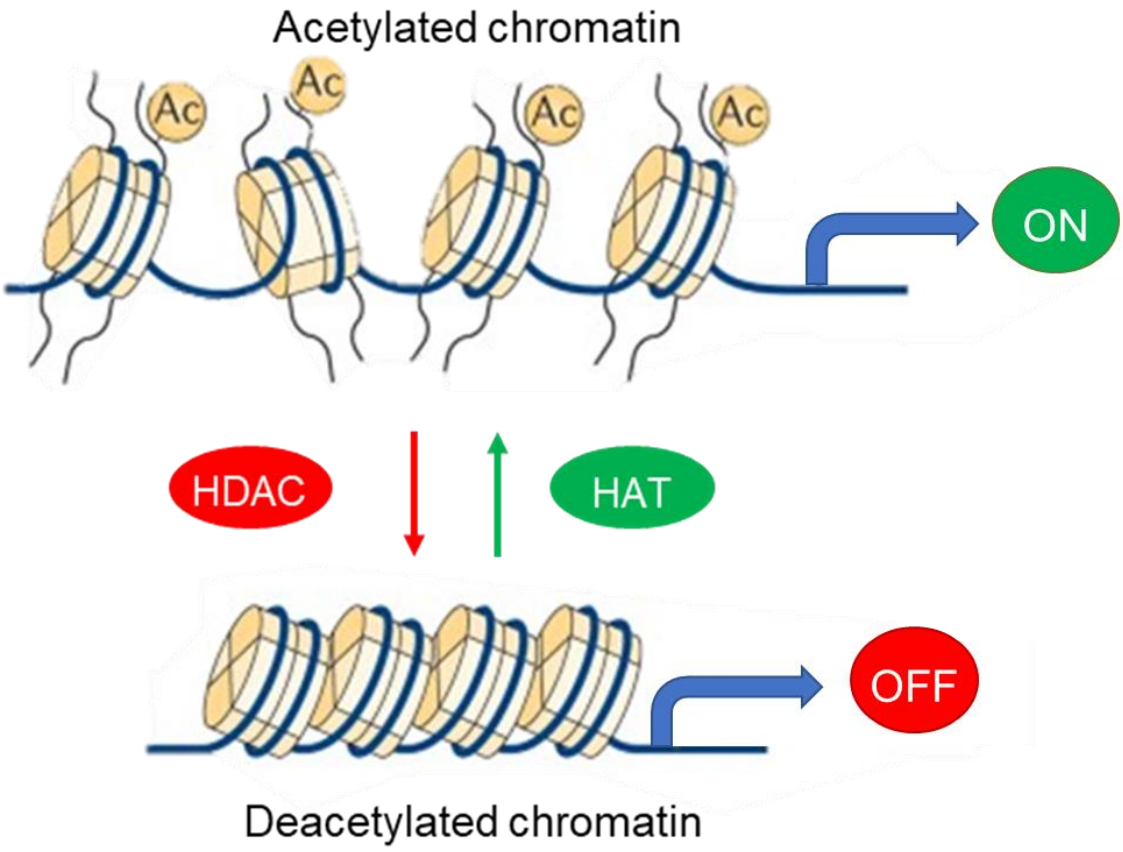

Figure 5: Schematic function of histone deacetylases (HDACs) and histone acetyltransferases (HATs)
Showing chromatin modulation according to the balance of HDACs and HATs. HDACs deacetylate histones, resulting in compact, densely-packed chromatin and a suppression of gene expression. In contrast, HATs acetylate histones, resulting in open, less densely-packed chromatin and gene expression (Adapted from Verdin and Ott, 2015).

1.4.2 Role of histone deacetylases in cancer development

An abnormal expression of HDACs is associated with the development of different cancer types, since HDACs are involved in several mechanisms, which can contribute to tumor development (Chen et al. 2020). Studies showed that aberrant expression of HDACs can decrease the transcription of tumor suppressor genes as well as promote oncogenic signaling (Chen, Zhao, and Zhao 2015; Li, Tian, and Zhu 2020).
A high level of HDACs has been shown to be associated with poor patient prognosis. It was shown that an increased expression of HDAC1, 2 and 3 correlates with poor patient outcomes in ovarian and gastric cancer (Weichert, Denkert, et al. 2008; Weichert, Roske, et al. 2008). In addition, a high level of HDAC8 in neuroblastoma, esophageal squamous cell carcinoma or cervical cancer is associated with an advance tumor stage and poor patient survival (Oehme et al. 2009).

A plethora of different studies has demonstrated that HDACs can support tumor progression by diverse cellular mechanisms (Fig. 6) (Hontecillas-Prieto et al. 2020).

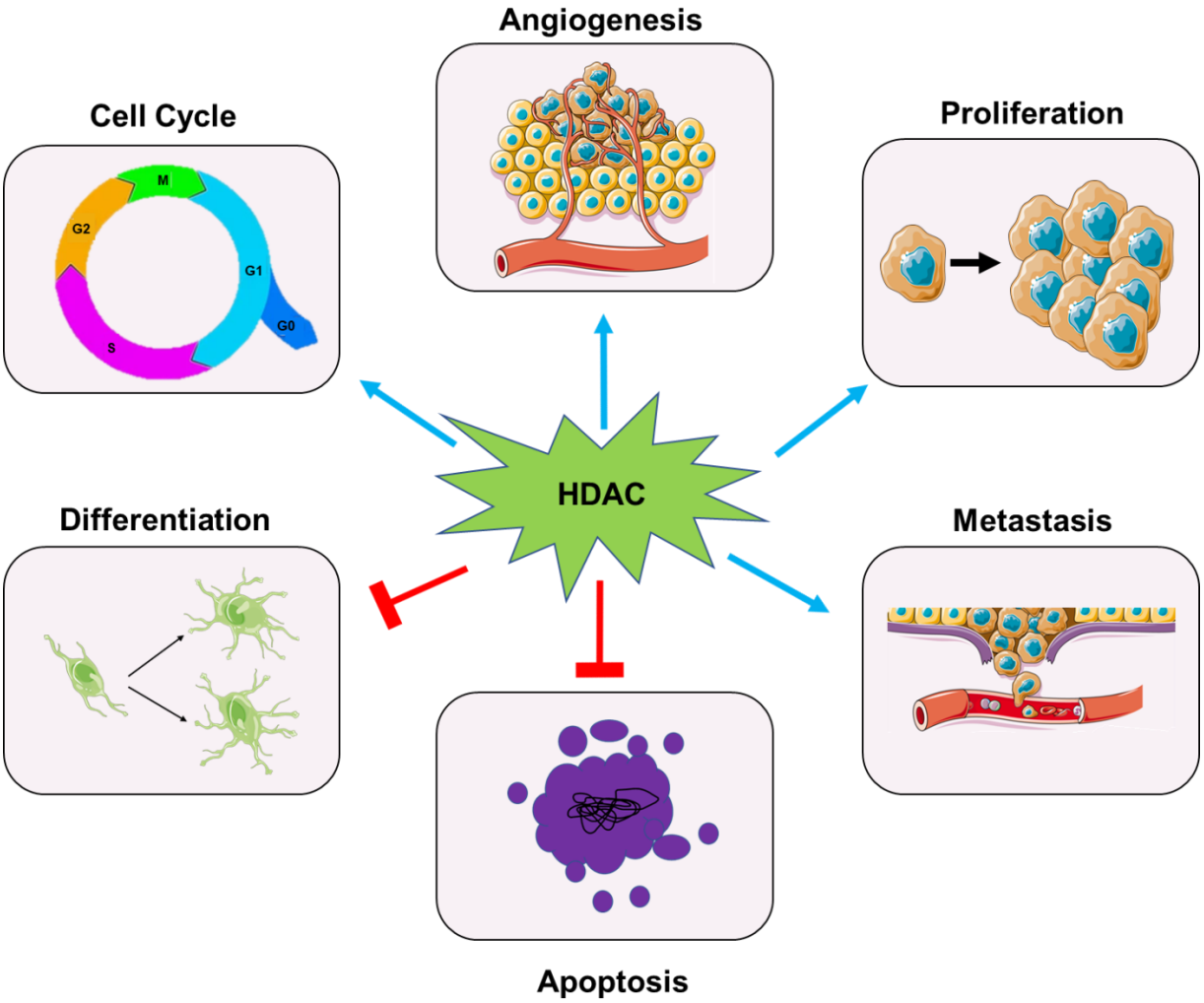

Figure 6: Role of HDACs in cancer progression
HDACs are inhibiting apoptosis and cell differentiation (inhibition: red arrow) and promote cell cycle progression, cell proliferation, angiogenesis as well as metastasis (promotion: blue arrow) (Hontecillas-Prieto et al. 2020).

HDACs have been shown to induce cell proliferation by deacetylating proteins involved in the cell cycle regulation (Glozak et al. 2005).

Furthermore, an overexpression of HDAC1, HDAC6, or HDAC8 lead to an increased cell invasion regulated by a higher expression of metalloproteinase-9, which mediates degradation and remodeling of the extracellular matrix, in breast cancer cell lines (Park et al. 2011). Moreover, it was reported that HDAC6 and HDAC8 can induce cancer cell migration and invasion by α-tubulin acetylation which leads to cancer progression in different cancer entities e.g. cervical cancer (Ding et al. 2014; Vanaja, Ramulu, and Kalle 2018).

Another possibility about how HDACs can influence cancer-associated pathways is by changing the expression of pro- and anti-apoptotic proteins, belonging to the B-cell lymphoma 2 family (Inoue et al. 2007). Additionally, it was reported that HDAC

inhibition can induce apoptosis by upregulation of cell surface death receptors and ligands, e.g. the Fas-receptor, apoptosis antigen 1 ligand or tumor necrosis factor receptor (Zhang and Zhong 2014).

Besides, HDACs are involved in the cellular mechanisms of hypoxia-induced angiogenesis. Previous studies revealed an overexpression of HDAC1, HDAC2 and HDAC3 in cancer cell lines, such as RCC and lung cancer cell lines, under hypoxic conditions (Kim et al. 2001). Moreover, it was described that high levels of HDAC1 mediated the suppression of the expression of the tumor suppressors p53 and von Hippel–Lindau protein, resulting in an overexpression of hypoxia-inducible Factor 1α and vascular endothelial growth factor (Kim et al. 2001; Deroanne et al. 2002).

The current knowledge about HDACs, their molecular functions and the cellular pathways that are affected by HDAC activities was significantly impacted and improved by the development of HDAC inhibitors (HDACi).

HDACi can be classified into different categories based on their functional range with inhibitors inhibiting all HDAC classes (not including sirtuins) being classified as pan-HDACi, whereas HDACi exclusively targeting specific HDACs being classified as selective HDACi (Ceccacci and Minucci 2016).

Some studies indicate that HDAC inhibition can result in a decreased tumor growth and an increased induction of apoptosis particularly in cancer cells, while minimally affecting normal tissue (Ungerstedt et al. 2005; Ceccacci and Minucci 2016).

In general, targeting HDACs with HDACi has shown clinical efficiency in different types of cancer, resulting in the FDA-approval of vorinostat and romidepsin for the treatment of cutaneous as well peripheral T-cell lymphoma (Grant et al. 2010; Iyer and Foss 2015). Additionally, it was shown that the treatment of diverse myeloma with the pan-HDACi panobinostat reveal clinical success as it was shown to increase the median progression-free survival of myeloma patients (Eleutherakis-Papaiakovou et al. 2020).

In previous reports, it was suggested that cancers with *BAP1* mutations could benefit of treatments with HDACi (Kuznetsov et al. 2019).

1.4.3 Efficiency of HDAC inhibitors in *BAP1*-mutated cancers

To date, several studies have investigated the efficiency of HDACi in tumors with *BAP1* mutations.

Previous studies suggest treating UM patients with HDACi. They reported that BAP1 loss causes hyperubiquitination of its target H2A, HDACi seems to prevent the

decrease excess of transcription factors to H2A. Therefore, HDACi suppressed tumor growth and reduced the metastatic spread of UM cells, resulting in a less aggressive phenotype (Landreville et al. 2012; Moschos et al. 2018).

Furthermore, it was shown that HDAC1, HDAC-3, and HDAC-8 are highly expressed in *BAP1*-mutant UM and are associated with an inflammatory phenotype, correlating with increased infiltrating leukocyte-derived cytokine production (Souri et al. 2021).

Another publication identified HDAC4 as a key target in *BAP1*-mutant UM. The authors demonstrated that the pan-HDAC inhibitor quisinostat lead to a decreased tumor growth and weight in *BAP1*-mutant UM tumors, but not in *BAP1*-wildtype UM, suggesting HDAC4 as the key target of quisinostat (Kuznetsoff et al. 2021).

Interestingly, BAP1 loss was found to increase the sensitivity to HDACi leading to a decrease of cell viability in mesothelioma. Additionally, an increased expression of HDAC1 and a decreased expression of HDAC2 were observed in *BAP1*-mutant mesothelioma tumors. Furthermore, HDACi sensitivity was induced due to *BAP1* alterations in mesothelioma cell lines (Sacco et al. 2015).

A phase lll clinical trial investigating the pan-HDACi vorinostat as a potential treatment option for malignant pleural mesothelioma patients revealed only minimal improvement in overall survival compared to the placebo control group (Krug et al. 2015). However, this clinical trial did not exclusively focus on *BAP1*-mutated malignant pleural mesothelioma patients, highlighting the need for additional studies focusing on HDACi in the context of *BAP1* loss/ mutation-associated malignancies.

1.5 Aim of the study

A loss of the tumor suppressor gene *BAP1* is associated with the development, progression and metastatic spread of several tumor entities, including clear cell renal cell carcinoma (ccRCC), uveal melanoma (UV) or intrahepatic cholangiocarcinoma (iCCA). In addition, cancer patients suffering from tumors containing a BAP1 inactivation show poor clinical response to standard therapies, highlighting the urgent clinical need for the identification of novel therapeutic targets.

Therefore, the aim of this study is the identification of a synthetically lethal target for *BAP1*-mutated tumors using a large-scale RNA interference screen.

The shRNA screen was conducted to identify synthetic lethal interactors with *BAP1* mutations using the BAP1-deficient cell line UMRC-6 reconstituted with an empty vector (control cell line) or wild-type *BAP1* expressing plasmid. We anticipated that the

knockdown of synthetically lethal genes within a BAP1 loss background results in a decrease of cell viability, proliferation and colony formation in BAP1 inactive cell lines, but not in wild-type *BAP1* expressing cell lines.

After the identification of the potential synthetically lethal target, we sought to characterize its specific role in *BAP1*-mutated tumors *in vitro* and investigate the effects of a synthetic lethal target inhibition on the growth of *BAP1*-mutated tumors *in vivo* using an iCCA murine xenograft model.

The identification of novel targets for BAP1-deficient tumors may pave the way for the development of specific therapies for cancers with mutations in *BAP1*.

2. Materials

2.1 Cell lines and bacterial strains

Name	Origin	Source	Growth Medium
786-O	Human (kidney carcinoma)	ATCC	RPMI
786-O Cas9	Human (kidney carcinoma)	Peña-Llopis Lab	RPMI
786-O sg*BAP1*	Human (kidney carcinoma)	Peña-Llopis Lab	RPMI
92-1	Human (uveal melanoma)	Michael Zeschnigk Lab	RPMI
92-1 B8-p.4 (sg*BAP1* #1)	Human (uveal melanoma)	Michael Zeschnigk Lab	RPMI
92-1 C8-p.4 (sg*BAP1* #2)	Human (uveal melanoma)	Michael Zeschnigk Lab	RPMI
Caki-1	Human (kidney carcinoma)	ATCC	McCoy's 5A
DH5α	Bacteria (*Escherichia coli*)	Invitrogen	LB-Medium
GP-293 (HEK293GP)	Human (kidney)	Stefan Fröhling Lab	DMEM
HEK293T	Human (embryonic kidney)	Stefan Fröhling Lab	DMEM
MDA-MB-231	Human (breast carcinoma)	Stefan Fröhling Lab / L. Garraway	DMEM
RCC4	Human (kidney carcinoma)	ATCC	RPMI
TFK-1	Human (cholangiocarcinoma)	Dr. Stephanie Rössler	RPMI
UMRC-6	Human (kidney carcinoma)	Sigma-Aldrich	DMEM

2.2 Plasmids

Plasmid name	Properties	Manufacture
pBabe-Hygro	Empty backbone Hygromycin resistance	Addgene #1765
pBH-BAP1-C91S-HA	Mutant *BAP1* Hygromycin resistance	Addgene #154021
pBH-BAP1-HA	Wild-type *BAP1* Hygromycin resistance	Addgene #154020
pLKO.1-HDAC1 #1	sh*HDAC1* Puromycin resistance	Sigma MISSION® TRCN0000195467
pLKO.1-HDAC1 #2	sh*HDAC1* Puromycin resistance	Sigma MISSION® TRCN0000195103
pLKO.1-HDAC4 #1	sh*HDAC4* Puromycin resistance	Sigma MISSION® TRCN0000004832
pLKO.1-HDAC4 #2	sh*HDAC4* Puromycin resistance	Sigma MISSION® TRCN0000314667
pMD2.G	Lentiviral envelope plasmid	Addgene #12259
psPAX2	Lentiviral packaging plasmid	Addgene #12260
pV2luc2	Luciferase expression YFP	Trumpp Lab (DKFZ)
pVSV-G	Retroviral packaging plasmid	Addgene #8454

2.3 Antibodies

Antibody (target)	Species/Manufacturer	Dilution
Primary antibodies		
Ⓟ-S6 (S240/244)	rabbit / Cell Signalling	1:1000
BAP1 Antibody (C-4)	mouse / Santa Cruz	1:500
HDAC1 (10E2)	mouse / Cell Signalling	1:1000
HDAC4 (D15C3)	rabbit / Cell Signalling	1:2000
S6 Ribosomal Protein (5G10) Rabbit mAb	rabbit / Cell Signalling	1:1000
β-Actin Antibody (C4) - HRP	mouse / Santa Cruz	1:1000
Secondary antibodies		
Anti-Mouse IgG (H+L) - HRP	goat / Dianova (Jackson ImmunoResearch)	1:2000
Anti-Rabbit IgG (H+L) - HRP	goat / Dianova (Jackson ImmunoResearch)	1:2000

2.4 Commercial kits

Kit	Manufacturer
AllPrep DNA/RNA Mini Kit	Qiagen
FITC Annexin V Apoptosis Detection Kit I	BD Bioscience
Plasmid Plus Midi Kit	Qiagen
QIAprep Spin Miniprep	Qiagen
Trans-Blot Turbo Transfer Kit	Bio-Rad Laboratories

2.5 Chemicals and reagents

Product	Manufacturer
4-20% Mini-PROTEAN TGX Precast Protein Gels, 10-well	Bio-Rad
4-20% Mini-PROTEAN TGX Precast Protein Gels, 15-well	Bio-Rad
6x loading dye	Thermo Fisher Scientific
Ampicillin	Karl Roth
Bovine serum albumin (BSA)	Sigma-Aldrich
CellTiter Glo®	Promega
Crystal violet	Sigma-Aldrich
Dimethyl sulfoxide (DMSO)	AppliChem
Dulbecco's Modified Eagle Medium (DMEM)	Gibco / Thermo Fisher Scientific
Dulbecco's Phosphate Buffered Saline (DPBS)	Gibco / Thermo Fisher Scientific
ECL Prime Western Blotting Detection Reagent	Sigma-Aldrich
Ethanol, absolute	Fisher BioReagents™/ Fisher Scientific
Fetal Bovine Serum (FBS)	Life Technologies / Thermo Fisher Scientific
Glycerol	Sigma-Aldrich
Glycine	Fisher Scientific
Halt™ Phosphatase Inhibitor Cocktail	Fisher Scientific
Halt™ Protease Inhibitor Cocktail	Thermo Fisher Scientific
HCl 37%	Sigma-Aldrich
Hygromycin B	Life Technologies / Thermo Fisher Scientific
Isoflurane	Apotheke Universitätsklinikum Essen
LB-Agar (Luria/Miller)	Roth
Luciferin	Biozol Diagnostica
Luria broth (LB) - Medium	Roth
Matrigel® Growth Factor Reduced (GFR) Phenol Red-free	Corning Inc.
McCoy's 5A Medium	Life Technologies
Methanol	J. T. Baker / Fisher Scientific
Nuclease-Free water	Qiagen

Product	Manufacturer
Opti-MEM Reduced Serum Medium	Life Technologies / Thermo Fisher Scientific
Penicillin/Streptomycin 10,000 U/mL	Life Technologies / Thermo Fisher Scientific
Precision Plus Protein™ Dual Color Standards	Bio-Rad Laboratories
ProLong mounting medium	ThermoFisher Scientific
Propidium iodide	Sigma-Aldrich
Protein Assay Dye Reagent Concentrate	Bio-Rad Laboratories
Puromycin Dihydrochloride-10 × 1 mL	Life Technologies
Quisinostat	Hölzel Diagnostika
RNAse	Qiagen
Roswell Park Memorial Institute (RPMI) 1640 medium	Gibco / Thermo Fisher Scientific
S.O.C medium	Fisher Scientific
SDS Solution 20%	Serva Electrophoresis
Sodium azide solution 1%	VWR
Sodium Chloride (NaCl)	Roth
Trans-Blot Turbo RTA Transfer Kit, nitrocellulose, mini	Bio-Rad
TransIT-LT1 transfection reagent	Mirus Bio
Tris	Karl Roth GmbH + Co
Triton X® 100	Roth
Trypan Blue solution 0.4%	VWR International
Trypsin-EDTA (0.25%)	Gibco / Thermo Fisher Scientific
Tween20	Promega

2.6 Buffers and solutions

Solution	Ingrediens
0.1% crystal violet solution	0.1% crystal violet 25% methanol
Antibody solution	Antibody (AB) diluted in: 5% BSA/TBS-T 0.05% sodium azide
Blocking solution	5% BSA in TBS-T
LB medium	25 g/l LB powder ddH2O
Propidium iodide (PI) staining solution	1 mg/mL propidium iodide 20% TritonX100 100 mg/mL RNase
Protein lysis buffer	50 mM Tris-HCl (pH 7.4) 250 mM NaCl 0.5% Igepal ddH2O
SDS running buffer (10 %)	30.2 g (MW 121.14) Tris Base 1 % SDS 144 g (MW 75.07) Glycine to 1000 m L ddH2O (pH 8.46)
TBS (10x)	500 mM Tris 1.5 M NaCl ddH2O (pH 7.6)
TBST buffer	1x TBS 0.1% Tween ddH2O
Transfer Buffer	2x Transfer Buffer from Trans-Blot Turbo Transfer Kit 20% Ethanol to 1000 mL ddH2O
Western blot stripping-solution	3 g Glycine 0.1% SDS 2 mL Tween20 to 200 mL ddH2O (pH 2.2)

2.7 Consumables

Product	Manufacturer
12-well Clear TC-treated plates	Corning Inc.
384 well plates, clear, with lid, CC	Fisher Scientific
96 well, white plate, clear Bottom	Santa Cruz
BD MICROLANCE cannula 22 G	BD Bioscience
BD MICROLANCE cannula 27 G	BD Bioscience
BioCoat™ control inserts (8.0 µm)	Corning
BioCoat™ GFR Matrigel Invasion Chambers (8.0 µm)	Corning
Cell Culture plate, 24-well	Sigma
ColiRollers™ plating beads	EMD Millipore
Combitips advanced® 5 mL	Eppendorf AG
Corning® 100 mm × 20 mm Dish	Corning Inc.
Corning® 28 mm Syringe Filter, 0.2 µL	Corning Inc.
Corning® 28 mm Syringe Filter, 0.45 µL	Corning Inc.
Costar® Disposable Serological Pipette (2 mL, 5 mL, 10 mL, 25 mL and 50 mL)	Corning Inc.
Countness™ cell counting chamber slides	Invitrogen
Cover slips 24×50 mm	VWR
CyroPure Tube 1.6 ml white	Sarstedt
CytoOne 6well plate, TC-treated	Starlab
Digital Caliper 150 MM	VWR
Ear piercing pliers	Roth
EasYFlask™ 25 cm^2	Thermo Fisher
EasYFlask™ 75 cm^2	Thermo Fisher
FACS tubes	Greiner Bio-One
Falcon® 14 mL Polypropylene Round-Bottom Tube	Neolab
Falcon® 50 mL Polypropylene Conical Tube	Neolab
Flask 175 cm^2	Corning Inc.
Glass Pasteur Pipettes, 145 mm	Brand
Microplate, 96 well, F-Bottom, clear	Greiner BioOne
Microplate, 96 well, FBottom, white	Greiner BioOne

Product	Manufacturer
Microscope slides	VWR
Pasteur pipettes, 230 mm	Karl Roth
RNase-Free 1.5 mL Microfuge Tubes	Ambion
SafeLock tube, 1.5 mL	Eppendorf
SafeSealTips® professional (10 µL, 20 µL, 200 µL and 1250 µL)	Biozym Scientific
TBC-needle 1 mL	Braun
UltraCruz™ Cell scraper, 39 cm	Santa Cruz

2.8 Equipment and Machines

Device	Manufacturer
Bead Bath M714	Lab ARMOR™
Centrifuge 5810 and 5810R Eppendorf	Eppendorf AG
CO2 Incubator HERACell 240i	Thermo Fisher Scientific
Countness II FL Automated Cell Counter	Thermo Fisher Scientific
FACSVantage SE with FACSDiVA Option	BD Bioscience
Flow cytometer BD FACSCelesta™	BD Bioscience
Ice pan (1 L, 4 L and 9 L)	Corning, Inc.
Incubator FD 23	Klaus Binder Labortechnik
IVIS Lumina II	Caliper Life Science
Maxisafe 2020 Safety cabinet/ cell culture hood	Fisher Scientific
Microplate reader Spark® 10M	Tecan Group
Microscope Slide Scanner Axio Scan.Z1	Carl Zeiss AG
Mini-Centrifuge 5424 and 5424R	Eppendorf AG
Mini-PROTEAN® Tetra Cell 4-gel	Bio-Rad Laboratories
Mini-PROTEAN® Tetra System	Bio-Rad Laboratories
Mr. Frosty™ Freezing Container	Thermo Fisher Scientific
Multipette® E3 Multi dispenser	Eppendorf AG
NanoDrop™ Lite Spectrophotometer	Thermo Fisher Scientific
Orbital Shaker-Incubator ES-20	Grant-bio / Fisher Scientific

Device	Manufacturer
pH Meter 766	Knick
Pipetboy Pipetus®	Hirschmann Laborgeräte GmbH
Pipettes (2 µL, 10 µL, 20 µL, 200 µL and 1000 µL)	Gilson
PowerPac HC Power Supply	Bio-Rad Laboratories
Primovert microscope	Carl Zeiss AG
Rocking platform Polymax 1040	Heidolph Instruments
Roller mixer/ Tube roller RS-TR05	Phoenix Instrument
T100™ Thermal Cycler	Bio-Rad Laboratories
ThermoMixer F1.5	Eppendorf AG
Trans-Blot® Turbo™	Bio-Rad Laboratories
Vortex Genie 2	Scientific Industries

2.9 Software

Product	Provider
BD FACSDiva FlowJo Software	BD Biosciences
D300eControl	Tecan
FlowJo Software	Tree Star Inc.
GraphPad Prism Version 9	GraphPad Software
ImageJ	Wayne Rasband
ImageLab™ Software	BioRad Laboratories
NanoDrop 200 1.4.1	Thermo Fisher Scientific
Servier Medical Art	Les Laboratoires Servier
SPARKCONTROL Dashboard	Tecan
Tick@Lab	A-Tune Software AG
Zen 2.6 (blue edition)	Carl Zeiss AG

3. Methods

3.1 Molecular biology methods

3.1.1 Bacteria transformation

Subcloning efficiency competent DH5α *E. coli* were used for the amplification of plasmid DNA under sterile conditions using a Bunsen burner. Frozen competent cells were thawed on ice.

The next steps were performed for sterility reasons next to the flame. For one reaction, 1 µL plasmid DNA was added in 25 µL of bacterial solution, mixed and incubated for 30 min on ice. Next, bacteria were heat-shocked at 42 °C for 75 sec followed by a second incubation on ice for 4 min. For cell recovery, 100 µL Super Optimal Broth was added to the cells. Cells were shacked (50 *g*) for 45 - 90 min at 37 °C. Afterwards, cells were plated with ColiRollers™ plating beads (EMD Millipore Corp.) on pre-warmed Luria broth (LB) -agar plates supplemented with 100 mg ampicillin per 1 L LB media and incubated at 37 °C overnight.

3.1.2 Plasmid DNA amplification and isolation

A single colony of the previously transformed DH5α *E. coli* was picked with a sterile pipet tip and utilized for plasmid DNA amplification. The bacteria derived from a single colony were incubated with 4 mL LB medium containing 100 µg/mL ampicillin at 37 °C in a shaking incubator at 45 *g* overnight. To further increase the amount of plasmid DNA, 25 µL of the overnight culture were added into two separate 50 mL tubes containing 20 mL LB medium with 100 µg/mL ampicillin. The tubes were incubated at 37 °C in a shaking incubator at 45 *g* overnight.

Alternatively, the overnight culture was used for glycerol stocks for long-term storage. For this purpose, 500 µL of the overnight culture were mixed with 40% glycerol in LB medium and stored at - 80 °C.

For plasmid DNA isolation, the two 50-mL tubes containing overnight cultured bacteria were pooled and centrifuged at 1,200 *g* for 15 min at 4 °C. The supernatant was discarded and the pellet was either stored at - 20 °C or directly used for plasmid DNA isolation.

Plasmid DNA from the bacteria pellet was extracted by using the QIAGEN Plasmid Plus Midi Kit according to manufacturers' protocol.

3.1.3 Determination of DNA concentration

The quantity and quality of eluted DNA was determined by measuring concentration and purity using a UV spectrophotometer (NanoDrop™ UV/VIS spectrophotometer). The concentration of DNA eluates was quantified by measuring the absorbance at 260 nm (A260). In addition, DNA purity was determined by measuring absorbance at 280 nm (proteins) as well as at 230 nm (chaotropic salts). Measured absorbances were used to calculate the A260/A280 and the A260/A230 ratio. Samples with a A260/A280 ratio between 1.8 – 2.0 as well as a A260/A230 ratio between 1.7 - 2.0 were assumed as high-quality samples, with minimal protein content or other contamination. Instrument calibration was performed prior to each experiment by utilization of elution buffer as blank value.

3.2. Protein isolation and analysis

3.2.1 Protein isolation

For protein isolation, 1×10^6 cells were seeded in 6-well microtiter plates and incubated at 37 °C in humidified atmosphere containing 5% CO_2 until reaching 80 – 90% confluency. The cell medium was removed and cells were washed with 2 mL cold PBS. Lysis was conducted by addition of 200 µL protein lysis buffer containing phosphatase inhibitor (Halt™ Phosphatase Inhibitor Cocktail) and proteinase inhibitor (Halt™ Protease Inhibitor Cocktail) to the cells and incubation for 10 min on ice. Afterwards, cells were scratched from the bottom of the 6-well microtiter plate with a cell scraper (UltraCruz™) on ice. Generated lysates were transferred to an Eppendorf 1.5 mL tube and centrifuged at 4 °C for 10 min at 5,000 *g* to separate cellular debris from the lysates. Cell lysates were stored at -20 °C until further processing.

3.2.2 Bradford protein assay

The protein concentrations were determined using the Bio-Rad Bradford protein assay. The Bradford reagent was used in a ratio of 1:5 with ddH_2O. For generation of a protein standard curve, a bovine serum albumin (BSA; 1 mg/mL) with a protein concentration range from 0 to 10 µg/mL was prepared. To measure the protein concentration of samples, 2 µL of the protein lysate was mixed with 198 µL of diluted Bradford reagent. The mixture was vortexed and incubated for 10 min at room temperature. The absorption was measured for each sample in duplicates at 595 nm using the Spark

Microplate Reader by Tecan. The absorption of the negative control (0 µg/mL BSA) was subtracted from every sample and the average of each duplicate was calculated. The generated BSA standard curve was used for the calculation of the protein concentrations of the respective lysates.

3.2.3 Western blot

For sample preparation, a lysate volume containing 10 µg protein was mixed with 1x loading buffer and ddH_2O to a total volume of 20 µL or 40 µL, respectively. Protein denaturation was performed by heating the samples at 95 °C for 10 min in a heat block. Afterwards, the whole sample volume was loaded onto a 10-well or 15-well Mini-PROTEAN® TGX™ 4 - 15% gel and run in 1x SDS running buffer at 120 V for approximately 1 h using the Bio-Rad Mini Protean Gel system.

Following, separated proteins were transferred from the gel to a nitrocellulose membrane (0.2 µm) using the Trans-Blot® Turbo™ RTA Mini Nitrocellulose Transfer Kit in a semidry Trans-Blot® Turbo™ Transfer system from Bio-Rad, applying the standard program for high molecular weight proteins.

To prevent unspecific antibody binding, the membrane was blocked by incubation with a 0.1% Tween 20 in TBS (TBS-T) solution containing 5% bovine serum albumin (BSA) for an hour at room temperature on a shaker. Next, the membrane was once washed with TBS-T for 5 min and incubated with the respective primary antibody (AB) diluted in 5% BSA/TBS-T overnight at 4 ˚C. All used primary AB and their corresponding dilutions are listed in Chapter 2.3.

On the next day, the membrane was washed three times for 10 min with TBS-T and incubated for an hour with a secondary antibody diluted 1:1000 in 5% BSA/TBST, which corresponded to the respective primary antibody species. Before protein detection, the membrane was washed three times for 10 min with TBST.

Lastly, the chemiluminescence signal from the secondary antibody was visualized on a ChemiDoc™ MP Imaging System (Bio-Rad), by adding Amersham™ ECL™ Prime western blotting detection reagent (1:1 dilution of Solution A and B) on the membrane.

3.2.4 Stripping of western blot membranes

For reusing the western blot membrane following a first target protein detection, membrane-bound primary and secondary antibodies were removed from the nitrocellulose membrane through membrane stripping. First, the membrane was

washed with 1x TBST-T for 10 min before incubation with mild stripping-solution for 15 min while shaking. Afterwards, the membrane was washed with ddH_2O for 10 min followed by a wash with TBST-T for 5 min. The membrane was blocked with 5% BSA/TBST for 1 h on RT before incubating it with a new primary antibody overnight.

3.3 Cell line establishment

3.3.1 Cell line cultivation and cryopreservation

Cell lines and their respective culture media are listed in Chapter 2.1. The cells were cultured on 37 °C and 5% CO_2 in a water-saturated atmosphere in cell culture flasks. Unless otherwise stated, cell culture media was supplemented with 10% fetal bovine serum (FBS) and 1% penicillin/streptomycin (P/S). The work was performed under sterile conditions using heat sterilized materials. Cells were split when reaching a confluency of 75 - 85%. For this purpose, medium was removed and the cells were washed with 5 mL PBS. With the use of Trypsin-EDTA, the cells were detached from the bottom of cell culture flask, before Trypsin-EDTA was diluted by the addition of fresh medium. The cell suspension was centrifuged at 150 *g* for 5 min and supernatant was discarded. The cell pellet was resuspended in 1 mL corresponding medium and the respective cell number was transferred into fresh cultivation medium. Cell number and viability were determined by trypan blue staining. For this procedure, 10 µL of the respective cell suspension were mixed with 10 µL trypan blue. 10 µL of the mixed solution were transferred to a cell counting chamber slide and automatically counted by Countness™ (Thermo Fisher Scientific).

For long-term storage, cells were cryopreserved by resuspending the cells in the respective complete growth medium supplemented containing 10% dimethyl sulfoxide (DMSO) and 30% FBS. Cryopreserved cells were stored in a freezer at - 150 °C.

3.3.2 Virus production and transduction

Virus transduced cell lines were generated by either retroviral or lentiviral transduction containing the respective plasmid of interest. All experiments involving virally transduced cell lines were performed following the official guidelines for laboratories of the Biosafety Level 2.

3.3.2.1 Retrovirus production and transduction

For generating stable TFK-1 and UMRC-6 cell lines expressing the empty vector (EV, control plasmid), wild-type *BAP1* (BAP1-wt) or p.C91S *BAP1* mutant plasmid cells were transduced with retrovirus and selected with hygromycin.

3.3.2.1.1 Retrovirus production

First, the retrovirus with the plasmid of interest was produced by seeding 1 × 10^6 GP-293 cells into a p100 dish with DMEM medium. On the next day, the transfection was performed. Therefore, a plasmid transfection mix was prepared, containing Opti-MEM, the packaging plasmid pVSV-G, the retroviral plasmid DNA of interest and the Transfection Reagent TransIT-LT1 (Table 1).

Table 1: Composition of the retroviral plasmid-transfection mix

Reagent	Amount per 10 cm plate
Opti-MEM	250 µL
pVSV-G (packaging plasmid)	3 µg
retroviral expression plasmid	3 µg
TransIT-LT1 (transfection reagent)	18 µL

The prepared plasmid-transfection mix was gently mixed by inverting ten times and incubated 30 min at room temperature. During incubation, the growth medium of GP-293 cells was replaced by 5 mL fresh complete DMEM medium. Next, the plasmid-transfection mix was dropwise added to the cells and cells were placed into the incubator. After 24 h of transfection, the medium of the GP-293 cells was discarded and replaced with 5 mL of fresh DMEM medium. The next day, the virus was harvested by collecting the medium of the GP-293. The virus could be harvested by repeating switching and collecting the media of the GP-293 for three days.

The retrovirus-containing medium was filtered through a 0.45-µL syringe filter and stored at 4 °C for short-term utilization or aliquoted and stored at - 80 °C for long-term storage.

3.3.2.1.2 Retrovirus transduction and antibiotic selection

Prior to transduction, 2.5 × 10^5 cells were seeded per 6-well plate to achieve a confluency of 30 - 40% and placed for incubation at 37 °C. On the next day, the medium was discarded and 1 mL of filtered retrovirus-containing medium was added to the cells. For transduction, cells were incubated for 48 h at 37 °C.

Following retrovirus-containing medium incubation, transduced cells were antibiotically selected with hygromycin, since the retroviral plasmid encoded a gene for hygromycin resistance, resulting in a directed selection of successfully transduced cells.

For antibiotic selection, the virus-containing medium was discarded and replaced with complete growth medium supplemented with 250 µg/ml hygromycin.

3.3.2.2 Lentivirus production and transduction

For generating stable cell lines expressing the knockdown of *HDAC1* and *HDAC4*, cell lines were transduced with lentivirus and selected with puromycin.

3.3.2.2.1 Lentivirus production

One day before transfection, 1 × 10^6 HEK293T cells were seeded into a 10-cm dish, to reach a target confluency of 50-60% at the time of transfection. On the next day, the transfection was performed. First, a plasmid-transfection mix of the psPAX2 packaging plasmid, pMD2.G envelope plasmid and OptiMEM was prepared according to Table 2. Next, 3 µg of desired pLKO.1-puro shRNA expression plasmids (compare Chapter 2.2) was added to the plasmid-transfection mix.

Table 2: Composition of the lentiviral plasmid-transfection mix

Reagent	Amount per 10 cm plate
Packaging plasmid (psPAX2)	1.8 µg
Envelop plasmid (pMD2.G)	0.3 µg
OptiMEM	20 µL

In addition to the plasmid-transfection mix, 18 µL of TransIT-LT1 transfection reagent were diluted with 270 µL OptiMEM to prepare a transfection mix. Afterwards, the plasmid-transfection mix with the corresponding expression plasmid was added to the diluted TransIT-LT1 reagent, gently mixed by inverting ten times and incubated for 30 minutes at RT.

Following, the growth medium of HEK293T cells, plated in 10-cm dishes on the previous day, was removed and replaced by 5 mL of fresh complete DMEM medium. The incubated plasmid-transfection mix was added dropwise to the cells, and plates

were gently mixed. Next, cells were incubated overnight at 37 °C. After approximately 16 h, transfection medium was removed and replaced by 5 mL of fresh DMEM medium. On the next day, the virus-containing medium was collected and stored at 4 °C. The procedure of medium replacement and virus harvest was repeated up to three times. Following, the virus-containing medium was filtered using a 0.45-µm sterile syringe filter and either immediately used or aliquoted and stored at - 80 °C for long-term storage.

3.3.2.2.2 Lentivirus transduction and antibiotic selection

Prior to transduction, 2.5 × 10^5 cells were seeded into each well of a 6-well tissue culture plate. On the next day, 1 mL of viral-containing medium was added to the cells Next, cells were incubated in a humidified incubator at 37 °C for 48 h. Afterwards, the virus containing medium was removed and replaced by the respective growth medium supplemented with the according amount of puromycin (see Table 3) to select for transduced cells.

Table 3: Puromycin concentration used for transduced cells selection

Cell line	Puromycin (µg/mL)
UMRC-6	2 µg/mL
TFK-1	1 µg/mL
786-O	2 µg/mL
Caki-1	2 µg/mL
RCC4	2 µg/mL
92-1	0.5 µg/mL

3.4 Proliferation and colony formation assays

To compare the growth rates of different cell lines upon shRNA-mediated knockdown Cell Titer-Glo 2.0 assays and colony formation assays were performed.

3.4.1 CellTiter-Glo 2.0 assay

The CellTiter-Glo 2.0 assay determines the number of viable cells in culture by quantifying ATP, which indicates the presence of metabolically active cells.

This assay was used to examine the cell viability and proliferation of the different cell lines upon shRNA-mediated knockdown.

500 cells were seeded in 100 µL medium into 7 different white-bottom 96-well plates in triplicates. After 30 min, a baseline measurement (day 0) was performed. The remaining six 96-well plates were incubated at 37 °C, 5% CO_2 for 24 h, 48 h, 72 h, 96 h, 120 h or 144 h before measurement.

Following the respective incubation time, 100 µL of CTG reagent (diluted 1:4 in PBS) was added to each well. The plates were shacked for 2 min and incubated for 8 min in the dark at room temperature to stabilize the luminescence signal. Following, live cell number was determined with the microplate reader Tecan SparkControl™ by detection of the luminescence signal, which is proportional to the number of living cells. Measured luminescence signals were normalized to the measurement of the baseline luminescence signal (day 0).

3.4.2 Colony formation assay

For the colony formation assay, either 1000 cells/well (TFK-1, UMRC-6, 786-O) or RCC4) or 3000 cells/well (Caki-1 or 92-1) were seeded into 6-well plates and cultured at 37 °C. Cells were allowed to grow for two weeks (UMRC-6, RCC4, Caki-1) or ten days (786-O, TFK-1 or 92-1) until the colonies were observed. Following, the medium was removed and cells were washed once with cold PBS. Colonies were fixed with cold 100% methanol for 10 min on ice and stained with 0.1% crystal violet solution on a shaking platform for 30 min. Cells were washed with H_2O and dried overnight at room temperature before imaging. After air drying, plates were scanned using Epson Perfection V850 Pro and analyzed with the Image J software.

3.5 Cell migration and invasion assay

The cell migration and invasion assay were used to study cell migration and invasion between HDAC1 expressed and *HDAC1* knockdown cell lines.

The migration and invasion assays were performed according to the manufacturer's recommendations by using 24-well transwell chambers (Corning) with 8.0-µm pore size polycarbonate membrane, which were either coated (invasion assay) or not coated (migration assay) with BioCoat GFR Matrigel.

First, 1×10^6 UMRC-6 cells were seeded into a 10-cm dish and incubated for around 16 h at 37 °C. The following day, cells were washed twice with PBS and starved by addition of DMEM medium containing 0.5% FBS (starvation medium) for 4 h. Simultaneously, trans-well chambers were incubated with prewarmed starvation medium for at least 2 h at 37 °C. After incubation, 750 µL DMEM medium supplemented with 10% FBS (to function as chemoattractant) was added into the lower chamber, and 500 µL starvation medium containing 3×10^4 cells were added into the upper chamber.

After 24 h incubation at 37 °C, the non-migratory cells and the Matrigel on the upper side of the membrane were removed with a cotton swab. The migrated or invasive cells on the bottom side of the membrane were then fixed with 70% ethanol for 1 h at room temperature and stained with a 0.1% crystal violet solution on a shaking platform for 20 min. After several washing steps with water, the membrane was removed with a scalpel from the insert and sticked with ProLong mounting medium on slides. Slides were scanned with the Axio Scanner Z.1. and five pictures per membrane of randomly chosen, separated areas were taken with a 10x objective magnification. The cells were counted and averaged to observe the cell number of migrated and invasive cells.

3.6 Flow cytometry

Flow cytometric experiments were conducted on a BD Celesta flow cytometer. The three lasers (blue (405nm), violet (488nm) and yellow/green (561nm)) and 13 filters enable concomitant detection of up to 10 colors. Intra- and inter-laser beam spillover correction was calculated with the corresponding FlowJo software.

3.6.1 Cell cycle analysis

Propidium iodide (PI) staining was performed for analyzing the cell cycle distribution of *HDAC1* knockdown cell lines. Thus, 1 × 10^6 cells were harvested and pelleted by centrifugation at 200 *g* for 5 min. The cell pellet was washed twice with cold PBS and each pellet was resuspended in 300 µL cold PBS and transferred to a FACS tube. The cells were subsequently fixed by dropwise addition of 700 µL 100% cold ethanol and incubated overnight at 4 °C. On the next day, the fixed cells were pelleted by centrifugation at 200 g and the cell pellet was resuspended once with 3 mL PBS and incubated for 15 min at RT. After centrifugation at 200 *g* for 5 min, the supernatant was discarded and cells were stained with 350 µL of PI staining-solution and incubated at least 30 minutes in the dark at 4°C before flow cytometry was carried out. Flow cytometry data were analyzed using the FlowJo software to calculate the percentage of cells in each cell cycle phase.

3.6.2 Apoptosis assay

The apoptotic rates of *HDAC1* and *HDAC4* knockdown cells were measured by flow cytometry using the Annexin V Apoptosis Detection kit I (BD Biosciences) according to the manufacturer's protocol.

First, cells with a concentration of 1 × 10^6 cells/mL were harvested. Afterwards, cells were washed with cold PBS, and centrifuged at 200 *g* for 5 min. Following, cells were washed with 2 mL 1x binding buffer (diluted 1 to 9 with distilled water) and centrifugation at 200 *g* for 5 min. Next, the cell pellet was resuspended in 100 µL 1x binding buffer and transferred into a FACS tube. The cells were stained by addition of 5 µL FITC-conjugated Annexin V and incubated 15 min at RT in the dark. Following the Annexin V staining, 2 mL of 1x binding buffer was added to the cells and the cells were centrifuged at 200 *g* on RT for 5 min. The supernatant was discarded and the cell pellet was resuspended in 200 µL of 1x binding buffer. Afterwards, 5 µL of PI solution was added to the cells and the solution was incubated for 15 min at room temperature in the dark. Following incubation, samples were analyzed by flow cytometry using lasers to detect FITC and PI. As controls and for determination of the appropriate flow cytometric laser settings, unstained cells, cells exclusively stained with FITC-annexin V and cells stained exclusively with PI were used. FACS data were analyzed using the software FlowJo to measure the percentage of cells in different apoptotic stages: Cells

which were Annexin V positive and PI negative were counted as early apoptotic cells, cells which were Annexin V and PI positive cells were assumed as late apoptotic cells.

3.7 Drug treatment

To compare the effect of Quisinostat on BAP1-competent and BAP1-null cell lines *in vitro*, cytotoxicity assays were performed.

Before performing the drug screen, the optimum cell number (to avoid too high confluency of cell at the end of the assay) was determined for each established and primary cell lines. For this purpose, a range of 100 to 2,500 cells/well from each well cell line were seeded as triplicates in both 384-well white flat bottom plates and 384-well clear flat bottom plates for visual inspection. The plates were incubated at 37 °C for 48 h and the optimum cell number was detected by performing CTG assay (see 3.4.1) and by visual inspection of each well under the microscope.

Quisinostat was dissolved in DMSO to reach a concentration of 100 mM and printed at nine concentrations ranging from 1 nM to 1 µM into triplicates in 384-well white flat bottom plates using a Tecan D300e Digital Dispenser (Tecan) and the corresponding software D300e Control (v3.1.3, Tecan). DMSO was used as a negative control to investigate the influence of the dissolvent on the cells. The drug pre-printed plates were stored at -80 °C until used.

Following pre-printed plate thawing at room temperature for at least 30 min, previously optimized cell numbers for each respective cell line were transferred into each well in 30 µL medium. The plates containing different concentrations of Quisinostat and cells were incubated at 37 °C and 5% CO_2 for 48 h before the CTG assay was conducted.

3.8 shRNA screen

To identify potential synthetic lethal interactors with BAP1 loss, Dr. Peña-Llopis performed a shRNA screen with isogenic cell lines. 2×10^{-6} UMRC-6 cells reconstituted with empty vector, wild-type *BAP1* and p.C91S mutant *BAP1* in 14 15-cm dishes were transduced for 24 h with the necessary amount of module 1 of the DECIPHER library, which covers 27,500 pooled shRNAs targeting 4,625 genes involved in the most important cell signaling pathways.

Cells were harvested after 3 days and after 12 days, splitting them every 3 days to enable enough doublings for the drop out of shRNAs synthetic lethal with BAP1 loss.

DNA was extracted and two rounds of PCR were conducted to amplify barcoded plasmids, which were sequenced by multiplexed high-throughput sequencing at the High-Throughput Sequencing Unit of the Genomics and Proteomics Core Facility at the German Cancer Research Center (DKFZ).

Thus, sequencing data was deconvoluted using the DECIPHER Bar Code Deconvoluter, to match the read counts of the exact barcode sequences to the corresponding shRNAs. Farther, shRNAs with less than 100 read counts for the baseline condition were excluded. Subsequently, the remaining read counts were normalized by dividing the individual counts of each shRNA by the mean of the total read counts. Following this internal normalization, the depletion ratio of each individual shRNA was calculated by division of the normalized read counts of the dropout sample by the normalized read counts of the baseline sample. Consequently, a depletion ratio below 1 indicates, that the respective shRNA reduced cell viability. The depletion ratios were further transformed to log2 fold change (LFC) scores using R. The obtained LFC scores of the different isogenic cell lines and conditions were rescaled using the peak median absolute deviation method (PMAD) of the NormLines pipeline from GenePattern (as described in Cheung et al., 2011). Following, the PMAD normalized LFC scores were analyzed with RIGER. RIGER calculates the differential effect between three independent replicates of UMRC-6 EV and three replicates of UMRC-6 BAP1-wt cells and ranked shRNAs accordingly. Thereby, the shRNAs, which were strongest depleted in UMRC-6 EV and least depleted in UMRC-6 BAP1-wt cells, received the highest scores. The single shRNA scores were assigned to their respective genes and grouped to become a normalized enrichment score (NES) of the target gene. The final output of the analysis was a list of ranked genes based on their NES. This hit list was further limited by excluding all hit genes with *p*-values greater than 0.05.

3.9 Microarray Analysis

Samples for microarray analysis of 786-O sgCas9 and sg*BAP1* containing shRNA for *HDAC1* or scrambled control were seeded in a ratio of 1×10^6 cell per 6-well plate. On the next day, the total RNAs were extracted using RNeasy (Qiagen) and quantified using Nanodrop. RNAs were hybridized on Affymetrix Clariom S human arrays by the Microarray Unit of the Genomics and Proteomics Core Facility at the German Cancer

Research Center (DKFZ). Quantile-normalized expression data were analyzed as previously described (Peña-Llopis *et al. EMBO J.* 2011).

3.10 *In vivo* experiments

Female nude mice (NMRI-Foxn1^{nu}) were used for all *in vivo* experiments, which were purchased from Envigo at an age of five weeks. All mice were acclimatized for at least one week before entering an experiment. Animals used in all experiments were approved by the LANUV (*Landesamt für Natur, Umwelt und Verbraucherschutz Nordrhein-Westfalen*) and has been assigned No. 81-02.04.2019.A185 by the commission.

3.10.1 *In vivo* experiments – Cell line generation

The BAP1-deficeint cell lines UMRC-6, TFK-1 and the breast cancer cell line MDA-MB-231 cell line, which were used for this project, were engineered by lentiviral transduction (as described in Chapter 3.3.2.2) to express yellow fluorescent protein (YFP) and Luciferase (Luc). To select only YFP/Luc positive cells, cells were sorted according to YFP fluorescence using BD FACSVantage SE with BD FACSDiVA Option (BD Biosciences). Afterwards, YFP+/Luc+ positive cells were transduced to express either an empty vector (EV) as a control, wild-type *BAP1* (BAP1-wt) or a plasmid encoding a mutated *BAP1* (p.C91S) plasmid (described in Chapter 3.3.1.2). Additionally, TFK-1 cell lines were transduced with shRNA plasmids to generate a *HDAC1* or *HDAC4* knockdown.

3.10.2 Establishment of a metastatic mouse model

For the establishment of a metastatic mouse model, Luc positive cell lines were injected into the heart of nude mice for systemic tumor cell dissemination. MDA-MB-231 cells were used as a control cell line as it was already reported that this cell line can develop successful metastasis after intracardiac injection into nude mice (Jenkins et al. 2005). Following, potential metastases were visualized with bioluminescence imaging (BLI).

3.10.2.1 Intracardiac injection of transduced and sorted tumor cells

For the establishment of a metastatic mouse model, the transduced BAP1-deficient ccRCC cell line UMRC-6 YFP^{+}/Luc^{+} (cell line of interest) as well as the transduced

MDA-MB-231 YFP$^+$/Luc$^+$ cell line (control cell line) were used for intracardiac injection. For this purpose, 1 × 10^5 cells in 0.1 mL PBS with 0.5% FBS were injected with a 27 G needle into the left ventricle of nude mice (6 –7 weeks of age), which obtain isoflurane anesthesia during the injection. Immediately after the procedure, whole body BLI (described in Chapter 3.10.2.2) was performed to confirm successful intracardiac tumor cell injection. BLI was performed weekly until the mice were sacrificed after 4 months following intracardiac injection.

3.10.2.2 Bioluminescence imaging

Bioluminescence is generated by an enzymatic reaction between the luciferase enzyme of luciferase-expressing cells and its substrate luciferin. The reactions between luciferase and luciferin result in an emission of light, which can be detected by detectors of the IVIS spectrum, enabling this technique to visualize luciferase-expressing, disseminated tumor cells within murine bodies following luciferin addition.

Therefore, BLI was used to follow *in vivo* tumor growth and development of metastases by using an IVIS Lumina II (Caliper Life Science) at the Imaging Center Essen (IMCES) of the University Hospital Essen.

Before performing BLI, luciferin was diluted in PBS (30 mg/mL), filtrated through a 0.2-µm filter and stored in the dark at –20 °C. Immediately before BLI, mice were injected intraperitoneally (i. p.) with 100 µL luciferin solution. After the injection, mice were placed into a narcosis chamber flooded with 2.5% isoflurane in oxygen. When the mice were narcoticized, they were placed into the IVIS spectrum. During BLI, mice were kept anesthetized with 2% isoflurane using a nose coin dispensing the isoflurane. Mice were imaged 10 min after the injection (optimum reaction time). Pictures exposed for 1 s, 10 s, 20 s and 1 min during imaging were taken.

3.10.3 Subcutaneous murine xenograft model

Tumor growth was compared between *HDAC1* knockdown and control cell lines using TFK-1 EV and BAP1-wt cell lines by performing subcutaneous (s. c.) injection in nude mice. Respective cells were prepared in Matrigel diluted 1:1 with PBS. Mice were s. c. injected with 100 µL cell solution (1 × 10^6 cells per injection) using a 22 G needle into the left flank of the mice. The subcutaneous tumor size was measured by a caliper and monitored with BLI imaging weekly (described in Chapter 3.10.2.2).

The tumor volume was determined by the following formula:

$$Tumor\ volume\ (mm^3) = \frac{length\ x\ width^2}{2}$$

3.11 Statistics

GraphPad Prism 9 software was used for statistical analysis applying two-tailed non-parametric Mann-Whitney test and ANOVA to determine statistical significance. If not stated otherwise, graphs show mean ± SEM. The following representations for *p*-values (level of significance) were used: $p<0.05$ (*), $p<0.01$ (**), $p<0.001$ (***) and $p<0.0001$ (****).

4. Results

4.1 Synthetic lethality screen

4.1.1 shRNA screen layout

A shRNA synthetic lethality screen was performed to identify genes that are essential in BAP1-deficient, but not in BAP1-expressing cell lines (Fig. 1). For the performed screen, the BAP1-depleted RCC cell line UMRC-6 was modified to either stably expressing an empty vector (EV) or wild-type *BAP1* (BAP1-wt) plasmid. Both cell lines were transduced using module 1 (targeting key signaling pathways related genes) of the Cellecta DECIPHER lentiviral shRNA library, which is a pooled barcoded shRNA library targeting over 11,000 human genes, with five or six shRNAs per gene.

After three days of transduction, a baseline sample of UMRC-6 EV and UMRC-6 BAP1-wt cell lines was collected. Afterwards, cells were selected with puromycin.

On day 12 after transduction, another round of samples was harvested and compared to the baseline samples by performing high-throughput (HT) sequencing. By using HT, genes essential in BAP1-deficient cancer cell lines were identified.

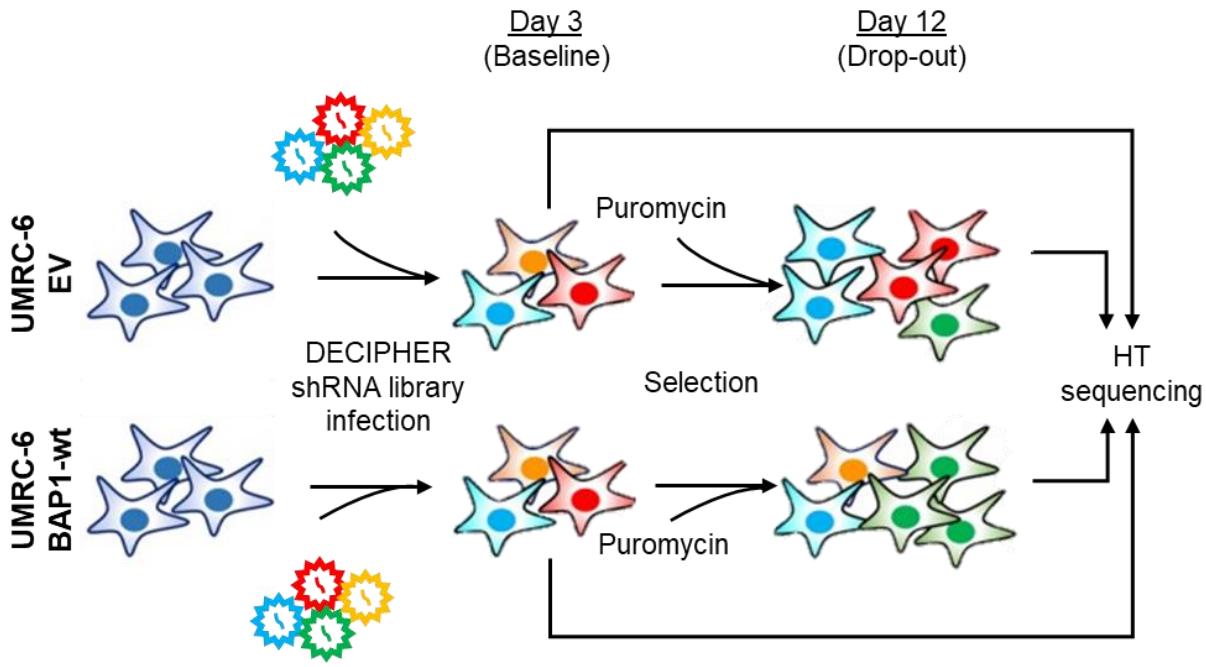

Figure 7: Scheme of the shRNA screen for identifying *BAP1*-specific vulnerabilities
UMRC-6 EV (BAP1-deficient) and UMRC-6 BAP1-wt (BAP1 expressed) cell lines were transduced in triplicates with a pooled DECIPHER shRNA library using lentiviral transfer. On day 3 after transduction, samples of both cell lines were harvested as baseline control. After selection of infected cells with puromycin, again samples of both cell lines were harvested on day 12 post-infection. Harvested samples were determined by high-throughput (HT) sequencing of vector barcodes. By detecting shRNAs that are depleted only in UMRC-6 EV cells and not in UMRC-6 BAP1-wt cells essential genes for *BAP1*-mutation were identified.

4.1.2 Identification of possible synthetic lethality genes

To identify genes causing synthetic lethality in BAP1-deficient cancer cells, data obtained from HT sequencing was analyzed using RIGER analysis as described in Chapter 3.8 (Fig. 8). Genes were scored based on their shRNA counts: Genes at the top of the ranking list have the lowest shRNA counts in the BAP1-deficient cells (UMRC-6 EV) while the genes at the bottom have the lowest shRNA counts in BAP1-expressing (UMRC-6 BAP1-wt) cells.

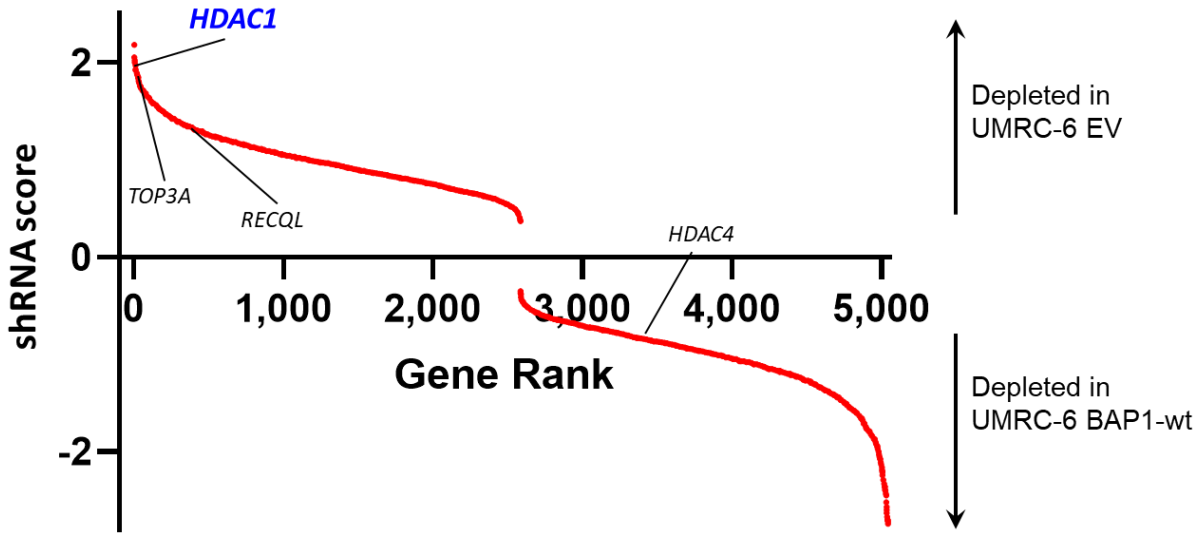

Figure 8: shRNA screen identifies novel synthetic lethal partners
Genes were ranked based on the power of the shRNAs to discriminate UMRC-6 EV cells and UMRC-6 BAP1-wt cells. Genes on top of the ranking list had lower shRNA counts in UMRC-6 EV cells and genes on the bottom had lower shRNA counts in UMRC-6 BAP1-wt cells. *HDAC1*, *TOP3A* and *RECQL* were identified as one of the best synthetic lethal hits based on the shRNA screen. In contrast, *HDAC4* is not showing enrichment in the shRNA screen.

With the shRNA screen we identified many genes which are essential in UMRC-6 EV cells but not in UMRC-6 BAP1-wt cells (Fig. 8). *RECQL* and *TOP3A (DNA Topoisomerase III Alpha*) were validated as UMRC-6 EV dependent genes and *HDAC4*, although it was published by *Kuznetsoff et al*. as a target for *BAP1*-mutant cancers, was not showing an enrichment in the performed shRNA screen.

In addition, *HDAC1* was ranked as one of the most prominent hits in the performed synthetic lethality screen.

As described in Chapter 1.4.2 HDACs are key players in cancer development and represent potential therapeutic targets for cancer therapy. Therefore, we picked *HDAC1* for further validation as a possible target for *BAP1*-mutant cancers.

4.2 Effect of *HDAC1* knockdown on BAP1-deficient cell lines

As *HDAC1* was identified in a synthetic lethality shRNA screen as a possible target for BAP1-deficient ccRCC cancer cells, we compared the effect of a *HDAC1* knockdown on BAP1-deficient cell lines: UMRC-6 (ccRCC) and TFK-1 (ICC), expressing either the EV, BAP1-wt or the BAP1 p.C91S mutant plasmids.

4.2.1 Generation of *HDAC1* knockdown in BAP1-deficient cell lines

For visualizing the success of the *HDAC1* knockdown in BAP1-loss cell lines (TFK-1 and UMRC-6) a western blot was performed (Fig. 9).

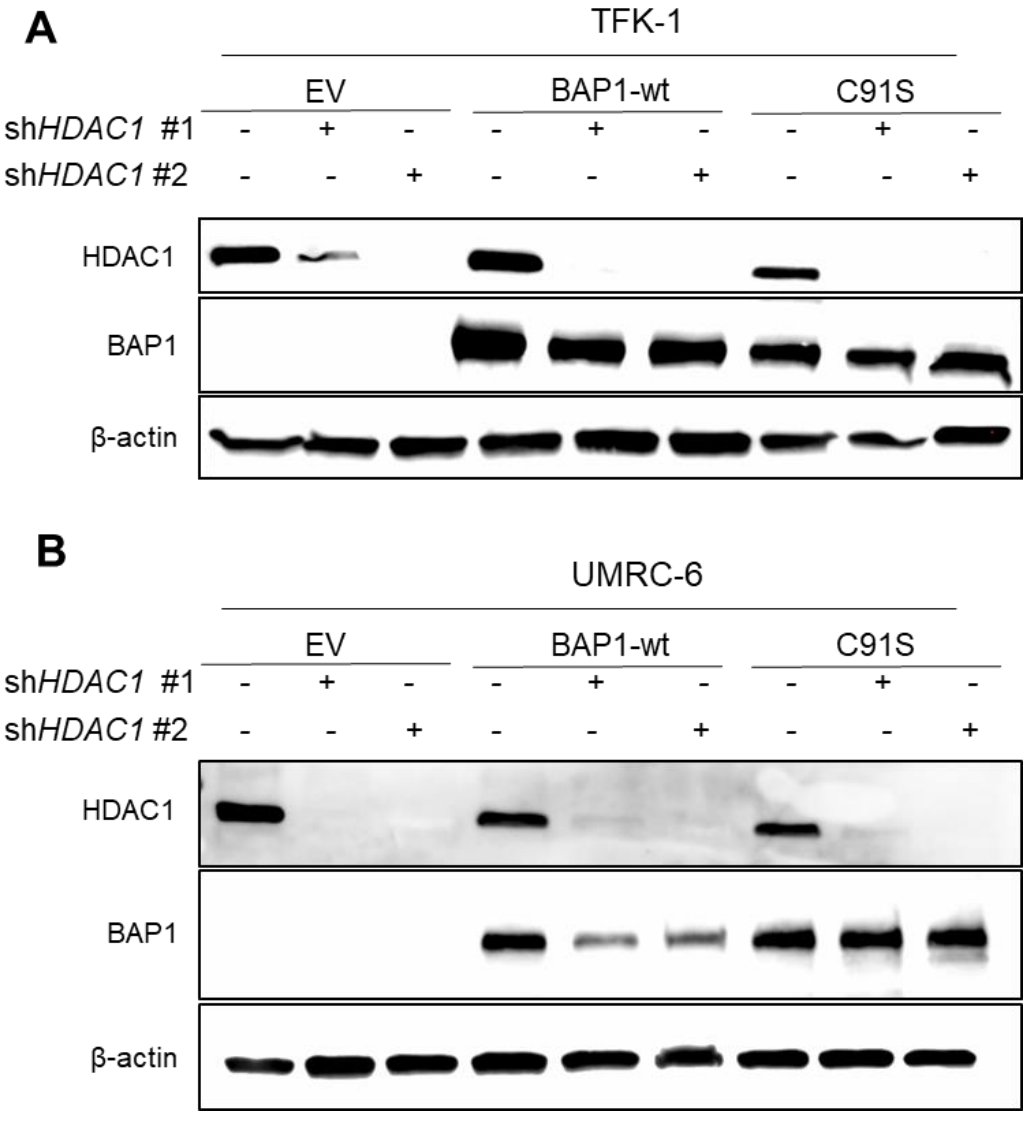

Figure 9: *HDAC1* knockdown in BAP1-deficient cell lines
Western Blot of A): TFK-1 (ICC) B): UMRC-6 (ccRCC) cell lines expressing the EV, BAP1-wt and BAP1 p.C91S (C91S) mutant plasmids. A stable shRNA knockdown of *HDAC1* in both cell lines with two different shRNAs (sh*HDAC1* #1 and sh*HDAC1* #2) was performed. β-actin was used as loading control. A): *N* = 3; B): *N* = 2.

A shRNA knockdown was performed in cell lines expressing wild-type *BAP1* (BAP1-wt) or with BAP1 loss (EV and C91S) (Fig. 3). The knockdown leads to a decrease of HDAC1 expression in both cell lines: TFK-1 and UMRC-6. Although, both shRNAs (sh*HDAC1* #1 and sh*HDAC1*#2) result in a successful knockdown of *HDAC1*, sh*HDAC1* #2 showed a more effective *HDAC1* knockdown, compared to sh*HDAC1* #1, which can be detected by western blot (Fig. 9).

4.2.2 Validation of *HDAC1* knockdown in BAP1-deficient cell lines

Next, a validation of the effect of *HDAC1* knockdown in BAP1-deficient cell lines was sought. Therefore, cell proliferation assays using the cell titer glow 2.0 method and colony formation assays were performed to compare effects of *HDAC1* knockdown on the cell survival and proliferation between BAP1-deficient cell lines expressing either EV, BAP1-wt or p.C91S plasmid (Fig. 10).

A *HDAC1* knockdown in TFK-1 and UMRC-6 cell lines led to a significant decrease of cell proliferation in EV and C91S expressed cell lines, but not in BAP1-wt expressed ones (Fig. 10A). This result was confirmed by analyzing the colony formation assay data (Fig. 10B and 10C). Although, the *HDAC1* knockdown showed no significant downregulation of colony formation in UMRC-6 EV and C91S cell lines a tendency of decreased number of colonies was visualized (Fig. 10B). In the TFK-1 EV and C91S cell lines sh*HDAC1* #2 showed a higher (significant) reduction of colony formation in comparison to sh*HDAC1* #1. These results can be explained by the stronger *HDAC1* knockdown with sh*HDAC1* #1 than sh*HDAC1* #2 in TFK-1 cell lines (see Fig. 9A).

However, *HDAC1* knockdown increased (especially sh*HDAC1* #2) the number of colonies in BAP1-wt expressed cell lines (Fig. 10B and Fig. 10C). Although, this effect was seen in both cell lines, it was stronger in TFK-1 BAP1-wt cells compared to UMRC-6 BAP1-wt cells.

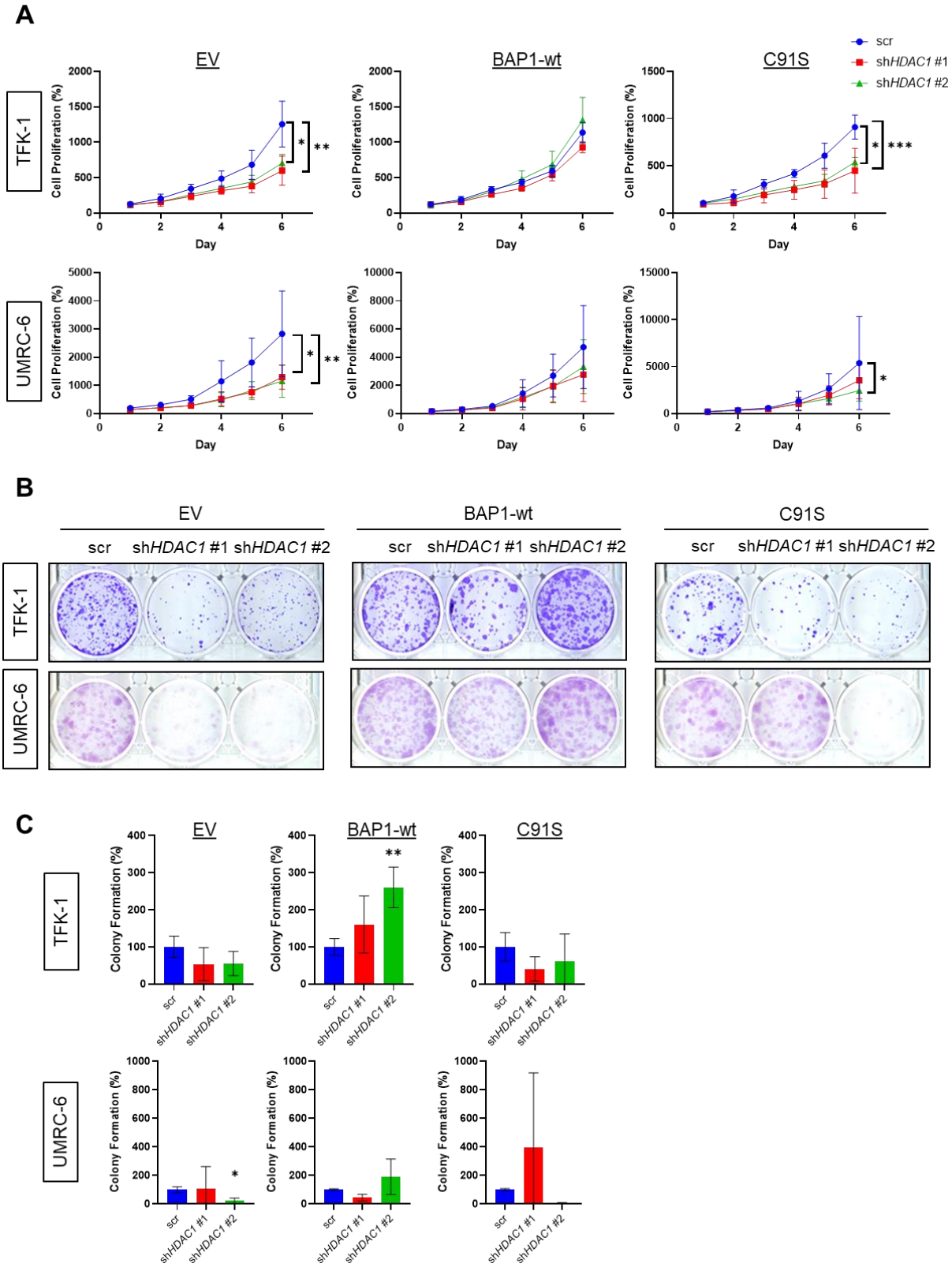
A
EV
BAP1-wt
C91S
scr
shHDAC1 #1
shHDAC1 #2
TFK-1
UMRC-6
Cell Proliferation (%)
Day
B
EV
BAP1-wt
C91S
scr
shHDAC1 #1
shHDAC1 #2
TFK-1
UMRC-6
C
EV
BAP1-wt
C91S
TFK-1
UMRC-6
Colony Formation (%)
scr
shHDAC1 #1
shHDAC1 #2

Figure 10: *HDAC1* knockdown decrease cell proliferation and colony formation of BAP1-deficient cell lines
A): Proliferation curves for TFK-1 and UMRC-6 cell lines expressing EV, BAP1-wt or BAP1 p.C91S mutant plasmid transduced with scrambled (Scr). control or two different shRNAs against *HDAC1*, normalized to data of day one. B-C): Representative colony formation assay (B) and its quantification (C) normalized to Scr of TFK-1 and UMRC-6 cells expressing the EV, BAP1-wt or p.C91S plasmid and transduced with Scr. control or sh*HDAC1* #1/#2. *N* = 3 for all experiments. Significance was assessed using nonparametric Kruskal-Wallis test. *p*-values: $p<0.05$ (*), $p<0.01$ (**) and $p<0.001$ (***).

4.3 Effect of *HDAC1* knockdown on BAP1-expressing cell lines

To validate *HDAC1* as a potential target in *BAP1*-mutant tumors and to demonstrate that *HDAC1* knockdown is only lethal in BAP1-deficient cancer cells, colony formations and cell survival assays were performed with two ccRCC cell lines (Caki-1 and RCC4) expressing endogenous wild-type *BAP1.*

4.3.1 Generation of *HDAC1* knockdown in BAP1-expressing cell lines

To visualize the knockdown of *HDAC1* in intrinsically BAP1-expressing cell lines a western blot was performed of Caki-1 and RCC4 cells (Fig. 11).

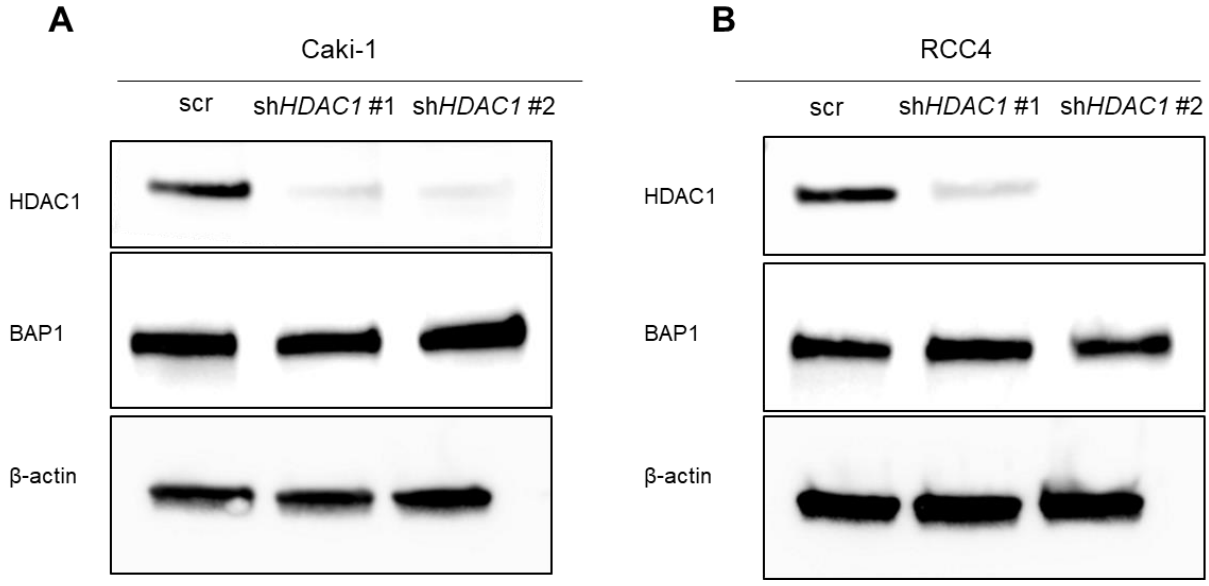

Figure 11: *HDAC1* knockdown in intrinsically BAP1-expressing cell lines
Western Blot of A): Caki-1 and B): RCC4 ccRCC cell lines. A stable shRNA knockdown of *HDAC1* in both cell lines with two different shRNAs (sh*HDAC1* #1 and sh*HDAC1* #2) was performed. β-actin was used as a control. *N* = 3 for all experiments.

The western blot in Figure 11 displays the protein expression of HDAC1, BAP1 and β-actin in Caki-1 and RCC4 *HDAC1* knockdown cell lines. For both cell lines a successful

knockdown of *HDAC1* can be *detected* using *both* shRNAs (sh*HDAC1* #1 and sh*HDAC1* #2). The second shRNA against *HDAC1* (sh*HDAC1* #2) is more efficient in preventing HDAC1 expression in both ccRCC cell lines compared to sh*HDAC1* #1 (Fig. 10B).

4.3.2 Validation of *HDAC1* knockdown in BAP1-expressing cell lines

The effect of *HDAC1* knockdown on Caki-1 and RCC4 cell lines was validated by performing proliferation and colony formation assays. Assumed, if *HDAC1* is a possible synthetic lethal interactor of *BAP1*-mutated tumors, a *HDAC1* knockdown should not have a strong effect on the proliferation and colony formation of BAP1-expressing cell lines compared to BAP1-deficient ones (Fig. 12).

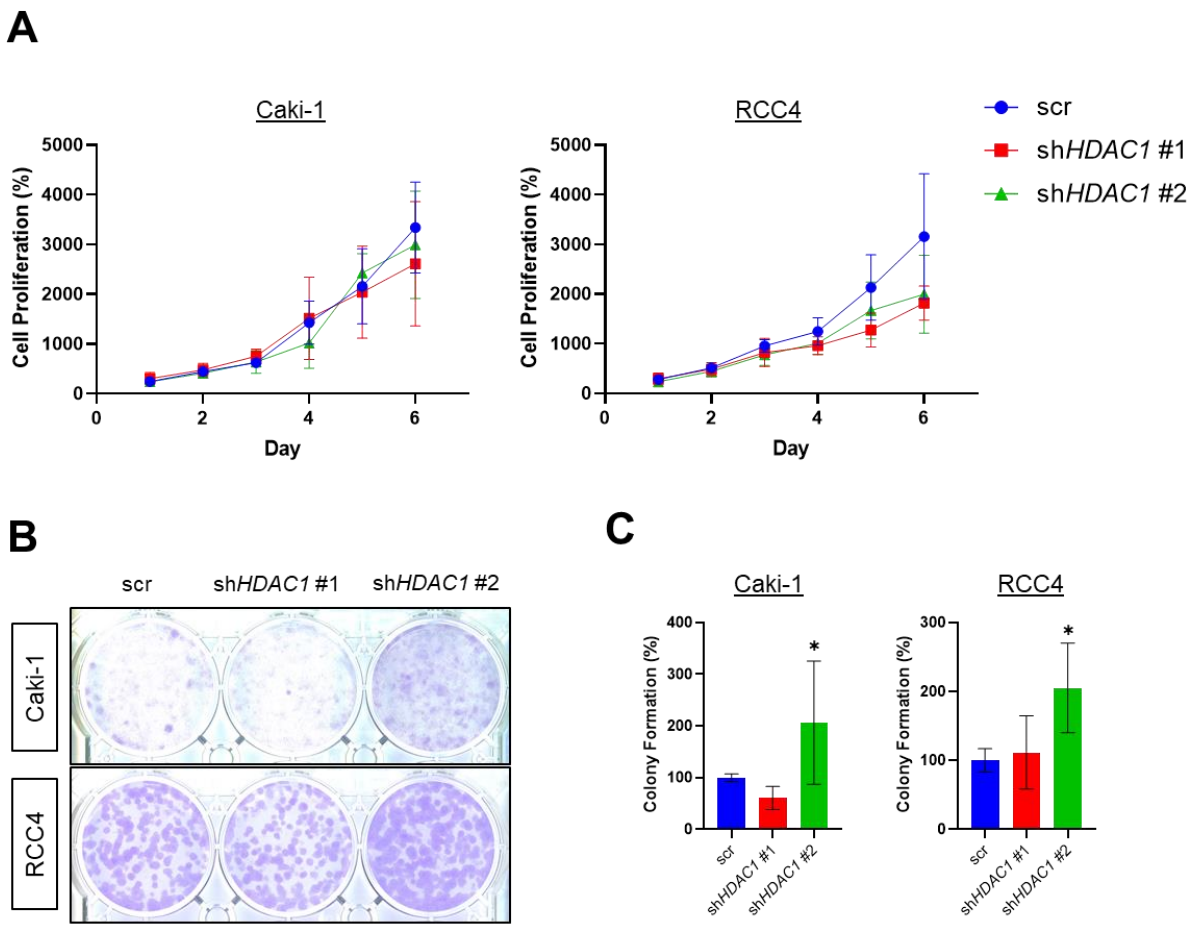

Figure 12: *HDAC1* knockdown has no effect on the proliferation of BAP1-expressing cell lines
A): Proliferation curves for Caki-1 and RCC4 (ccRCC) cell lines transduced with Scr control or two different shRNAs against *HDAC1* (sh*HDAC1* #1/ #2), normalized to data of day one. B-C): Representative colony formation assay (B) and its quantification (C) normalized to the control cell line (Scr) of Caki-1 and RCC4 cells cell lines. *N* = 3 for all experiments. Significance was assessed using nonparametric Kruskal-Wallis test. *p*-values: $p<0.05$ (*).

Although, the *HDAC1* knockdown decreased slightly the cell viability of RCC4 cells, no significant difference between the proliferation rate of control (Scr) and *HDAC1* knockdown (sh*HDAC1 #1* and sh*HDAC1 #2)* cell lines in both intrinsically BAP1-expressing cells were detected (Fig. 12A).

These findings were confirmed with the colony formation results of the Caki-1 and RCC4 cell lines (Fig. 12B). As already for the proliferation, *HDAC1* knockdown using sh*HDAC1* #1 showed no significant effect on the colony formation number of both BAP1-expressing cell lines. Moreover, sh*HDAC1* #2 cell lines exhibited a significant increase of colony formation in Caki-1 and RCC4 cells (Fig. 12B).

4.4 Comparison of the effect of *HDAC1* and *HDAC4* knockdown on BAP1-expressing and *BAP1* knockout cell lines

BAP1 knockout 786-O (RCC) and 92-1 (UM) cell lines were used to uncover whether HDAC1 is a stronger candidate than HDAC4 to target *BAP1*-mutated cancers since HDAC4 was previously suggested to be an important target of *BAP1*-mutated UM tumors (Kuznetsov *et al.,*2019).

4.4.1 Generation and characterization of *HDAC1* and *HDAC4* knockdown in renal cancer *BAP1* knockout cells

4.4.1.1 Establishment of *HDAC1* and *HDAC4* knockdown in *BAP1* knockout RCC cells

The success of the *HDAC1* and *HDAC4* knockdown in 786-O Cas9 (BAP1-expressing) and 786-O sg*BAP1* (*BAP1* knockout) cell lines was visualized with western blot (Fig. 13).

The representative western blot in Figure 13 show the difference in the expression of BAP1 between control (786-O transfected with Cas9 only) and *BAP1* knockout cells (786-O cells transfected with BAP1 guide RNA). In addition, a decrease in the protein levels of HDAC1 and HDAC4 was observed after the transduction of 786-O cell lines with shRNA #2 but not shRNA #1 against their corresponding targets *HDAC1* and *HDAC4.*

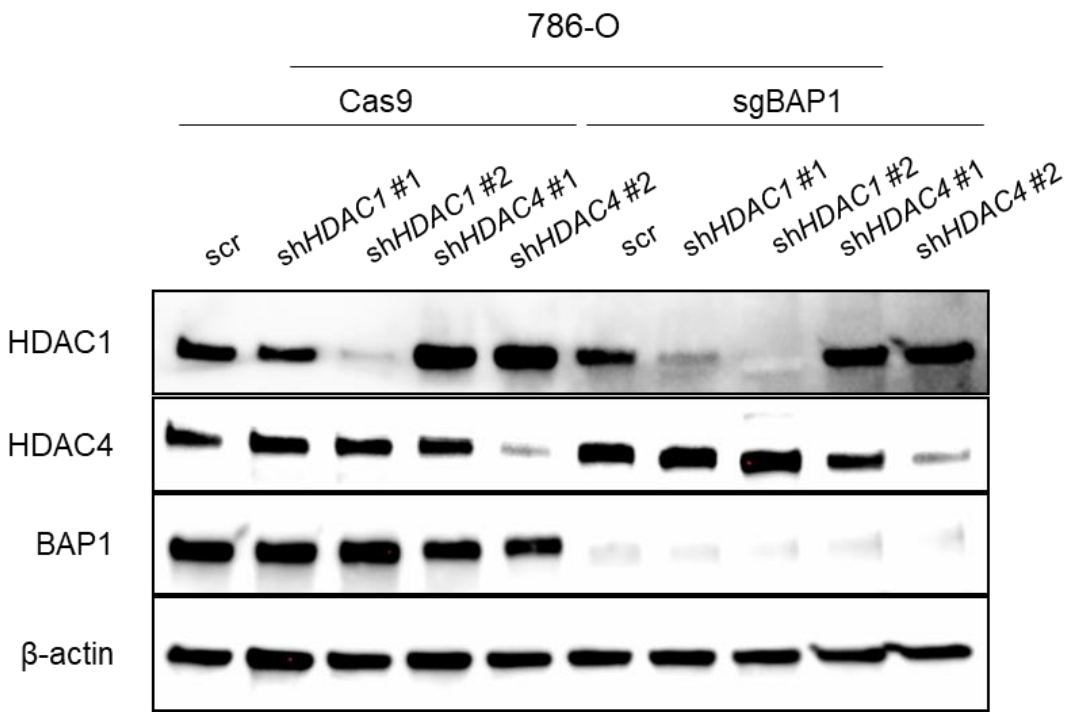

Figure 13: Generation of *HDAC1* and *HDAC4* knockdown in a renal cell carcinoma cell line
Western Blot of 786-O cell lines expressing BAP1 (Cas9) or containing a *BAP1* knockout (sg*BAP1*) transduced with a stable shRNAs against *HDAC1* (sh*HDAC1* #1 and sh*HDAC1* #2) or *HDAC4* (sh*HDAC4* #1 and sh*HDAC4* #2). β-actin was used as a control. *N* = 3.

4.4.1.2 Characterization of the effects of a *HDAC1* knockdown on *BAP1* knockout RCC cells

To analyze the effects of a *HDAC1* knockdown on BAP1-expressing and *BAP1* knockout 786-O cell lines, proliferation and colony formation assays were performed.

The proliferation assay firm up that *HDAC1* knockdown led to a significant decrease in proliferation in *BAP1* knockout (sg*BAP1*) 786-O cells but showed no effect in BAP1-expressing (Cas9) 786-O cells (Fig. 14A). Furthermore, HDAC1-expressing 786-O sg*BAP1* cells exhibit a 4x higher cell viability in comparison to HDAC1 knockdown cells on the 7th day of the CellTiter-Glo assay.

Additionally, the colony formation assay confirmed the strong effect of a *HDAC1* knockdown on *BAP1* knockout cells (Fig. 14B and 14D). Representative colony formations pictures of 786-O cell lines demonstrated that less colonies formed in *BAP1* knockout (sg*BAP1*) cells compared to BAP1-expressing (Cas9) cells after *HDAC1* knockdown (Fig. 14B and 14D). Nevertheless, *HDAC1* knockdown led to a significant reduction in the number of the colonies formed by both *BAP1* knockout and BAP1-expressing 786-O cell lines in comparison to HDAC1-expressing (Scr) 786-O cell lines (Fig. 14C). However, the comparison of the colony formation rate of the

786-O Cas9 and the 786-O sg*BAP1* cell lines showed a significant decrease in colony formation in 786-O sg*BAP1* sh*HDAC1* #2 cells compared to 786-O Cas9 sh*HDAC1* #2 cells (Fig. 14D).

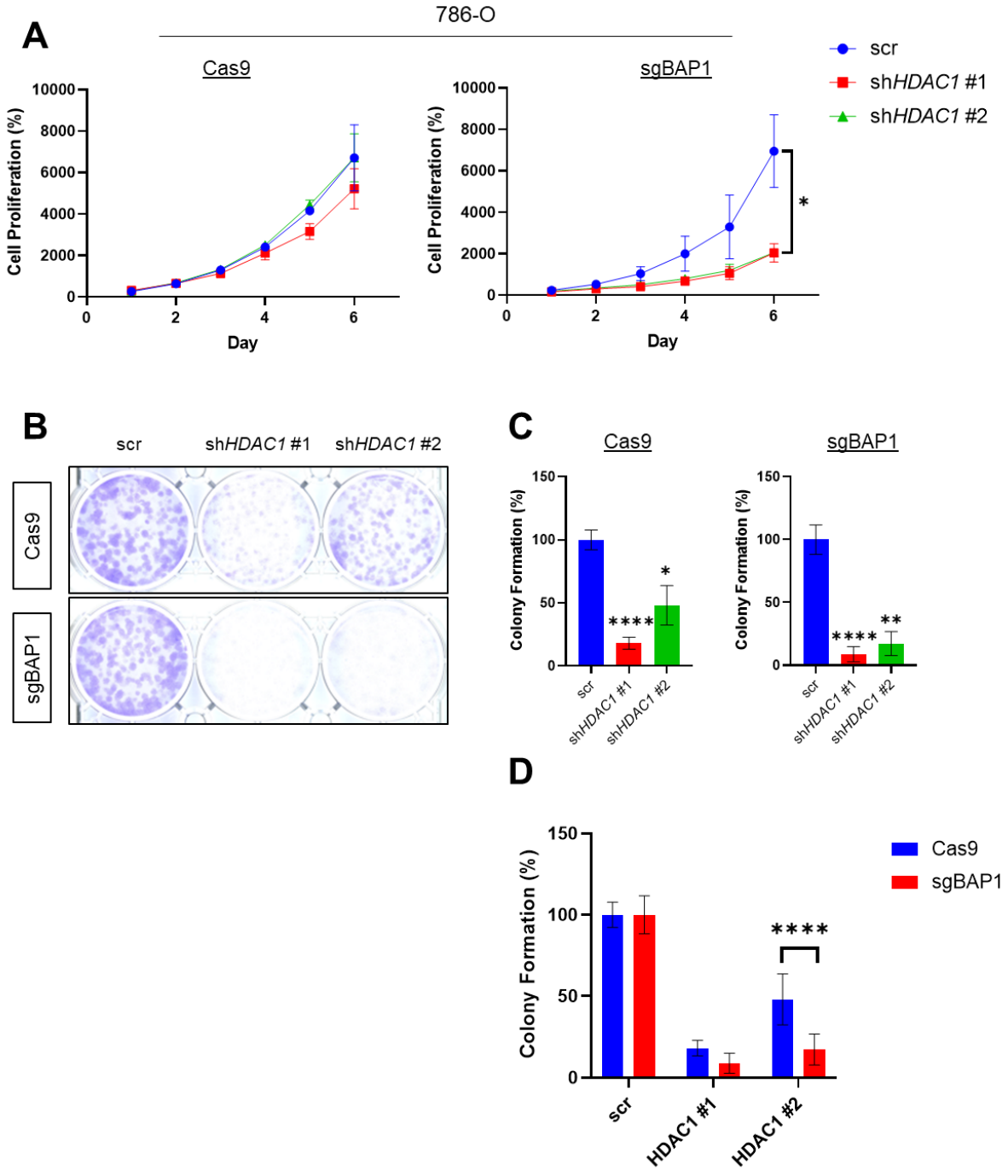

Figure 14: Knockdown of *HDAC1* results in decreased proliferation and colony formation in *BAP1*-knockout cells.
786-O (renal cell carcinoma) cells expressing BAP1 (Cas9) or containing a *BAP1* knockout (sg*BAP1*) transduced with Scr control or two different shRNAs against *HDAC1*. A): Proliferation curves for 786-O cell lines normalized to data of day one. B): Representative colony formation assay (C-D) and its quantification normalized to Scr of 786-O Cas9 or sgBAP1 cells. *N* = 3 for all experiments. Significance was assessed using A-C) nonparametric Kruskal-Wallis test and D) two-way ANOVA test. *p*-values: $p<0.05$ (*), $p<0.01$ (**) and $p<0.001$ (***).

4.4.1.3 Characterization of the effects of a *HDAC4* knockdown on *BAP1* knockout RCC cells

For the comparison of the effect of *HDAC1* and *HDAC4* knockdown on 786-O cell lines we performed proliferation and colony formation for *HDAC4* knockdown 786-O cell lines too.

In contrast to *HDAC1* (Fig. 14), *HDAC4* knockdown had no significant effect on the proliferation or the colony formation of both BAP1-expressing and *BAP1* knockout 786-O cell lines (Fig. 15A and 15D).

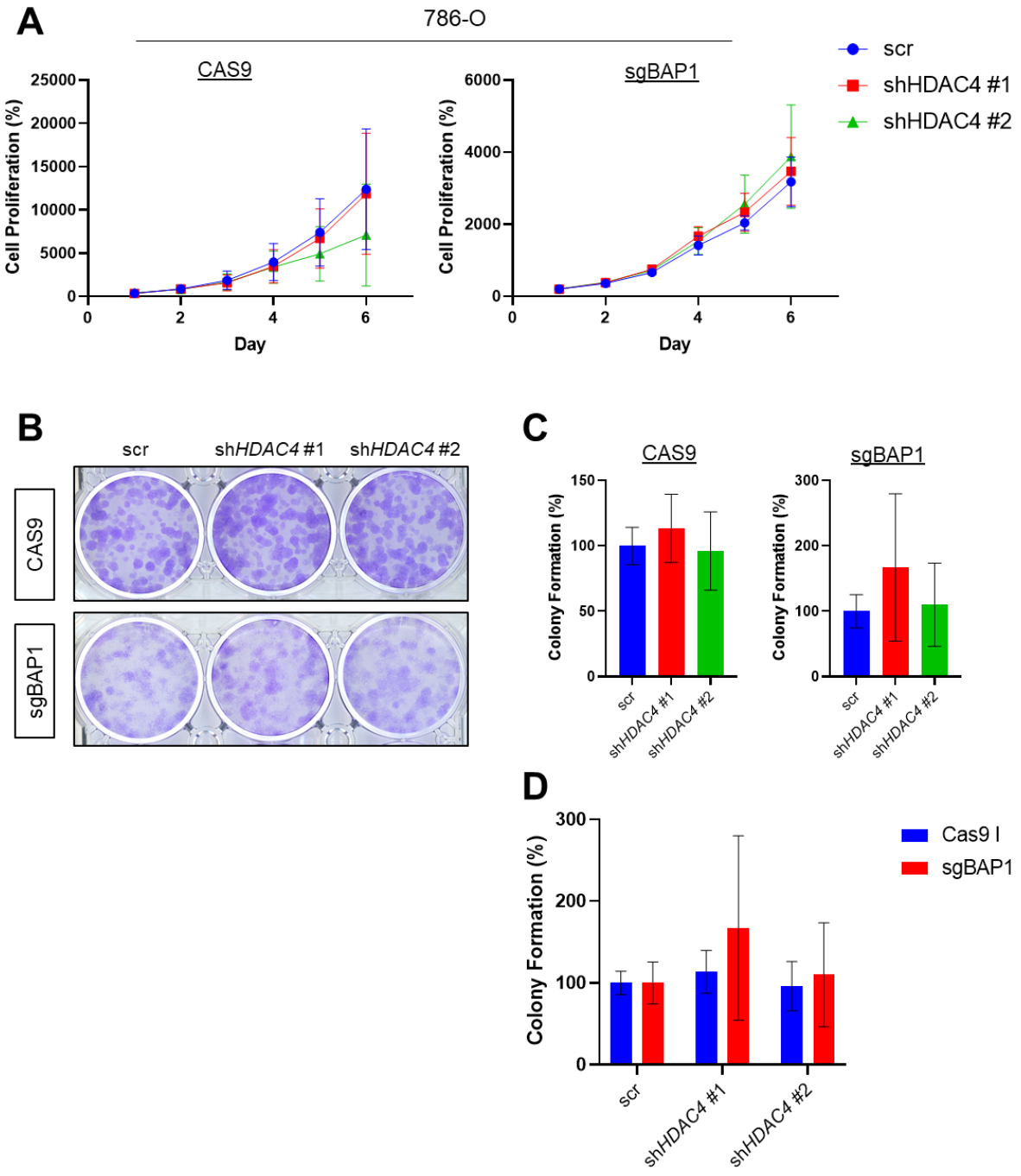

Figure 15: *HDAC4* knockdown shows no effect on *BAP1* knockout cells
786-O (renal cell carcinoma) cells expressing BAP1 (Cas9) or containing a *BAP1* knockout (sg*BAP1*) transduced with Scr control or two different shRNAs against *HDAC4*. A): Proliferation curves for 786-O cell lines normalized to data of day one. B): Representative colony formation assay (C-D) and its quantification normalized to Scr of 786-O Cas9 or sgBAP1 cells. *N* = 3 for all experiments. Significance was assessed using A-C) nonparametric Kruskal-Wallis test and D) two-way ANOVA test.

4.4.2 Generation and characterization of *HDAC1* and *HDAC4* knockdown in uveal melanoma *BAP1* knockout cells

4.4.2.1 Establishment of *HDAC1* and *HDAC4* knockdown in 92-1 *BAP1* knockout cells

To compare the effect of *HDAC1* and *HDAC4* knockdown on UM 92-1 cell lines, expressing BAP1 (WT) or containing a *BAP1* knockout (sg*BAP1* #1 and sg*BAP1* #2), the UM cell lines were transduced with shRNAs against *HDAC1* (sh*HDAC1* #1 or sh*HDAC1* #2) or against *HDAC4* (sh*HDAC4* #1 or sh*HDAC1* #2).

The success of these knockdowns was visualized by performing western blotting (Fig. 16).

Figure 16 demonstrates the reduction in the protein expression of HDAC1 and HDAC4 after transduction with shRNAs against the mentioned targets in 92-1 cell lines. As already showed before for the other cell line models (Fig. 9, Fig. 11 and Fig.13), the second shRNA against *HDAC1* (sh*HDAC1* #2) led to a stronger decrease of HDAC1 protein expression than the first one (sh*HDAC1* #1) in 92-1 cell lines (Fig. 16A). However, the sh*HDAC4* #1 shRNA guided to a lower HDAC4 protein expression than sh*HDAC4* #2 in the 92-1 cell line (Fig. 16B).

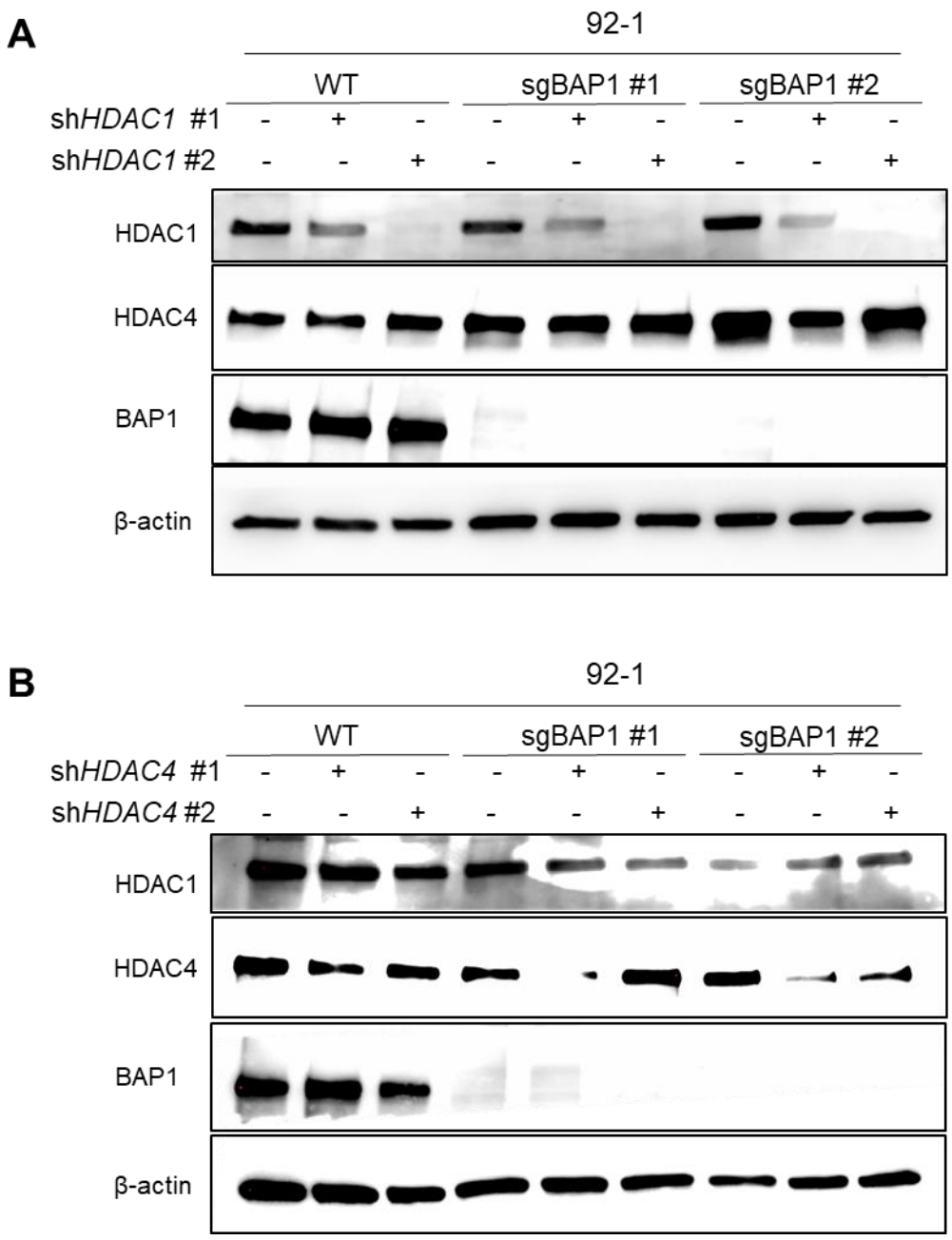

Figure 16: Generation of a *HDAC1* and a *HDAC4* knockdowns in UM 92-1 cell lines
Western Blot of three different 92-1 (UM) cell lines: 1. expressing BAP1 (WT) or 2-3. containing a *BAP1* knockout (sg*BAP1* #1 and sg*BAP1* #2) transduced with a stable shRNAs against *HDAC1* (sh*HDAC1* #1 and sh*HDAC1* #2) or *HDAC4* (sh*HDAC4* #1 and sh*HDAC4* #2). β-actin was used as a control. *N* = 3.

4.4.2.2 Comparison of the effect of *HDAC1* and *HDAC4* knockdown on 92-1 cell lines with *BAP1* knockout

To solidify HDAC1 as a more effective target than HDAC4 for *BAP1*-mutant tumor entities, the effect of *HDAC1* and *HDAC4* knockdown on the 92-1 UM cell lines was compared by performing proliferation and colony formation assays (Fig. 17).

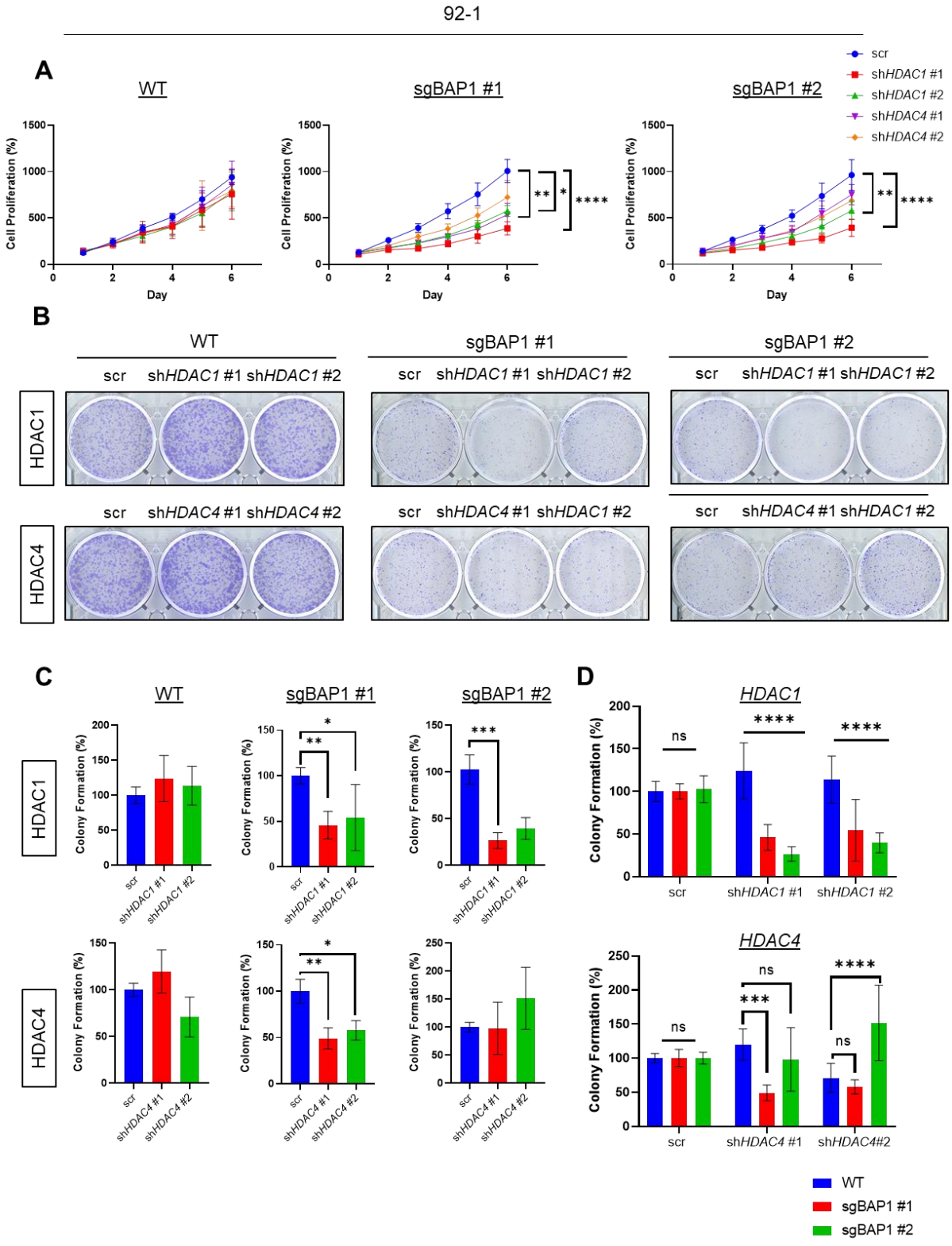

Figure 17: *HDAC1* knockdown has a stronger effect on UM *BAP1* knockout cells than a *HDAC4* knockdown

92-1 (UM) cells expressing BAP1 (WT) or containing a *BAP1*-knockout (sg*BAP1* #1 and sg*BAP1* #2) transduced with a control plasmid (Scr) or two different shRNAs against *HDAC1 (shHDAC1 #1 or shHDAC1 #2) or HDAC4 (shHDAC4 #1 or shHDAC4 #2).* A): Proliferation curves for 92-1 cell lines normalized to data of day one. B): Representative colony formation assay (C-D) and its quantification normalized to Scr of 92-1 Cas9 or sgBAP1 cells. *N* = 3 for all experiments. Significance was assessed using A-C) nonparametric Kruskal-Wallis test and D) two-way ANOVA test. *p*-values: $p<0.05$ (*), $p<0.01$ (**), $p<0.001$ (***) and $p<0.0001$ (****).

Knockdown of *HDAC1* and *HDAC4* did not affect the proliferation ability of 92-1 WT cells (Fig. 17A). In contrast, knockdown of *HDAC1* and *HDAC4* significantly decreased the cell viability of 92-1 *BAP1* knockout cell lines. After a *HDAC1* knockdown a significantly lower proliferation rate was seen in both 92-1 *BAP1* knockout cell lines (sg*BAP1* #1 and sg*BAP1* #2), however for HDAC4 only one of the shRNAs (sh*HDAC4* #1) demonstrated a decrease in the proliferation ability in the same cell lines. Further, only a knockdown of *HDAC1* and not of *HDAC4* was associated with a decrease in proliferation in the second *BAP1* knockout cell line (sg*BAP1* #2) (Fig. 17.A).

Results from the colony formation assays underline that *HDAC1* as well as *HDAC4* knockdown did not have any effect on the growth rate of the 92-1 WT cell line (Fig. 17B and 17C). Nevertheless, in both 92-1 *BAP1* knockout (sg*BAP1* #1 and sg*BAP1* #2) cell lines, the knockdown of *HDAC1* led to a significant decrease in colony formation (Fig. 17C and 17D). In contrast, *HDAC4* knockdown had only a significantly effect on the colony growth rate in one of the 92-1 *BAP1* knockout (sgBAP1 #1) cell lines (Fig. 17C and 17D).

4.5 Efficiency of HDAC1 inhibition in RCC cell lines

Since *HDAC1* knockdown effectively prevented cell growth and proliferation in *BAP1*-deficient cells, the pan-HDAC inhibitor quisinostat was used to validate HDAC1 as a target in clinical settings.

As quisinostat has the highest selectivity and potency for HDAC1 compared to other HDACs (Venugopal et al. 2013; Lo Cascio et al. 2021), quisinostat was used to compare the effect of HDAC1 inhibition on the cell viability of BAP1-expressing and

BAP1-deficient renal cancer cell lines (Fig. 18).

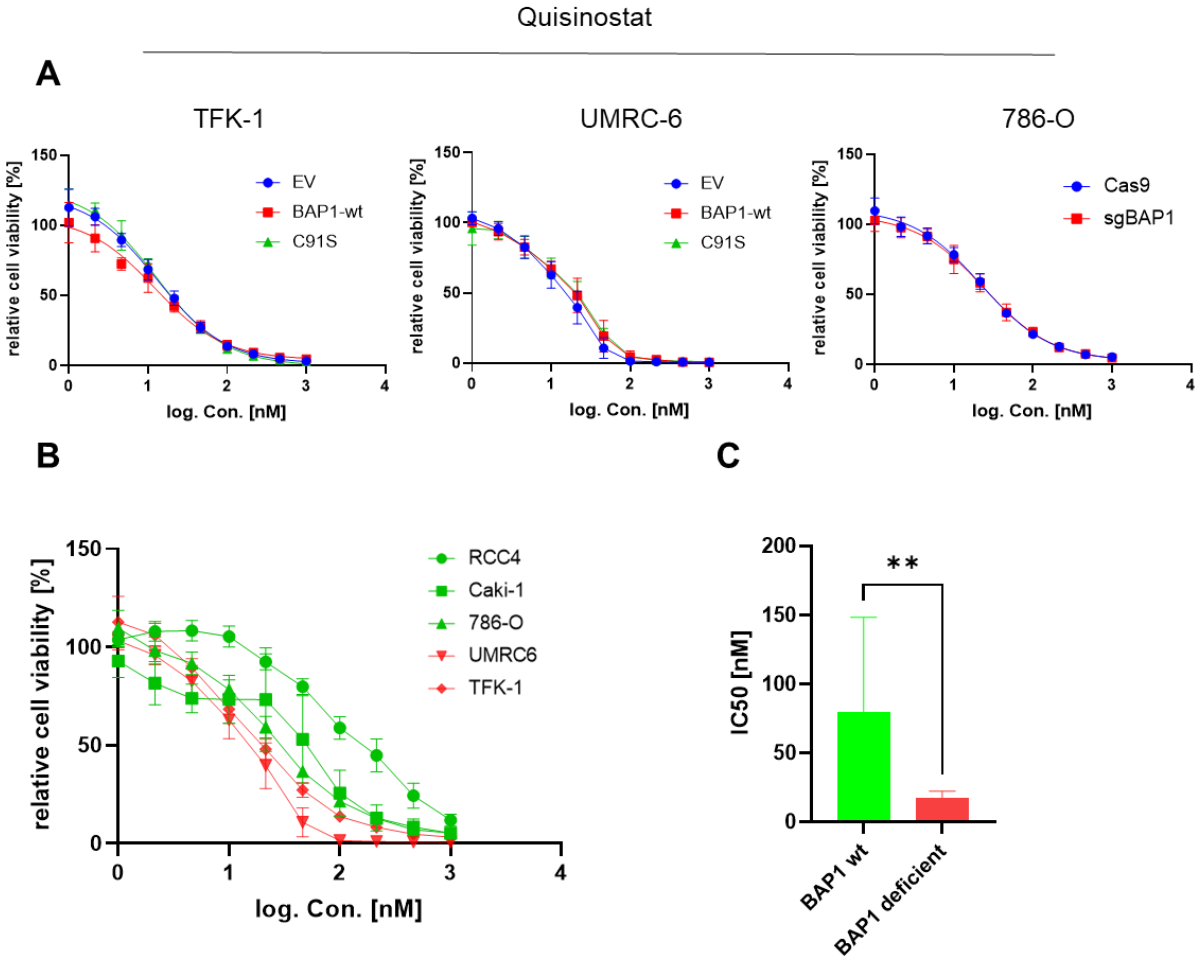

Figure 18: HDAC1 inhibition decreased cell viability of BAP1-loss cell lines
Dose-response curves of renal carcinoma cell lines treated with quisinostat (from 1nM to 1µM) for three days. A) Dose-response curves of A) TFK-1 and UMRC-6 cell lines expressing EV, BAP1-wt or BAP1 p.C91S mutant plasmid and 798-O *BAP1* knockout (sg*BAP1*) and Cas9 control cell line. Comparison of B) dose-response curves and C) IC50 of BAP1-expressing (green symbols) and BAP1-deficient (red symbols) cell lines. Cell viability is present as normalized values in percentage to DMSO controls. *N* = 3 for all experiments. Significance was assessed using nonparametric Mann-Whitney test. *p*-value: $p<0.01$ (**).

No difference in cell viability was observed between the EV, BAP1-wt and p.C91S transduced cell lines (both TFK-1 and UMRC-6) when the cells were treated with quisinostat (Fig. 18A). Similarly, HDAC1 inhibition with quisinostat did not show any difference in cell viability between BAP1-expressing (Cas9) and *BAP1* knockout (sg*BAP1*) 786-O cell lines.

Conversely, intrinsically parental BAP1 competent cell lines, RCC4, Caki-1 and 786-O cells, were less sensitive to HDAC1 inhibition with quisinostat compared to BAP1-deficient cell lines, UMRC-6 and TFK-1 (Fig. 18A).

The IC50 values for BAP1-deficient cell lines were, in total, significantly lower compared to BAP1-expressing cell lines (Fig. 18C). In total, IC50 values for BAP1-expressing cell lines were six times higher than the IC50 values of BAP1-deficient cell lines, indicating the higher sensitivity for quisinostat in BAP1-deficient cells.

4.6 Association between HDAC1 inhibition and cell migration/ invasion in *BAP1* knockout cells

In order to further validate *HDAC1* as synthetic lethal partner of *BAP1*-mutated tumors, an established trans-well model was used to assess the effects of *HDAC1* knockdown on the migratory and invasive capacity of 786-O BAP1-expressing and 786-O *BAP1* knockout cells *in vitro* (Fig. 19).

HDAC1 knockdown resulted in a suppression of cell migration of *BAP1* knockout cells comparing to BAP1-expressing 786-O cells (Fig. 19 B). However, the number of migrated and invasive cells between HDAC1 competent and knockout cells was not statistically significant, although the migrated and invasive cell numbers were lower in *BAP1* knockout 786-O cells compared to BAP1-expressing 786-O cells (Fig. 19B and 19C).

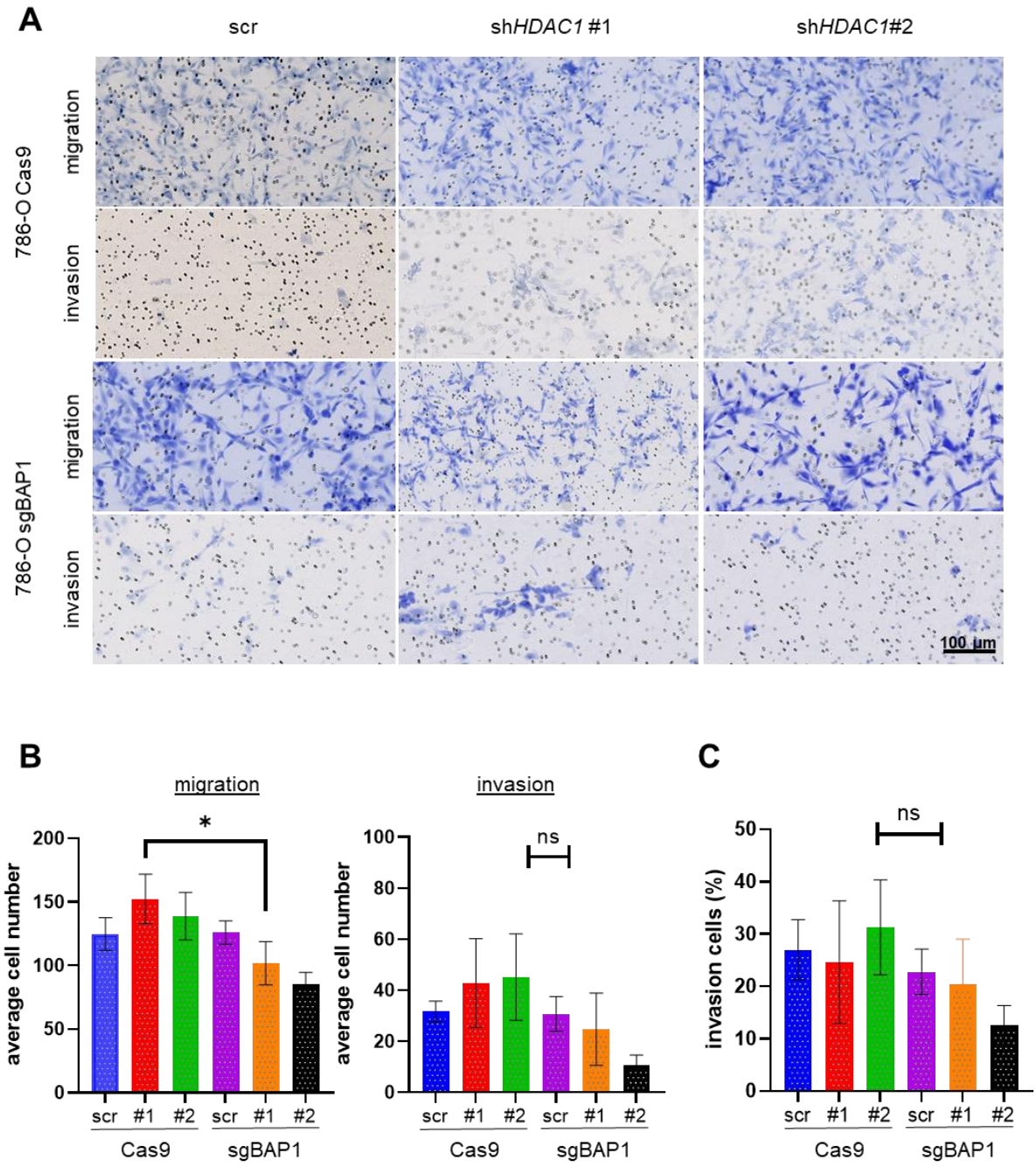

Figure 19: Suppression of HDAC1 decreased cell migration in 786-O cells with *BAP1* knockout
The effect of a *HDAC1* knockdown (#1 and #2) on migration and invasion of 786-O cell lines expressing BAP1 (Cas9) or containing a *BAP1* knockout (sg*BAP1*) were calculated by performing trans-well migration/ invasion assay. A) Representative migration and invasion pictures. Scale bar: 100 µm. B) Average cell number of migrated and invaded cells counted of five independent pictures of two membranes for each experiment C) Relative invasion was calculated by dividing the mean number of invading by the mean number of migrating cells. *N* = 3 for all experiments. Significance was assessed using nonparametric Kruskal-Wallis test. *p*-value: $p<0.05$ (*).

4.7 *HDAC1* knockdown leads to a G1-Arrest in *BAP1* knockout cells

As previously showed, *HDAC1* knockdown led to decrease in proliferation and growth rates of BAP1-deficient cells (see Chapter 4.2.4.4). Therefore, cell cycle analysis was performed to evaluate whether a cell cycle arrest is the reason (or not) of the decrease in proliferation and growth (Fig. 20).

For the cell cycle arrest assay BAP1-deficient TFK-1 and UMRC-6 cell lines expressing one of the three plasmids: EV (control), BAP1-wt or p.C91S (*BAP1* inactive mutant) were used. *HDAC1* knockdown did not caused any difference or change in the distribution of cells through the different cell cycle phases (G0/G1, S-Phase and G2/M) (Fig. 20A) in both TFK-1 and UMRC-6 cell lines.
In contrast, the difference in the distribution of cells through distinct cell cycle phases was observed between BAP1-expressing (Cas9) and *BAP1* knockout (sgBAP1) 786-O cells (Fig. 20B and 20C).
HDAC1 knockdown increased the numbers of the cells arrested in G0/G1 phase and significantly reduced the numbers of cells arrested in S-Phase in *BAP1* knockout 786-O cells compared to BAP1-expressing 786-O cell lines.
Overall, these results suggest that *HDAC1* knockdown leads to a reversible arrest in the G1 phase of the cell cycle in *BAP1* knockout cells, but has no effect on the cell cycle distribution of the three plasmids model cell lines.

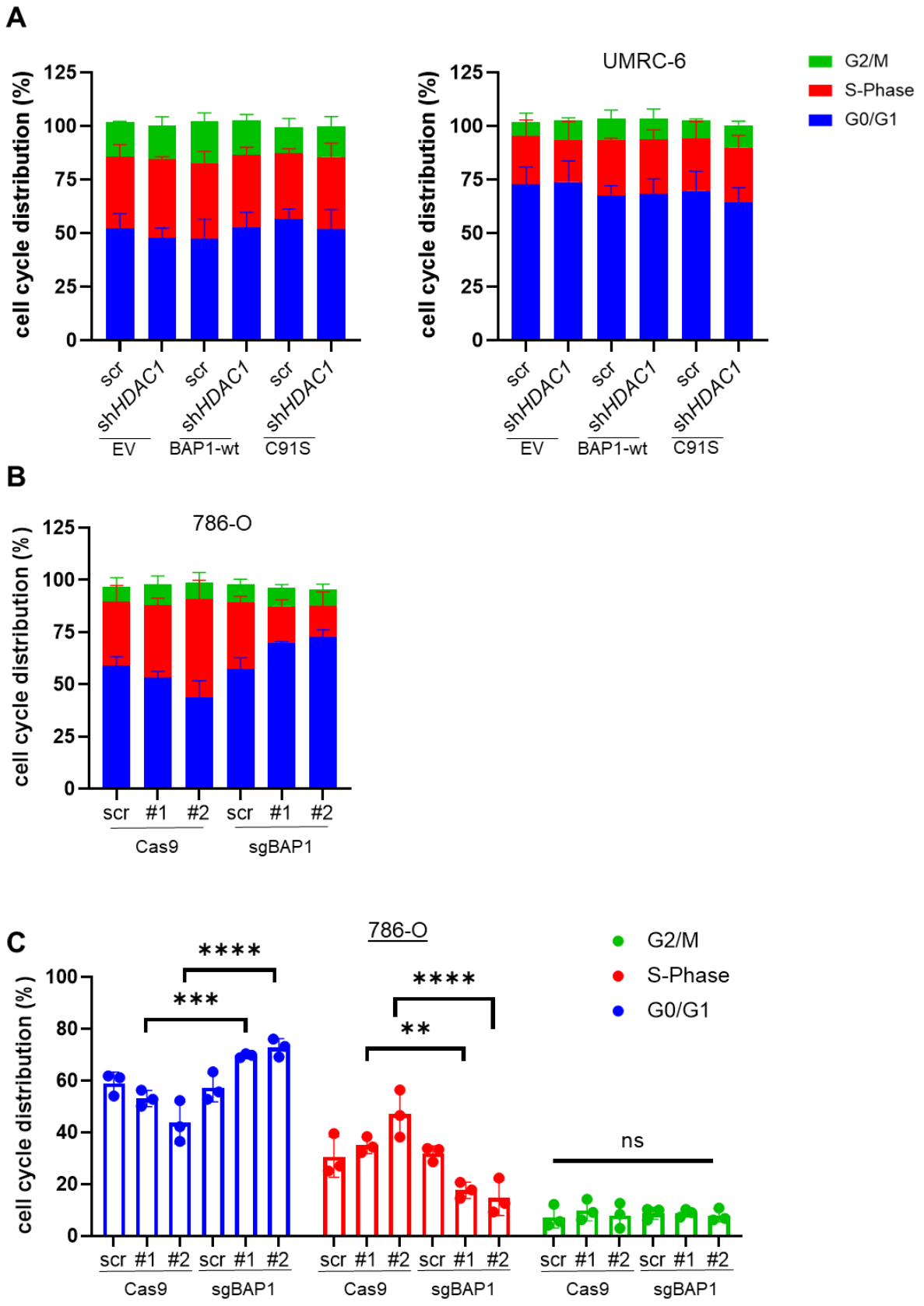
A
cell cycle distribution (%)
125
100
75
50
25
0
scr
shHDAC1
EV
BAP1-wt
C91S
UMRC-6
G2/M
S-Phase
G0/G1
B
786-O
scr #1 #2 scr #1 #2
Cas9
sgBAP1
C
786-O
****
***
****
**
ns
scr #1 #2 scr #1 #2
Cas9
sgBAP1

Figure 20: Influence of *HDAC1* knockdown on cell cycle distribution in BAP1-deficient cell lines
For cell cycle distribution analyses, PI-staining was performed and fixed cells were measured via flow cytometry. The effect of *HDAC1* knockdown (sh*HDAC1* #1 and sh*HDAC1* #2) on the cell cycle distribution of A) TFK-1 and UMRC-6 cell lines expressing EV (control), BAP1 wt or p.C91S (BAP1 mutant) as well as on B-C) 786-O cells expressing BAP1 (Cas9) or containing a *BAP1* knockout (sg*BAP1*) was analyzed. *N* = 3 for all experiments. Significance was assessed using nonparametric Kruskal-Wallis test. *p*-values: $p<0.01$ (**), $p<0.001$ (***) and $p<0.0001$ (****).

4.8 Influence of *HDAC1* knockdown on apoptosis

To see whether the G0/G1 arrest upon *HDAC1* knockdown in *BAP1* knockout 786-O cells was caused by the induction of apoptosis, 786-O cell lines with annexin V (AV) and PI to determine the number of cells in early (AV positive and PI positive) and late (AV negative and PI positive) apoptosis (Fig. 21). Additionally, the same staining was conducted with *HDAC4* knockdown 786-O cell lines to compare the efficiency of HDAC1 with HDAC4 as targets for *BAP1*-mutated cancers.

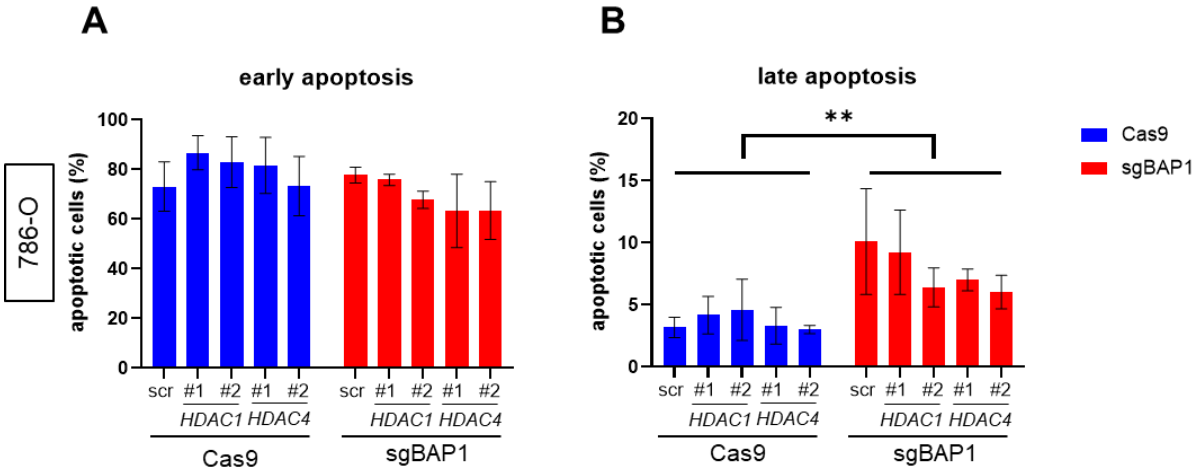

Figure 21: Influence of *HDAC1* knockdown on apoptosis in 786-O cell lines
For the apoptosis *assay*, cells were stained with PI and annexin V (AV), fixated and measured via flow cytometry. 786-O cells expressing BAP1 (Cas9, blue) or containing a *BAP1*-knockout (sg*BAP1*, red) were transduced with sh*HDAC1* (#1 and #2) or with sh*HDAC4* (#1 and #2) and the apoptosis of the cells was determined. A) Early apoptosis (PI positive and AV positive) B) Late apoptosis (PI positive and AV negative). *N* = 3 for all experiments. Significance was assessed using nonparametric Mann-Whitney test. *p*-value: $p<0.01$ (**).

Figure 21 is representing the percentage of 786-O cells located in early and late apoptotic stages. First, no shift of cell numbers in the early apoptosis stage after a *HDAC1* or *HDAC4* knockdown in 786-O cell lines was determined (Fig. 21A). However, a tendency of cell reduction in the late apoptosis stage after HDAC1 and HDAC4 suppression in 786-O *BAP1* knockout (sg*BAP1*) cells was detected (Fig. 21B). Furthermore, a significant increase of cell in the late apoptosis stage in the 786-O

BAP1 knockout cell line compared to BAP1-expressing (Cas9) cell line was investigated.

4.9 Xenograft tumor models

4.9.1 Metastatic mouse model

HDACs are involved in metastasis progression. Therefore, a metastatic mouse model was established to analyze the association of HDAC1 inhibition and metastatic ability in *BAP1*-mutated cancers.

For this, BAP1-deficient UMRC-6 cells were injected into the left ventricle via intracardiac injection of nude mice. Afterwards, metastatic spread was followed by using bioluminescence imaging. In addition, a metastatic breast cancer cell line MDA-MB-231 was used as a control cell line since it was showed that these cells successfully develop metastases after intracardiac injection into nude mice (Jenkins et al. 2005).

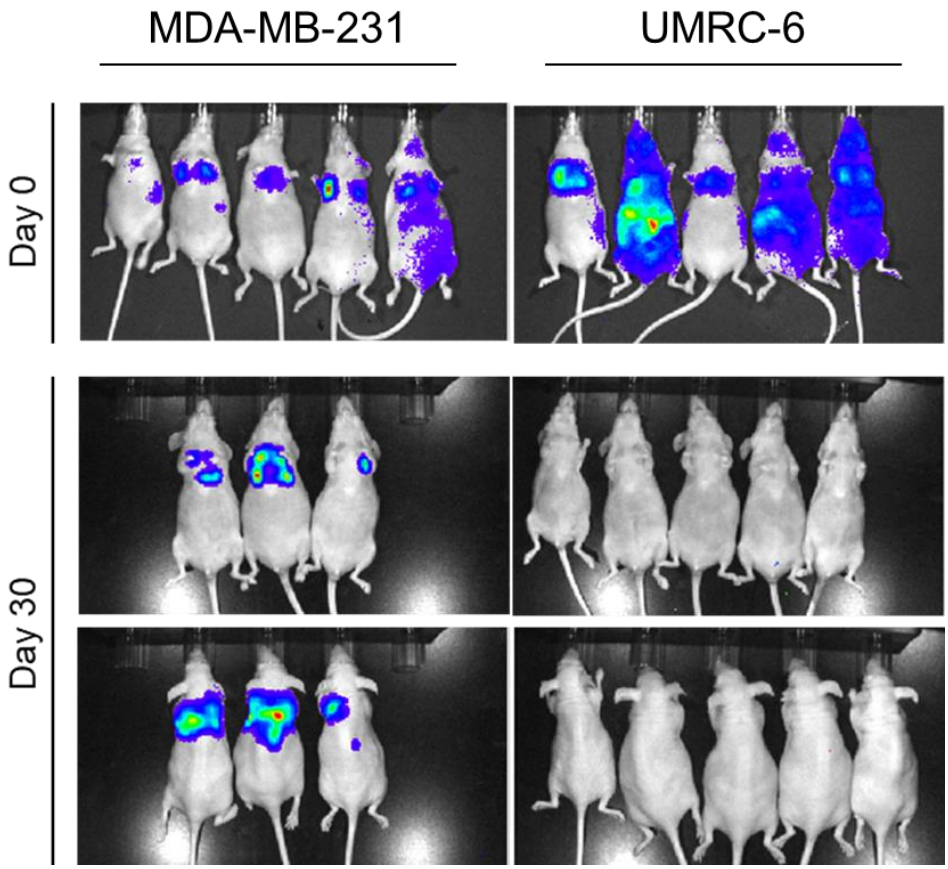

Figure 22: UMRC-6 cells are not forming metastasis
MDA-MB-231 (metastatic breast cancer cells, control group) and UMRC-6 (ccRCC, group of interest) cells were injected via intracardiac injection into the left heart ventricle. Bioluminescence was performed directly after injection (Day 0). Afterwards, two times a week until day 30 after injection. Five mice per group were used. After 30 days only three mice of the MDA-MB-231 group survived.

Figure 22 is representing the bioluminescence imaging of nude mice directly after intracardiac injection of MDA-MB-231 and UMRC-6 cells. However, bioluminescence floating over the whole body of nude mice was a sign of successful intracardiac injection. After 30 days, only the control group MDA-MB-231 showed bioluminescence signal.

The bioluminescence images from the control group indicate that MDA-MB-231 cells formed metastases especially in lung, heart and liver after intracardiac injection. Moreover, only three mice of the control group survived for 30 days after injection and the other two mice died possibly because of metastatic disease.

In contrast, mice injected with UMRC-6 cells (group of interest) survived for 30 days and none of them showed any signal on the day 30, indicating that UMRC-6 cells were not able to develop metastasis after injection.

4.9.2 Cholangiocarcinoma xenograft mouse model

The *in vitro* results indicated that *HDAC1* knockdown decreased the proliferation of BAP1-deficient cancer cells (described in Chapter 4.2-4.4). Therefore, the behavior of tumor growth of BAP1-deficient cells with or without a *HDAC1* knockdown was investigated to validate *HDAC1* as a possible synthetic lethal partner of *BAP1*-mutated cancers *in vivo*.

To establish the murine xenograft model, cholangiocarcinoma TFK-1 cells were injected subcutaneously (s. c.) into nude mice and followed the tumor growth.

4.9.2.1 Characterization of *in vivo* cell line xenografts

TFK-1 cell lines were used to generate the subcutaneous mouse model. First, TFK-1 cells were transduced with a Luc-Venus plasmid (pV2luc2) expressing luciferase and YFP. Luciferase expression was used to visualize the tumors growth over time noninvasively by bioluminescence imaging. On the other hand, YFP expression was used for cell sorting. After sorting, cells were transduced again with plasmids expressing EV, BAP1-wt or p.C91S.

Before these cell lines were used to create a xenograft mouse model, they were characterized *in vitro* (Fig. 23).

The success of the transduction of TFK-1 cells with the three plasmids (EV, BAP1-wt and p.C91S) was confirmed via western blot (Fig. 23A). The TFK-1 EV cells did not express BAP1 and TFK-1 BAP1-wt and C91S cells showed a BAP1 protein expression, although the BAP1 expression was higher in BAP1-wt cells than in C91S cells.

The CellTiter-Glo assay showed a significant decrease in cell proliferation in BAP1-wt and *BAP1*-mutant (C91S) TFK-1 cells compared to EV-expressing TFK-1 cells. However, only BAP1-wt, but not C91S, TFK-1 cells presented a lower colony number compared to EV TFK-1 cells (Fig. 23C and 23D).

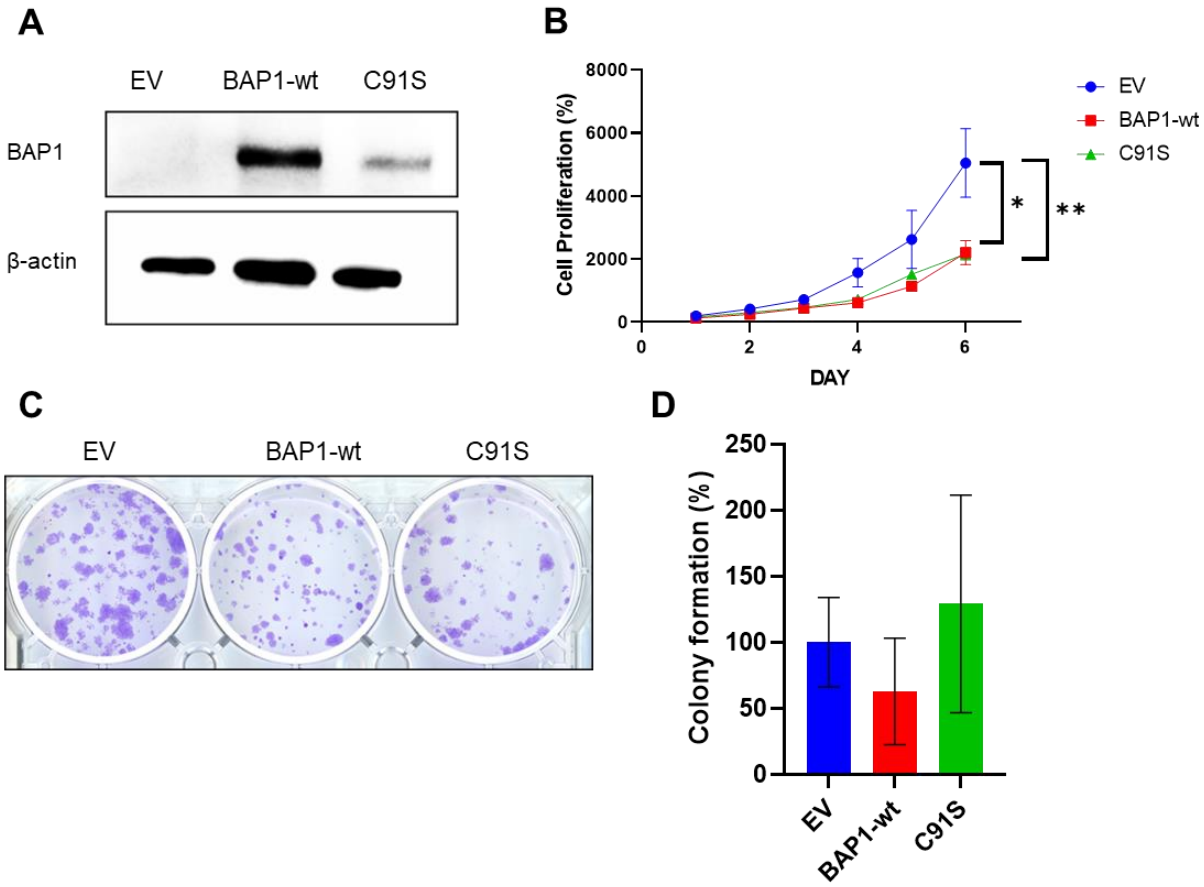

Figure 23: Characterization of TFK 1 Luc-Venus cell line
The TFK-1 cell line was transduced and sorted for a Luciferase/YFP expressing plasmid. Afterwards, TFK-1 cells were transduced with EV, BAP1-wt or a p.C91S (*BAP1*-mutant) expressing plasmid. The three cell lines were analyzed by performing A) western blot, B) proliferation assay and C-D) colony formation assay. *N* = 3 for all experiments. Significance was assessed using nonparametric Kruskal-Wallis test. *p*-values: $p<0.05$ (*), $p<0.01$ (**).

4.9.1.2 Validation of synthetic lethality of *HDAC1* knockdown with BAP1 loss in TFK-1 cell lines *in vivo*

The BAP1-deficient TFK-1 cell line was used to investigate the association of *HDAC1* and tumor growth of *BAP1*-mutated tumors. TFK-1 EV and TFK-1 BAP1-wt cells described in Chapter 4.9.1.1 were transduced with sh*HDAC*1 or Scr (control) plasmids and injected subcutaneously into the left flank of nude mice. Throughout the experiment, the tumor sizes were measured weekly with bioluminescence imaging and manually with a caliper.

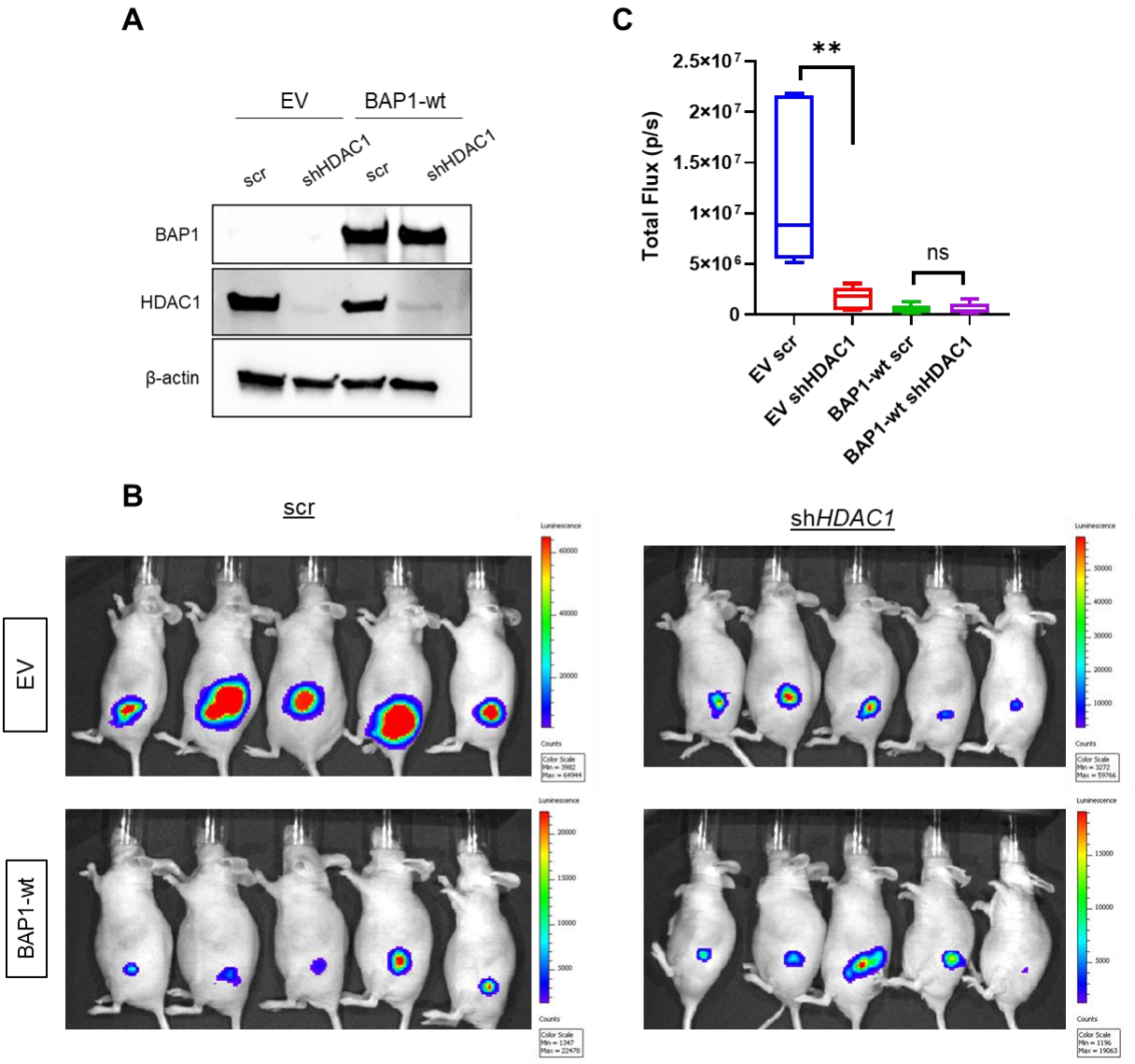

Figure 24: Bioluminescence images of TFK-1 cell lines
A *HDAC1* knockdown was performed in TFK-1 EV and BAP1-wt cell lines. A) The knockdown of *HDAC1* was validated by western blotting. Cells were injected into the left flank of nude mice and the mice were imaged every week with an IVIS Lumina II (bioluminescence imager). B) Bioluminescence pictures were taken after eight weeks of injection C) and the total flux from each image was quantified.
Five mice per group were used. Significance was assessed using nonparametric Kruskal-Wallis test. *p*-value: $p<0.01$ (**).

The success of the *HDAC1* knockdown in the TFK-1 cell lines was verified by western blot, where sh*HDAC1* cell lines are showing a clearly downregulation of HDAC1 protein expression (Fig. 24A).

The bioluminescence imaging clarified the effect of a *HDAC1* knockdown on BAP1-defient cell lines (Fig. 24B and 24C). The bioluminescent pictures were taken eight weeks after cell injection (Fig. 24B) showing that the *BAP1*-depleted control tumors (TFK-1 EV Scr) were growing faster than the BAP1-expressing tumors (TFK-1 BAP1-wt Scr) (Fig. 24C). The *HDAC1* knockdown led to a decrease in tumor size in tumors with BAP1 loss while it had no effect on the tumor size in BAP1-wt tumors (Fig. 24C).

The results of the bioluminescence imaging were confirmed by the manual measurements of the tumor volume with the caliper (Fig. 25A). After four weeks of subcutaneous injection of TFK-1 cells, the tumors started to grow with different rates (Fig. 25B). The tumor growth of TFK1 BAP1-wt Scr and TFK-1 EV sh*HDAC1* were similar. In contrast, TFK-1 BAP1-wt sh*HDAC1* tumors were growing faster compared to the tumor size of BAP1-wt ones. Moreover, the TFK-1 EV Scr tumors showed in comparison to the other tumor groups the fastest growth rate. The tumor volume of TFK-1 EV Scr was significantly bigger than the other tumors after eight weeks of subcutaneous injection (Fig. 25C). However, the volume of TFK-1 EV sh*HDAC1* tumors were decreased in comparison of the control TFK-1 EV tumors. Besides, the *HDAC1* knockdown did not had any effect on the tumor volume of TFK-1 BAP1-wt ones.

The *in vivo* results underline that *HDAC1* knockdown only affects *BAP1*-mutated cancers and not BAP1-expressing tumors, strongly suggesting a synthetic lethal interaction of HDAC1 with BAP1 loss *in vivo*.

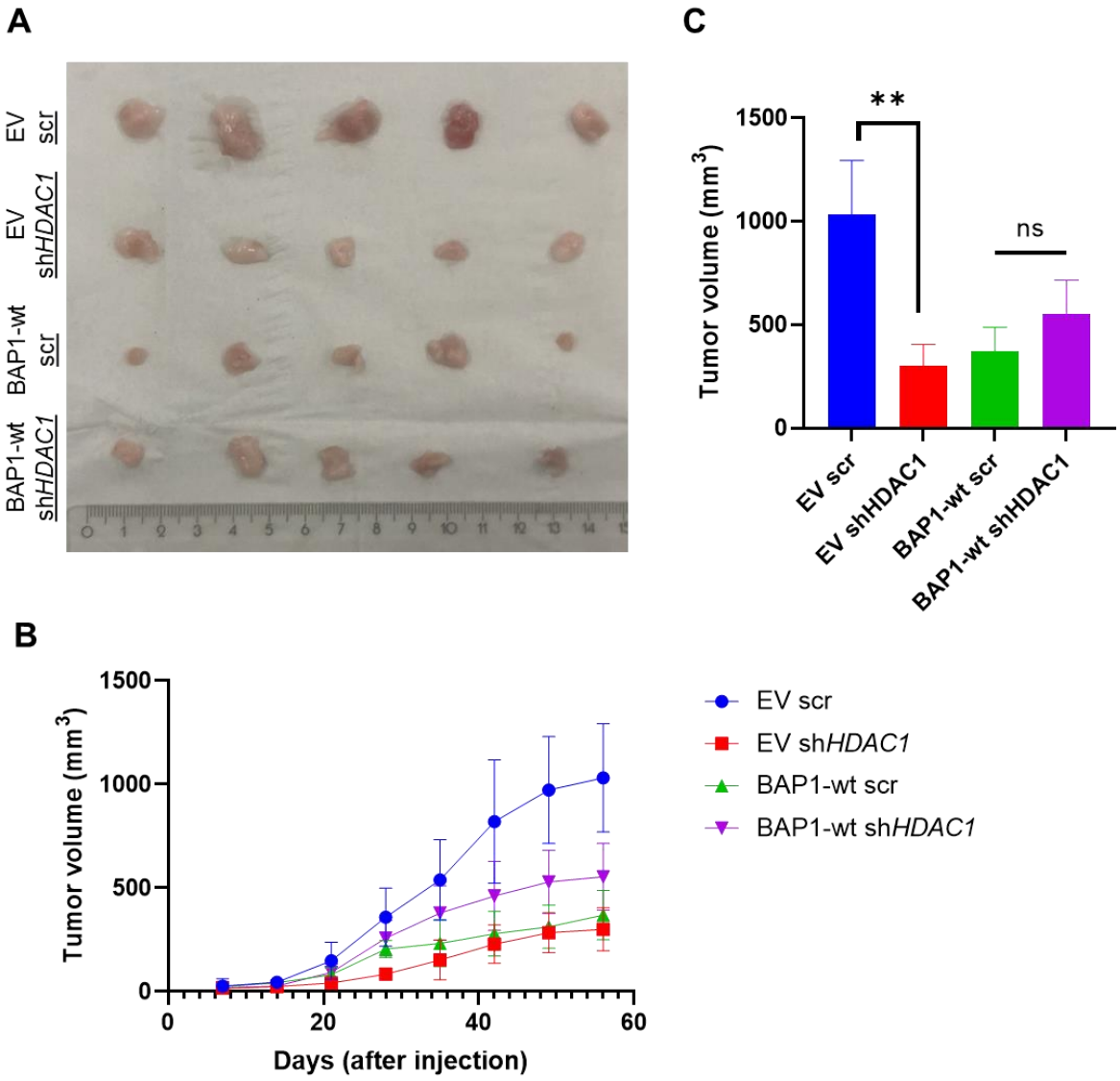

Figure 25: *HDAC1* knockdown decreases tumor growth of BAP1-deficient tumors
TFK-1 EV and BAP1-wt transduced with Scr (control) or sh*HDAC1* and injected subcutaneously into the left flanks of nude mice. A) Picture of comparison of xenograft tumors after eight weeks of injection. B) Tumor sizes were measured every week for 56 days with a caliper. C) The tumor volume of the last measurement was quantified. Five mice per group were used. Significance was assessed using nonparametric Kruskal-Wallis test. *p*-value: $p<0.01$ (**).

5. Discussion

Curative treatment is the desired goal for every cancer patient, but for most tumor entities, curative treatment options are – due to multifactorial reasons - currently rare. This unfortunate reality also holds true for cancer patients with *BAP1* mutations, which are showing frequently a poor overall survival (Uner et al. 2021; Wang et al. 2016; da Costa et al. 2019; Kapur et al. 2013).

Recently, it was reported that early detection and screening for *BAP1*-mutated tumors can be life saving for different tumor entities, however, the detection of *BAP1*-mutated tumors at an early stage is a rare clinical event and most patients are diagnosed at a later disease stage (Kittaneh and Berkelhammer 2018).

Notably, several studies suggested the clinical administration of PARP-1 inhibitors for several different *BAP1*-mutated tumors; even though, a recently published clinical report showed only limited effects of the PARP-Inhibitor olaparib on the treatment of mesothelioma, including patients with *BAP1* mutations, showing no improvement of the overall survival of mesothelioma patients after olaparip treatment (Sabbatino et al. 2020; de Koning et al. 2019; Hassan et al. 2019).

To meet this still unmet clinical need, we performed a synthetic lethality screen to identify a potential target for *BAP1*-mutated tumors (Fig. 6).

5.1 HDAC1 as a target in *BAP1*-mutated tumors

Synthetic lethality screens are performed to identify tumor-specific vulnerabilities which are associated with tumor-specific mutations that can be therapeutically targeted.

A shRNA screen was conducted to identify synthetically lethal interactors with BAP1 deficiency using the BAP1-deficient cell line UMRC-6, which got reconstituted with an empty vector as a control cell line or a wild-type BAP1-expressing plasmid, respectively. We expected that the knockdown (KD) of synthetically lethal genes of *BAP1*-mutated tumors results in decreased cell viability, proliferation and colony formation in *BAP1*-mutant cell lines, but not in *BAP1*-wildtype expressing cell lines (Fig. 7). Using the Cellecta DECIPHER lentiviral shRNA library for our synthetic lethality screen identified several potential synthetically lethal candidates for *BAP1*-mutated tumors (Fig. 7, Fig. 8 and Supplementary Fig. 1).

First, we performed a shRNA screen, which included two biological replicates. In the shRNA library screen, there was an overexpression of DNA double-strand break (DSB)

repair genes in the top candidate hits (Supplementary Fig. 1). Two of the most prominent genes were *TOP3A* and *RECQL* both playing a crucial role in DSB repair machinery. Therefore, at the beginning the investigations focused on *TOP3A* and *RECQL* as potential synthetically lethal targets of tumors with *BAP1* mutations. Interestingly, *BAP1* mutations have been shown to play a crucial role in the DSB repair pathway, specifically in the homologous recombination pathway (Ismail et al. 2014; Carbone, Arron, et al. 2020). Thus, BAP1 deficiency is associated with defects in the repair of DSBs. Based on this observation, it was suggested to treat patients with *BAP1*-mutated tumors by inhibiting genes involved in the DSB repair machinery (Carbone, Arron, et al. 2020). However, so far, there is a lack of knowledge on inhibition of BAP1-target proteins involved in the DSB repair pathway.

The proliferation assay results of this study (Supplementary Fig. 2) demonstrated that the knockdown of *RECQL* as well as a *TOP3A* decreased the proliferation of BAP1-wt expressing as well as of BAP1-inactive (EV and p.C91S mutant) UMRC-6 cell lines, indicating that *RECQL* and *TOP3A* might not be synthetically lethal targets for BAP1-mutated tumors, since both knockdowns showed a *BAP1*-independent effect on the cell proliferation. These observations were supported by results from additional proliferation and colony formation assays in different RCC and ICCA cell lines, which were generated by our laboratory (data not shown).

Afterwards, performing a second synthetic lethality screen using three biological replicates, *HDAC1* was identified as one potential synthetically lethal target of *BAP1* mutated tumors (Fig. 8). Since HDACs have been shown to regulate the expression and activity of numerous proteins, which are involved in tumor progression and initiation (Glozak et al. 2005), and since previous studies revealed that tumors with BAP1 loss can be sensitive to HDAC inhibitors, we decided to focus our investigations on *HDAC1* as a potential synthetically lethal target.

The proliferation assays of the BAP1-deficient cell lines TFK-1 and UMRC-6 containing a *HDAC1* knockdown showed a significant decrease of cell viability in cells not expressing *BAP1* (EV) and cells expressing mutant *BAP1* (p.C91S) in comparison to the wild-type *BAP1* expressing cells (*BAP1*-wt) (Fig. 10A). In addition, colony formation assays revealed that the BAP1-deficient *HDAC1* knockdown cell lines expressing EV and p.C91S plasmids showed a tendency of reduced colony formation compared to wild-type *BAP1* cell lines (Fig. 10B and 10C). The possibility of identifying *HDAC1* as a potential synthetic lethal partner with *BAP1* vulnerabilities could be manifested by

the use of generated *BAP1* knockout cell lines using 786-O (RCC) and 92-1 (UM) cells (Fig. 13 and Fig. 16). The results of the proliferation and colony formation assays of 786-O and 92-1 cell lines showed a suppression of their cell growth and cell viability only in the combination of BAP1 loss and *HDAC1* knockdown, emphasizing the strong effect of a *HDAC1* knockdown in *BAP1* knockout cell lines, but not in *BAP1*-wt expressing cells (Fig. 14 and Fig. 17). These findings additionally supported the further investigation of *HDAC1* as a potential synthetically lethal target for BAP1-deficient tumors.

In the past, different studies highlighted the importance of HDAC1 as a key player for cancer progression. Studies focusing on HDACs and small interfering RNA revealed an important role of HDACs in the regulation of proliferation and cancer cell survival (Glaser et al. 2003). Further, it was reported that HDAC1 can promote proliferation of breast cancer cells by suppressing the transcription of the estrogen receptor alpha (Kawai et al. 2003).

In addition to the above-mentioned studies, the data presented in this work indicate that HDAC1 particularly increased the proliferation of BAP1-deficient tumor cells (Fig. 10, Fig. 14 and Fig. 17), but not in tumor cells expressing the wild-type *BAP1* protein (Fig. 12). Furthermore, the proliferation of Caki-1 and RCC4 cells – which are BAP1-wt expressing ccRCC cell lines – was not affected by a knockdown of HDAC1 (Fig. 12). To further understand the role and importance of HDAC1 as a target protein in other BAP1-deficient cancer types, the effect of HDAC1 inhibition on additional BAP1-deficient tumor types as well as the effects of HDAC1 inhibition on normal tissues needs to be further investigated in the future.

Previously generated data by our laboratory (data not shown) showed a significant overexpression of HDAC1 in BAP1-deficient UM cell lines in comparison to *BAP1*-wt expressing cells lines. These data are in line with observations from other groups, who reported an overexpression of HDAC1 at the mRNA and protein level in different tumor entities, including colon, breast, prostate, gastric, pancreatic and lung cancer as well as in hepatocellular carcinoma (Wilson et al. 2006).

Another evidence for HDAC1 being a potential synthetically lethal target in *BAP1*-mutant tumors is based on the observation that the HDAC1 inhibitor quisinostat decreased the cell viability of BAP1-deficient cancer cell lines stronger than the cell viability of BAP1-expressing cancer cell lines (Fig. 18B and 18C).

Previously, quisinostat has shown antitumor effects in advanced solid tumors, such as metastatic melanoma, with prolonged clinical responses in patients and without causing severe side effects in comparison to other HDACi (Morales Torres et al. 2020; Venugopal et al. 2013).

Moreover, a recent study demonstrated that quisinostat treatment inhibited tumor growth in a BAP1-deficient UM xenograft model (Kuznetsoff et al. 2021). Interestingly, the same study showed that quisinostat did not affect the tumor growth of BAP1-wt expressing UM tumors, although the authors claim that the effect was mediated by HDAC4.

Even though quisinostat is a pan-HDACi, which can inhibit different classes of HDAC proteins simultaneously, it was shown that quisinostat is inhibiting HDAC1 with a higher sensitivity than other HDACs (Venugopal et al. 2013; Lo Cascio et al. 2021). However, whether the effect of quisinostat on cell viability of BAP1-deficient tumor cells is exclusively mediated by inhibition of HDAC1 or whether a concomitant inhibition of different HDAC proteins is responsible for the observed effects in the abovementioned experiments needs to be further addressed.

In contrast to the abovementioned parental BAP1-deficient and *BAP1*-wt expressing tumor cell lines, quisinostat exhibited no differential effect on the cell viability of BAP1-deficient cell lines (UMRC-6 and TFK-1 cells), which were reconstituted with an EV, a *BAP1*-wt expressing plasmid and a mutated, dysfunctional BAP1-expressing plasmid (p.C91S) as well between 786-O *BAP1* knockout and 786-O BAP1-wt cells (Fig. 18A). A potential reason for this discordant result could be that the reintroduction of BAP1 into BAP1-deficient cells was not sufficient to fully compensate and restore BAP1 protein function. In addition, it is possible that a portion of the BAP1-reconstituted cells might have had a decreased BAP1 protein expression in comparison the other BAP1-reconstituted cells. This could potentially result in an increased proliferation rate of the BAP1-reconstituted cells with decreased BAP1 protein levels, resulting in a relative increase of these cells during the course of cell cultivation, concomitantly decreasing the relative number of cells with a higher BAP1 protein expression. This might explain the diminished effect of quisinostat on the cell viability of the BAP1-reconstituted (BAP1-wt) cells in comparison to BAP1-deficient cells (EV).

However, additional experiments focusing on the potential benefit of HDAC1 inhibitors in *BAP1*-mutated tumors should be conducted to enable evidence-based decision-making on potential HDAC1-targeted therapies in the future.

A novel HDAC1 inhibitor, CBUD-1001, showed anti-tumor effects by inducing tumor cell apoptosis and repressing the epithelial-to-mesenchymal transition in colorectal cancer cells (Kim et al. 2020). Further investigations comparing the sensitivity of CBUD-1001 on BAP1-deficient and BAP1-expressing cancer cells could help to shed light on HDAC1 as a synthetically lethal target for *BAP1*-mutated tumors.

Besides promoting proliferation and cell survival, HDACs have been shown to play a crucial role in cell migration and invasion (Jeon and Lee 2010), so we sought to investigate the association between HDAC1 and the migration and invasion of 786-O *BAP1* knockout cells (Fig. 19). The results indicated that the *HDAC1* knockdown suppressed the migration of BAP1-deficient cells stronger than the migration of BAP1-expressing cells (Fig. 19A and 19B). Moreover, *BAP1* knockout cells showed a tendency of decreased invasion following *HDAC1* knockdown (Fig 19A - 19C).

In the past, studies revealed a correlation between HDAC1 expression and cancer cell invasion in different cancers, including glioma, liver cancer and RCC (Xie et al. 2012; Park et al. 2011; Ramakrishnan et al. 2016).

One of these studies reported that HDAC1 promotes the invasion of RCC cells by increasing the expression of the matrix metalloprotease-2 /9, indicating an important role of HDAC1 in tumor progression and metastatic spread of RCC (Ramakrishnan et al. 2016).

In addition to the investigations focusing on tumor cell migration and invasion *in vitro*, we sought to examine the impact of cancer cell-derived HDAC1 expression on the metastatic ability of BAP1-deficient ccRCC cells (UMRC-6) *in vivo* by establishing a metastatic ccRCC mouse model in nude mice through intracardiac injection of tumor cells (Fig. 23). In comparison to MDA-MB-231 cells, which formed metastasis and served as a control for the successful establishment of the experimental *in vivo* system, UMRC-6 cells did not form metastasis in the injected nude mice (Jenkins et al. 2005). This finding is in agreement with previous studies that reported that the UMRC-6 cell line is not able to form tumors in nude mice (Grossman, Wedemeyer, and Ren 1985), therefore, another renal cell carcinoma BAP1-deficient cell line should be chosen to investigate the metastatic role of HDAC1 in *BAP1*-mutated tumor cells in future experiments.

Most importantly, by using a subcutaneous xenograft mouse model of BAP1-deficient intrahepatic cholangiocarcinoma (TFK-1), a significant decrease of tumor growth by either the knockdown of *HDAC1* or the reconstitution of wild-type *BAP1* without any

additional effect by the combination of both could be identified (Fig. 24 and Fig. 25). This finding indicated that HDAC1 inhibition might lead to a less aggressive phenotype of *BAP1*-mutated tumors, validating HDAC1 as a synthetic lethal interactor of iCCA BAP1 loss tumors *in vivo* and hinting towards a clinical benefit of HDAC1-targeted therapies for patients with *BAP1*-mutated tumors.

The obtained results are supported by a study showing that HDACs are involved in tumor growth and tumor cell survival (Schmidt et al. 2021). In addition, it was shown that HDAC1 is involved in the modulation of angiogenesis by the regulation of the transcription factor hypoxia-inducible factors 1 α (HIF-1α). HDAC1 is directly blocking the degradation of HIF-1α through its deacetylation (Yoo, Kong, and Lee 2006). HIF-1α itself can increase the transcription of numerous angiogenesis-associated genes, thereby supporting tumor cells survival and tumor growth (Carmeliet et al. 1998).

Moreover, it was found that an overexpression of HDAC1 correlated with poor patient prognosis and survival in different tumor entities (Cao, Song, et al. 2017; Cao, Yue, et al. 2017). Future clinical trials could particularly focus on the recruitment of BAP1-deficient cancer patients to gain more insights into *HDAC1* as a synthetically lethal target and to increase our understanding of the role of HDAC1 in BAP1-deficient tumors.

6.2 Comparison of the effect of HDAC1 and HDAC4 inhibition on BAP1-deficient tumor cells

As described above, HDAC1 has been shown to support tumor cell survival and growth by different cellular mechanisms. However, HDAC1 is not the only HDAC family member that can support *BAP1*-mutated cancer cells, since Kuznetsoff and colleagues also identified HDAC4 as a key target in *BAP1*-mutant UM (Kuznetsoff et al. 2021).

In the past, several studies showed tumor promoting functions of HDAC4 in different cancer types (Zeng et al. 2016; Cai et al. 2018). Like HDAC1, HDAC4 can support tumor growth by HIF-1α stabilization (Geng et al. 2011). For this stabilization, HDAC4 directly binds to HIF-1α, forming a complex that regulates HIF-1α-mediated gene expression, glycolysis and chemoresistance of cancer cells.

In addition, studies demonstrated an association between HDAC4 overexpression and poor patient survival in different cancer types, including esophageal, ovarian and pancreatic carcinoma (Fan et al. 2021; Zhou, Xu, et al. 2018; Zeng et al. 2016).

However, focusing on the results of our shRNA library screen, *HDAC4* was not significantly enriched in *BAP1*-mutated tumor cells (Fig. 8). Thus, we were interested in performing a side by side comparison between HDAC1 and HDAC4 to investigate which target has a higher effectiveness for the treatment of *BAP1*-mutated cancer patients. For this side-by-side comparison, we performed proliferation and colony formation assays of *BAP1* knockout 786-O and 92-1 cells containing either a *HDAC1* knockdown or a *HDAC4* knockdown (Fig. 13 – Fig. 17).

In comparison to *HDAC1* knockdown, *HDAC4* knockdown did not show a strong effect on the proliferation and colony formation of the UM 92-1 *BAP1* knockout cell line (Fig. 17). Moreover, the *HDAC4* knockdown did not affect the cell viability and the cell growth of the RCC 786-O *BAP1* knockout cell line at all, in contrast to *HDAC1* knockdown, which led to a significant decrease of proliferation and colony formation of the 786-O *BAP1* knockout cell line (Fig. 14 and Fig 15).

In support of our data, a previous study demonstrated a link between *HDAC1* inhibition and cancer progression, whereby *HDAC4* inhibition only minimally affected the cell proliferation of different cancer cell lines (Glaser et al. 2003). Our data indicate that HDAC4 plays a role in specific BAP1-deficient cell lines e.g. in UM cell lines, but not in all *BAP1*-mutant cell lines from different tumor entities, whereby *HDAC1* seems to be important in different cancers with *BAP1* mutations.

6.3 Characterizing HDAC1-mediated inhibitory mechanism on BAP1-deficient cells

As our previous data identified HDAC1 as a potential target for *BAP1*-mutated tumors, we next wanted to investigate the role of HDAC1 in BAP1-deficient cancer cells to understand the mechanism behind the antiproliferative effect of HDAC1 inhibition.

First, we investigated, whether other HDAC proteins compensated the HDAC1 loss following HDAC1 inhibition in *BAP1*-mutated cancer cells. Therefore, we performed a microarray analysis on 786-O BAP1-expressing and *BAP1* knockout cells, each containing either a *HDAC1* knockdown or a scrambled control plasmid, to compare the mRNA expression levels of different HDAC proteins (HDAC1-10) between the two different cell lines (Supplementary Fig 2). The microarray analysis revealed no upregulated mRNA expression of the investigated HDAC proteins, indicating the absence of a compensatory effect after *HDAC1* knockdown in the investigated cell

lines. However, even though mRNA expression data indicate the absence of a compensatory effect of other HDACs, it is still thinkable that other, mRNA expression level-independent HDAC-mediated processes can facilitate *HDAC1* loss-initiated compensatory effects. One such process could be an altered HDAC protein stability and turnover rate, resulting in an increased amount of functional HDACs, without affecting the expression level of the respective e.g. reported in Jamaladdin and colleagues (2014). In this report, it was demonstrated that HDAC1 and HDAC2 inhibition leads to an increase of HDAC3 protein levels, but did not affect the *HDAC3* gene expression levels (Jamaladdin et al. 2014). Furthermore, it is possible that HDAC proteins reveal an altered activity following the *HDAC1* knockdown, which can also not be detected by the used microarray analysis (Lagger et al. 2002). Therefore, further investigations addressing the above-mentioned scenarios need to be conducted to finally exclude a HDAC-mediated compensatory effect following the *HDAC1* loss.
Interestingly, the experiments of this project revealed a downregulation of the *HDAC2* expression in 786-O *BAP1* knockout cells in comparison to 786-O BAP1-expressing cells. These results are consistent with studies from other groups, demonstrating that an inactivation of *BAP1* resulted in a downregulation of *HDAC2* expression (Sacco et al. 2015). In addition, a report showed that inhibition of either *HDAC1* or *HDAC2* in mice, using a *HDAC1* or *HDAC2* knockout mouse model, resulted in the reciprocal upregulation of the respective other protein (Winter et al. 2013). In our studies, we did not observe a reciprocal regulation of HDAC2 following the *HDAC1* knockdown in our cell lines, suggesting that the HDAC2 expression is dependent on the BAP1 expression status of the respective tumor cells.

Next, we investigated the association between HDAC1 inhibition and the decrease of proliferation of BAP1-deficient cancer cells.
Previous studies revealed that *BAP1* loss is associated with an increase of cancer cell proliferation and progression in several tumor entities (Qin et al. 2015; Carbone, Harbour, et al. 2020). In addition, it was reported that HDAC1 inhibition triggers cell cycle blockade and apoptosis in cancer cells (Zhou, Cai, et al. 2018).
Therefore, we performed flow cytometry-based cell cycle analysis, which indicated that the *HDAC1* knockdown resulted in a G1 arrest and a decreased proliferation and colony formation in *BAP1* knockout cells compared to BAP1-wt expressing cells (Fig. 10, Fig. 14, Fig. 17, Fig. 20B and 20C).

Importantly, other reports about the relation of HDAC1 inhibition and G1 arrest are supporting our data. One report demonstrated that *HDAC1* knockdown led to G1 arrest in mouse embryonic fibroblast cells (Wilting et al. 2010). In addition, it was reported that HDAC1 inhibition resulted not only in a G1 arrest, but also decreased the G2-M arrest in pancreatic cancer cells which was leading to apoptosis in the reported cell lines (Du et al. 2014). However, the effect of HDAC1 inhibition on the G2-M arrest was not observed in the conducted *in vitro* experiments and might be explained by the use of different tumor entities in our project in contrast to the other reported study (Fig. 20). In comparison to influencing the cell cycle, HDAC1 inhibition did not affect apoptosis induction in *BAP1* knockout cells (Fig. 21). These results are supported by a study demonstrating an association between HDAC1 inhibition and G1 arrest, but not between HDAC1 inhibition and apoptosis induction *in vivo,* even though another study also suggested that HDAC1 inhibition leads to an increased apoptosis of cancer cells *in vitro* (Yamaguchi et al. 2010).

Recently, it was published that HDAC1 regulates the cell cycle through the tumor suppressor p21 in an apoptosis-independent manner (Sankala et al. 2007). Therefore, HDAC1 is binding to the promoter region of the *p21* gene (Yamaguchi et al. 2010) and induce a G1-arrest in cells without influencing the apoptosis level of cells.

The p21 protein is a member of the CIP/WAF family and plays a key role in cell cycle regulation, cell differentiation and senescence (Campisi 2013). Further, the p21 expression was shown to be upregulated following HDAC1 inhibition in different cancer types (Glozak and Seto 2007). Additional research focusing on the association between HDAC1 inhibition and p21 expression as well p21 targeted gene expression could help to uncover cellular signaling pathways, in which HDAC1 might be involved in *BAP1*-mutated cancers.

At last, previous data generated in our lab indicated that BAP1 is directly binding to the promoter site of *HDAC1*, suggesting that BAP1 is suppressing the transcription of *HDAC1* resulting in a decrease of proliferation. However, the precise role of BAP1 as a negative regulator of HDAC1 should be investigated further in the future to gain deeper insights into HDAC1 inhibitor-mediated mechanisms of action in *BAP1*-mutated tumors.

6.4 Conclusion and outlook

In summary, our study provided strong evidence for the synthetic lethality between HDAC1 and BAP1 in tumor development via *in vitro* and *in vivo* experiments. We show that *HDAC1* knockdown decreased cell proliferation, colony formation and migration as well as the tumor growth in the context of BAP1 loss. We propose that this effect is based on the G1 cell cycle arrest regulated due to HDAC1 in BAP1-deficient cancer cells. Furthermore, we demonstrated that HDAC1 regulate the progression of BAP1-deficient cancer types independent of apoptosis pathways.

In the future, deeper characterizations of the mechanisms behind the association of HDAC1 inhibition and BAP1 deficiency can provide higher evidence of the benefit using *HDAC1* as a novel therapeutic target for *BAP1*-mutated cancers. Therefore, the comparison of the expression levels of diverse genes such as p21 in BAP1-expressing with *BAP1*-knockout cell lines after a *HDAC1* knockdown can give us evidence in which cell signaling pathway HDAC1 is involved in cancers with *BAP1* mutations.

In addition, as inhibition with the HDAC1 inhibitor quisinostat on BAP1-deficient cancer cells resulted in a decrease of cell viability, the next step is to test this HDAC1 inhibitor *in vivo* as well as in patient-derived organoids from renal cell carcinoma and uveal melanoma generated in our group in collaboration with the departments of Urology and Ophthalmology. These pre-clinical models might clarify the therapeutic benefit of quisinostat for cancer patients with *BAP1* mutations.

6. References

Abdel-Rahman, M. H., R. Pilarski, J. B. Massengill, B. B. Christopher, and F. H. Davidorf. 2011. 'Lack of GNAQ germline mutations in uveal melanoma patients with high risk for hereditary cancer predisposition', *Fam Cancer*, 10: 319-21.

Alley, E. W., J. Lopez, A. Santoro, A. Morosky, S. Saraf, B. Piperdi, and E. van Brummelen. 2017. 'Clinical safety and activity of pembrolizumab in patients with malignant pleural mesothelioma (KEYNOTE-028): preliminary results from a non-randomised, open-label, phase 1b trial', *Lancet Oncol*, 18: 623-30.

Amato, R. J. 2000. 'Chemotherapy for renal cell carcinoma', *Semin Oncol*, 27: 177-86.

Andrici, J., B. Goeppert, L. Sioson, A. Clarkson, M. Renner, A. Stenzinger, M. Tayao, N. Watson, M. Farzin, C. W. Toon, R. C. Smith, A. Mittal, J. S. Samra, T. J. Hugh, A. Chou, R. T. Lawlor, W. Weichert, P. Schirmacher, N. Sperandio, A. Ruzzenente, A. Scarpa, and A. J. Gill. 2016. 'Loss of BAP1 Expression Occurs Frequently in Intrahepatic Cholangiocarcinoma', *Medicine (Baltimore)*, 95: e2491.

Baas, P., and L. Schunselaar. 2018. 'MS31.02 Clinical Implementation of BAP1 Inhibitors', *Journal of Thoracic Oncology*, 13: S305-S06.

Banales, J. M., J. J. G. Marin, A. Lamarca, P. M. Rodrigues, S. A. Khan, L. R. Roberts, V. Cardinale, G. Carpino, J. B. Andersen, C. Braconi, D. F. Calvisi, M. J. Perugorria, L. Fabris, L. Boulter, R. I. R. Macias, E. Gaudio, D. Alvaro, S. A. Gradilone, M. Strazzabosco, M. Marzioni, C. Coulouarn, L. Fouassier, C. Raggi, P. Invernizzi, J. C. Mertens, A. Moncsek, S. Rizvi, J. Heimbach, B. G. Koerkamp, J. Bruix, A. Forner, J. Bridgewater, J. W. Valle, and G. J. Gores. 2020. 'Cholangiocarcinoma 2020: the next horizon in mechanisms and management', *Nat Rev Gastroenterol Hepatol*, 17: 557-88.

Bhattacharya, S., P. Hanpude, and T. K. Maiti. 2015. 'Cancer associated missense mutations in BAP1 catalytic domain induce amyloidogenic aggregation: A new insight in enzymatic inactivation', *Sci Rep*, 5: 18462.

Bononi, A., C. Giorgi, S. Patergnani, D. Larson, K. Verbruggen, M. Tanji, L. Pellegrini, V. Signorato, F. Olivetto, S. Pastorino, M. Nasu, A. Napolitano, G. Gaudino, P. Morris, G. Sakamoto, L. K. Ferris, A. Danese, A. Raimondi, C. Tacchetti, S. Kuchay, H. I. Pass, E. B. Affar, H. Yang, P. Pinton, and M. Carbone. 2017. 'BAP1 regulates IP3R3-mediated Ca(2+) flux to mitochondria suppressing cell transformation', *Nature*, 546: 549-53.

Braconi, C., and T. Patel. 2010. 'Cholangiocarcinoma: new insights into disease pathogenesis and biology', *Infect Dis Clin North Am*, 24: 871-84, vii.

Bridgewater, J., P. R. Galle, S. A. Khan, J. M. Llovet, J. W. Park, T. Patel, T. M. Pawlik, and G. J. Gores. 2014. 'Guidelines for the diagnosis and management of intrahepatic cholangiocarcinoma', *J Hepatol*, 60: 1268-89.

Butt, Z., N. D. Parikh, J. L. Beaumont, S. K. Rosenbloom, K. L. Syrjala, A. P. Abernethy, A. B. Benson, 3rd, and D. Cella. 2012. 'Development and validation of a symptom index for advanced hepatobiliary and pancreatic cancers: the National Comprehensive Cancer Network Functional Assessment of Cancer Therapy

(NCCN-FACT) Hepatobiliary-Pancreatic Symptom Index (NFHSI)', *Cancer*, 118: 5997-6004.

Cai, J. Y., T. T. Xu, Y. Wang, J. J. Chang, J. Li, X. Y. Chen, X. Chen, Y. F. Yin, and X. J. Ni. 2018. 'Histone deacetylase HDAC4 promotes the proliferation and invasion of glioma cells', *Int J Oncol*, 53: 2758-68.

Campagne, A., M. K. Lee, D. Zielinski, A. Michaud, S. Le Corre, F. Dingli, H. Chen, L. Z. Shahidian, I. Vassilev, N. Servant, D. Loew, E. Pasmant, S. Postel-Vinay, M. Wassef, and R. Margueron. 2019. 'BAP1 complex promotes transcription by opposing PRC1-mediated H2A ubiquitylation', *Nat Commun*, 10: 348.

Campisi, J. 2013. 'Aging, cellular senescence, and cancer', *Annu Rev Physiol*, 75: 685-705.

Cao, L. L., X. Song, L. Pei, L. Liu, H. Wang, and M. Jia. 2017. 'Histone deacetylase HDAC1 expression correlates with the progression and prognosis of lung cancer: A meta-analysis', *Medicine (Baltimore)*, 96: e7663.

Cao, Lin-Lin, Zhihong Yue, Lianhua Liu, Lin Pei, Yue Yin, Li Qin, Jie Zhao, Huixin Liu, Hui Wang, and Mei Jia. 2017. 'The expression of histone deacetylase HDAC1 correlates with the progression and prognosis of gastrointestinal malignancy', *Oncotarget*, 8: 39241-53.

Carbone, M., S. T. Arron, B. Beutler, A. Bononi, W. Cavenee, J. E. Cleaver, C. M. Croce, A. D'Andrea, W. D. Foulkes, G. Gaudino, J. L. Groden, E. P. Henske, I. D. Hickson, P. M. Hwang, R. D. Kolodner, T. W. Mak, D. Malkin, R. J. Monnat, Jr., F. Novelli, H. I. Pass, J. H. Petrini, L. S. Schmidt, and H. Yang. 2020. 'Tumour predisposition and cancer syndromes as models to study gene-environment interactions', *Nat Rev Cancer*, 20: 533-49.

Carbone, M., J. W. Harbour, J. Brugarolas, A. Bononi, I. Pagano, A. Dey, T. Krausz, H. I. Pass, H. Yang, and G. Gaudino. 2020. 'Biological Mechanisms and Clinical Significance of BAP1 Mutations in Human Cancer', *Cancer Discov*, 10: 1103-20.

Carbone, M., H. Yang, H. I. Pass, T. Krausz, J. R. Testa, and G. Gaudino. 2013. 'BAP1 and cancer', *Nat Rev Cancer*, 13: 153-9.

Carmeliet, P., Y. Dor, J. M. Herbert, D. Fukumura, K. Brusselmans, M. Dewerchin, M. Neeman, F. Bono, R. Abramovitch, P. Maxwell, C. J. Koch, P. Ratcliffe, L. Moons, R. K. Jain, D. Collen, and E. Keshert. 1998. 'Role of HIF-1alpha in hypoxia-mediated apoptosis, cell proliferation and tumour angiogenesis', *Nature*, 394: 485-90.

Carvajal, R. D., G. K. Schwartz, T. Tezel, B. Marr, J. H. Francis, and P. D. Nathan. 2017. 'Metastatic disease from uveal melanoma: treatment options and future prospects', *Br J Ophthalmol*, 101: 38-44.

Ceccacci, E., and S. Minucci. 2016. 'Inhibition of histone deacetylases in cancer therapy: lessons from leukaemia', *Br J Cancer*, 114: 605-11.

Chen, A., F. E. Kleiman, J. L. Manley, T. Ouchi, and Z. Q. Pan. 2002. 'Autoubiquitination of the BRCA1*BARD1 RING ubiquitin ligase', *J Biol Chem*, 277: 22085-92.

Chen, C. Y., C. C. Chen, W. Y. Chuang, Y. L. Leu, S. H. Ueng, C. Hsueh, C. T. Yeh, and T. H. Wang. 2020. 'Hydroxygenkwanin Inhibits Class I HDAC Expression and Synergistically Enhances the Antitumor Activity of Sorafenib in Liver Cancer Cells', *Front Oncol*, 10: 216.

Chen, H. P., Y. T. Zhao, and T. C. Zhao. 2015. 'Histone deacetylases and mechanisms of regulation of gene expression', *Crit Rev Oncog*, 20: 35-47.

Chen, M., Y. Ye, H. Yang, P. Tamboli, S. Matin, N. M. Tannir, C. G. Wood, J. Gu, and X. Wu. 2009. 'Genome-wide profiling of chromosomal alterations in renal cell carcinoma using high-density single nucleotide polymorphism arrays', *Int J Cancer*, 125: 2342-8.

Chin, A. I., J. S. Lam, R. A. Figlin, and A. S. Belldegrun. 2006. 'Surveillance strategies for renal cell carcinoma patients following nephrectomy', *Rev Urol*, 8: 1-7.

Choudhary, C., C. Kumar, F. Gnad, M. L. Nielsen, M. Rehman, T. C. Walther, J. V. Olsen, and M. Mann. 2009. 'Lysine acetylation targets protein complexes and co-regulates major cellular functions', *Science*, 325: 834-40.

Choueiri, T. K., and R. J. Motzer. 2017. 'Systemic Therapy for Metastatic Renal-Cell Carcinoma', *N Engl J Med*, 376: 354-66.

Chung, Y. E., M. J. Kim, Y. N. Park, J. Y. Choi, J. Y. Pyo, Y. C. Kim, H. J. Cho, K. A. Kim, and S. Y. Choi. 2009. 'Varying appearances of cholangiocarcinoma: radiologic-pathologic correlation', *Radiographics*, 29: 683-700.

Cuyas, E., B. Corominas-Faja, J. Joven, and J. A. Menendez. 2014. 'Cell cycle regulation by the nutrient-sensing mammalian target of rapamycin (mTOR) pathway', *Methods Mol Biol*, 1170: 113-44.

da Costa, W. H., A. F. Fares, S. M. Bezerra, M. A. Morini, L. A. de Toledo Benigno, D. A. Clavijo, L. Fornazieri, M. M. Rocha, I. W. da Cunha, and S. de Cassio Zequi. 2019. 'Loss of BAP1 expression in metastatic tumor tissue is an event of poor prognosis in patients with metastatic clear cell renal cell carcinoma', *Urol Oncol*, 37: 78-85.

de Koning, L., D. Decaudin, R. El Botty, A. Nicolas, G. Carita, M. Schuller, B. Ouine, A. Cartier, A. Naguez, J. Fleury, V. Cooke, A. Wylie, P. Smith, E. Marangoni, D. Gentien, D. Meseure, P. Mariani, N. Cassoux, S. Piperno-Neumann, S. Roman-Roman, and F. Nemati. 2019. 'PARP Inhibition Increases the Response to Chemotherapy in Uveal Melanoma', *Cancers (Basel)*, 11.

Delcuve, G. P., D. H. Khan, and J. R. Davie. 2012. 'Roles of histone deacetylases in epigenetic regulation: emerging paradigms from studies with inhibitors', *Clin Epigenetics*, 4: 5.

Denton, M. D., C. C. Magee, C. Ovuworie, S. Mauiyyedi, M. Pascual, R. B. Colvin, A. B. Cosimi, and N. Tolkoff-Rubin. 2002. 'Prevalence of renal cell carcinoma in patients with ESRD pre-transplantation: a pathologic analysis', *Kidney Int*, 61: 2201-9.

Deroanne, C. F., K. Bonjean, S. Servotte, L. Devy, A. Colige, N. Clausse, S. Blacher, E. Verdin, J. M. Foidart, B. V. Nusgens, and V. Castronovo. 2002. 'Histone deacetylases inhibitors as anti-angiogenic agents altering vascular endothelial growth factor signaling', *Oncogene*, 21: 427-36.

Diener-West, M., S. M. Reynolds, D. J. Agugliaro, R. Caldwell, K. Cumming, J. D. Earle, B. S. Hawkins, J. A. Hayman, I. Jaiyesimi, J. M. Kirkwood, W. J. Koh, D. M. Robertson, J. M. Shaw, B. R. Straatsma, J. Thoma, and Group Collaborative Ocular Melanoma Study. 2005. 'Second primary cancers after enrollment in the COMS trials for treatment of choroidal melanoma: COMS Report No. 25', *Arch Ophthalmol*, 123: 601-4.

Ding, N., L. Ping, L. Feng, X. Zheng, Y. Song, and J. Zhu. 2014. 'Histone deacetylase 6 activity is critical for the metastasis of Burkitt's lymphoma cells', *Cancer Cell Int*, 14: 139.

Du, L., A. L. Risinger, J. B. King, D. R. Powell, and R. H. Cichewicz. 2014. 'A potent HDAC inhibitor, 1-alaninechlamydocin, from a Tolypocladium sp. induces G2/M cell cycle arrest and apoptosis in MIA PaCa-2 cells', *J Nat Prod*, 77: 1753-7.

Duvic, M., and J. Vu. 2007. 'Vorinostat in cutaneous T-cell lymphoma', *Drugs Today (Barc)*, 43: 585-99.

Edmunds, J. W., L. C. Mahadevan, and A. L. Clayton. 2008. 'Dynamic histone H3 methylation during gene induction: HYPB/Setd2 mediates all H3K36 trimethylation', *EMBO J*, 27: 406-20.

Eleutherakis-Papaiakovou, E., N. Kanellias, E. Kastritis, M. Gavriatopoulou, E. Terpos, and M. A. Dimopoulos. 2020. 'Efficacy of Panobinostat for the Treatment of Multiple Myeloma', *J Oncol*, 2020: 7131802.

Esnaola, N. F., J. E. Meyer, A. Karachristos, J. L. Maranki, E. R. Camp, and C. S. Denlinger. 2016. 'Evaluation and management of intrahepatic and extrahepatic cholangiocarcinoma', *Cancer*, 122: 1349-69.

Fan, Q., L. Li, T. L. Wang, R. E. Emerson, and Y. Xu. 2021. 'A Novel ZIP4-HDAC4-VEGFA Axis in High-Grade Serous Ovarian Cancer', *Cancers (Basel)*, 13.

Farley, M. N., L. S. Schmidt, J. L. Mester, S. Peña-Llopis, A. Pavia-Jimenez, A. Christie, C. D. Vocke, C. J. Ricketts, J. Peterson, L. Middelton, L. Kinch, N. Grishin, M. J. Merino, A. R. Metwalli, C. Xing, X. J. Xie, P. L. M. Dahia, C. Eng, W. M. Linehan, and J. Brugarolas. 2013. 'A novel germline mutation in BAP1 predisposes to familial clear-cell renal cell carcinoma', *Mol Cancer Res*, 11: 1061-71.

Figueiredo, C. R., H. Kalirai, J. J. Sacco, R. A. Azevedo, A. Duckworth, J. R. Slupsky, J. M. Coulson, and S. E. Coupland. 2020. 'Loss of BAP1 expression is associated with an immunosuppressive microenvironment in uveal melanoma, with implications for immunotherapy development', *J Pathol*, 250: 420-39.

Fitzmaurice, C., D. Dicker, A. Pain, H. Hamavid, M. Moradi-Lakeh, M. F. MacIntyre, C. Allen, G. Hansen, R. Woodbrook, C. Wolfe, R. R. Hamadeh, A. Moore, A. Werdecker, B. D. Gessner, B. Te Ao, B. McMahon, C. Karimkhani, C. Yu, G. S. Cooke, D. C. Schwebel, D. O. Carpenter, D. M. Pereira, D. Nash, D. S. Kazi, D. De Leo, D. Plass, K. N. Ukwaja, G. D. Thurston, K. Yun Jin, E. P. Simard, E. Mills, E. K. Park, F. Catala-Lopez, G. deVeber, C. Gotay, G. Khan, H. D. Hosgood, 3rd, I. S. Santos, J. L. Leasher, J. Singh, J. Leigh, J. B. Jonas, J. Sanabria, J. Beardsley, K. H. Jacobsen, K. Takahashi, R. C. Franklin, L. Ronfani, M. Montico, L. Naldi, M. Tonelli, J. Geleijnse, M. Petzold, M. G. Shrime, M. Younis, N. Yonemoto, N. Breitborde, P. Yip, F. Pourmalek, P. A. Lotufo, A.

Esteghamati, G. J. Hankey, R. Ali, R. Lunevicius, R. Malekzadeh, R. Dellavalle, R. Weintraub, R. Lucas, R. Hay, D. Rojas-Rueda, R. Westerman, S. G. Sepanlou, S. Nolte, S. Patten, S. Weichenthal, S. F. Abera, S. M. Fereshtehnejad, I. Shiue, T. Driscoll, T. Vasankari, U. Alsharif, V. Rahimi-Movaghar, V. V. Vlassov, W. S. Marcenes, W. Mekonnen, Y. A. Melaku, Y. Yano, A. Artaman, I. Campos, J. MacLachlan, U. Mueller, D. Kim, M. Trillini, B. Eshrati, H. C. Williams, K. Shibuya, R. Dandona, K. Murthy, B. Cowie, A. T. Amare, C. A. Antonio, C. Castaneda-Orjuela, C. H. van Gool, F. Violante, I. H. Oh, K. Deribe, K. Soreide, L. Knibbs, M. Kereselidze, M. Green, R. Cardenas, N. Roy, T. Tillmann, Y. Li, H. Krueger, L. Monasta, S. Dey, S. Sheikhbahaei, N. Hafezi-Nejad, G. A. Kumar, C. T. Sreeramareddy, L. Dandona, H. Wang, S. E. Vollset, A. Mokdad, J. A. Salomon, R. Lozano, T. Vos, M. Forouzanfar, A. Lopez, C. Murray, and M. Naghavi. 2015. 'The Global Burden of Cancer 2013', *JAMA Oncol*, 1: 505-27.

Forsythe, J. A., B. H. Jiang, N. V. Iyer, F. Agani, S. W. Leung, R. D. Koos, and G. L. Semenza. 1996. 'Activation of vascular endothelial growth factor gene transcription by hypoxia-inducible factor 1', *Mol Cell Biol*, 16: 4604-13.

Geng, H., C. T. Harvey, J. Pittsenbarger, Q. Liu, T. M. Beer, C. Xue, and D. Z. Qian. 2011. 'HDAC4 protein regulates HIF1alpha protein lysine acetylation and cancer cell response to hypoxia', *J Biol Chem*, 286: 38095-102.

Glaser, K. B., J. Li, M. J. Staver, R. Q. Wei, D. H. Albert, and S. K. Davidsen. 2003. 'Role of class I and class II histone deacetylases in carcinoma cells using siRNA', *Biochem Biophys Res Commun*, 310: 529-36.

Glozak, M. A., N. Sengupta, X. Zhang, and E. Seto. 2005. 'Acetylation and deacetylation of non-histone proteins', *Gene*, 363: 15-23.

Glozak, M. A., and E. Seto. 2007. 'Histone deacetylases and cancer', *Oncogene*, 26: 5420-32.

Gnarra, J. R., K. Tory, Y. Weng, L. Schmidt, M. H. Wei, H. Li, F. Latif, S. Liu, F. Chen, F. M. Duh, and et al. 1994. 'Mutations of the VHL tumour suppressor gene in renal carcinoma', *Nat Genet*, 7: 85-90.

Grant, C., F. Rahman, R. Piekarz, C. Peer, R. Frye, R. W. Robey, E. R. Gardner, W. D. Figg, and S. E. Bates. 2010. 'Romidepsin: a new therapy for cutaneous T-cell lymphoma and a potential therapy for solid tumors', *Expert Rev Anticancer Ther*, 10: 997-1008.

Grossman, H. B., G. Wedemeyer, and L. Q. Ren. 1985. 'Human renal carcinoma: characterization of five new cell lines', *J Surg Oncol*, 28: 237-44.

Guo, G., Y. Gui, S. Gao, A. Tang, X. Hu, Y. Huang, W. Jia, Z. Li, M. He, L. Sun, P. Song, X. Sun, X. Zhao, S. Yang, C. Liang, S. Wan, F. Zhou, C. Chen, J. Zhu, X. Li, M. Jian, L. Zhou, R. Ye, P. Huang, J. Chen, T. Jiang, X. Liu, Y. Wang, J. Zou, Z. Jiang, R. Wu, S. Wu, F. Fan, Z. Zhang, L. Liu, R. Yang, X. Liu, H. Wu, W. Yin, X. Zhao, Y. Liu, H. Peng, B. Jiang, Q. Feng, C. Li, J. Xie, J. Lu, K. Kristiansen, Y. Li, X. Zhang, S. Li, J. Wang, H. Yang, Z. Cai, and J. Wang. 2011. 'Frequent mutations of genes encoding ubiquitin-mediated proteolysis pathway components in clear cell renal cell carcinoma', *Nat Genet*, 44: 17-9.

Gupta, M. P., A. M. Lane, M. M. DeAngelis, K. Mayne, M. Crabtree, E. S. Gragoudas, and I. K. Kim. 2015. 'Clinical Characteristics of Uveal Melanoma in Patients With Germline BAP1 Mutations', *JAMA Ophthalmol*, 133: 881-7.

Hagiwara, M., A. Fushimi, K. Matsumoto, and M. Oya. 2021. 'The Significance of PARP1 as a biomarker for Predicting the Response to PD-L1 Blockade in Patients with PBRM1-mutated Clear Cell Renal Cell Carcinoma', *Eur Urol*.

Halestrap, A. P. 2006. 'Calcium, mitochondria and reperfusion injury: a pore way to die', *Biochem Soc Trans*, 34: 232-7.

Harbour, J. W. 2012. 'The genetics of uveal melanoma: an emerging framework for targeted therapy', *Pigment Cell Melanoma Res*, 25: 171-81.

Harbour, J. W., and D. L. Chao. 2014. 'A molecular revolution in uveal melanoma: implications for patient care and targeted therapy', *Ophthalmology*, 121: 1281-8.

Harbour, J. W., M. D. Onken, E. D. Roberson, S. Duan, L. Cao, L. A. Worley, M. L. Council, K. A. Matatall, C. Helms, and A. M. Bowcock. 2010. 'Frequent mutation of BAP1 in metastasizing uveal melanomas', *Science*, 330: 1410-3.

Harrison, S. L., K. D. Mann, and M. S. Pearce. 2013. 'Early life influences kidney function at age 63-64 years, but so does adult body size: results from the newcastle thousand families birth cohort', *PLoS One*, 8: e66660.

Hassan, R., B. Morrow, A. Thomas, T. Walsh, M. K. Lee, S. Gulsuner, M. Gadiraju, V. Panou, S. Gao, I. Mian, J. Khan, M. Raffeld, S. Patel, L. Xi, J. S. Wei, M. Hesdorffer, J. Zhang, K. Calzone, A. Desai, E. Padiernos, C. Alewine, D. S. Schrump, S. M. Steinberg, H. L. Kindler, M. C. King, and J. E. Churpek. 2019. 'Inherited predisposition to malignant mesothelioma and overall survival following platinum chemotherapy', *Proc Natl Acad Sci U S A*, 116: 9008-13.

Helgadottir, H., and V. Hoiom. 2016. 'The genetics of uveal melanoma: current insights', *Appl Clin Genet*, 9: 147-55.

Henkind, P., and M. S. Roth. 1971. 'Breast carcinoma and concurrent uveal melanoma', *Am J Ophthalmol*, 71: 198-203.

Hontecillas-Prieto, L., R. Flores-Campos, A. Silver, E. de Alava, N. Hajji, and D. J. Garcia-Dominguez. 2020. 'Synergistic Enhancement of Cancer Therapy Using HDAC Inhibitors: Opportunity for Clinical Trials', *Front Genet*, 11: 578011.

Hsieh, J. J., M. P. Purdue, S. Signoretti, C. Swanton, L. Albiges, M. Schmidinger, D. Y. Heng, J. Larkin, and V. Ficarra. 2017. 'Renal cell carcinoma', *Nat Rev Dis Primers*, 3: 17009.

Hyder, O., I. Hatzaras, G. C. Sotiropoulos, A. Paul, S. Alexandrescu, H. Marques, C. Pulitano, E. Barroso, B. M. Clary, L. Aldrighetti, C. R. Ferrone, A. X. Zhu, T. W. Bauer, D. M. Walters, R. Groeschl, T. C. Gamblin, J. W. Marsh, K. T. Nguyen, R. Turley, I. Popescu, C. Hubert, S. Meyer, M. A. Choti, J. F. Gigot, G. Mentha, and T. M. Pawlik. 2013. 'Recurrence after operative management of intrahepatic cholangiocarcinoma', *Surgery*, 153: 811-8.

Inoue, S., J. Riley, T. W. Gant, M. J. Dyer, and G. M. Cohen. 2007. 'Apoptosis induced by histone deacetylase inhibitors in leukemic cells is mediated by Bim and Noxa', *Leukemia*, 21: 1773-82.

Ismail, I. H., R. Davidson, J. P. Gagne, Z. Z. Xu, G. G. Poirier, and M. J. Hendzel. 2014. 'Germline mutations in BAP1 impair its function in DNA double-strand break repair', *Cancer Res*, 74: 4282-94.

Iyer, S. P., and F. F. Foss. 2015. 'Romidepsin for the Treatment of Peripheral T-Cell Lymphoma', *Oncologist*, 20: 1084-91.

Jamaladdin, S., R. D. Kelly, L. O'Regan, O. M. Dovey, G. E. Hodson, C. J. Millard, N. Portolano, A. M. Fry, J. W. Schwabe, and S. M. Cowley. 2014. 'Histone deacetylase (HDAC) 1 and 2 are essential for accurate cell division and the pluripotency of embryonic stem cells', *Proc Natl Acad Sci U S A*, 111: 9840-5.

Janzen, N. K., H. L. Kim, R. A. Figlin, and A. S. Belldegrun. 2003. 'Surveillance after radical or partial nephrectomy for localized renal cell carcinoma and management of recurrent disease', *Urol Clin North Am*, 30: 843-52.

Jarnagin, W. R., S. Weber, S. K. Tickoo, J. B. Koea, S. Obiekwe, Y. Fong, R. P. DeMatteo, L. H. Blumgart, and D. Klimstra. 2002. 'Combined hepatocellular and cholangiocarcinoma: demographic, clinical, and prognostic factors', *Cancer*, 94: 2040-6.

Jenkins, D. E., Y. S. Hornig, Y. Oei, J. Dusich, and T. Purchio. 2005. 'Bioluminescent human breast cancer cell lines that permit rapid and sensitive in vivo detection of mammary tumors and multiple metastases in immune deficient mice', *Breast Cancer Res*, 7: R444-54.

Jensen, D. E., M. Proctor, S. T. Marquis, H. P. Gardner, S. I. Ha, L. A. Chodosh, A. M. Ishov, N. Tommerup, H. Vissing, Y. Sekido, J. Minna, A. Borodovsky, D. C. Schultz, K. D. Wilkinson, G. G. Maul, N. Barlev, S. L. Berger, G. C. Prendergast, and F. J. Rauscher, 3rd. 1998. 'BAP1: a novel ubiquitin hydrolase which binds to the BRCA1 RING finger and enhances BRCA1-mediated cell growth suppression', *Oncogene*, 16: 1097-112.

Jensen, D. E., and F. J. Rauscher, 3rd. 1999. 'BAP1, a candidate tumor suppressor protein that interacts with BRCA1', *Ann N Y Acad Sci*, 886: 191-4.

Jenuwein, T., and C. D. Allis. 2001. 'Translating the histone code', *Science*, 293: 1074-80.

Jeon, H. W., and Y. M. Lee. 2010. 'Inhibition of histone deacetylase attenuates hypoxia-induced migration and invasion of cancer cells via the restoration of RECK expression', *Mol Cancer Ther*, 9: 1361-70.

Johansson, P. A., V. Nathan, L. M. Bourke, J. M. Palmer, T. Zhang, J. Symmons, M. Howlie, A. M. Patch, J. Read, E. A. Holland, H. Schmid, S. Warrier, W. Glasson, V. Hoiom, K. Wadt, G. Jonsson, H. Olsson, C. Ingvar, G. Mann, K. M. Brown, N. K. Hayward, and A. L. Pritchard. 2019. 'Evaluation of the contribution of germline variants in BRCA1 and BRCA2 to uveal and cutaneous melanoma', *Melanoma Res*, 29: 483-90.

Kaelin, W. G., Jr. 2007. 'The von Hippel-Lindau tumor suppressor protein and clear cell renal carcinoma', *Clin Cancer Res*, 13: 680s-84s.

Kalirai, H., A. Dodson, S. Faqir, B. E. Damato, and S. E. Coupland. 2014. 'Lack of BAP1 protein expression in uveal melanoma is associated with increased

metastatic risk and has utility in routine prognostic testing', *Br J Cancer*, 111: 1373-80.

Kapitsinou, P. P., and V. H. Haase. 2008. 'The VHL tumor suppressor and HIF: insights from genetic studies in mice', *Cell Death Differ*, 15: 650-9.

Kapur, P., S. Peña -Llopis, A. Christie, L. Zhrebker, A. Pavia-Jimenez, W. K. Rathmell, X. J. Xie, and J. Brugarolas. 2013. 'Effects on survival of BAP1 and PBRM1 mutations in sporadic clear-cell renal-cell carcinoma: a retrospective analysis with independent validation', *Lancet Oncol*, 14: 159-67.

Karlsson, J., L. M. Nilsson, S. Mitra, S. Alsen, G. V. Shelke, V. R. Sah, E. M. V. Forsberg, U. Stierner, C. All-Eriksson, B. Einarsdottir, H. Jespersen, L. Ny, P. Lindner, E. Larsson, R. Olofsson Bagge, and J. A. Nilsson. 2020. 'Molecular profiling of driver events in metastatic uveal melanoma', *Nat Commun*, 11: 1894.

Kawai, H., H. Li, S. Avraham, S. Jiang, and H. K. Avraham. 2003. 'Overexpression of histone deacetylase HDAC1 modulates breast cancer progression by negative regulation of estrogen receptor alpha', *Int J Cancer*, 107: 353-8.

Khan, S. A., M. B. Toledano, and S. D. Taylor-Robinson. 2008. 'Epidemiology, risk factors, and pathogenesis of cholangiocarcinoma', *HPB (Oxford)*, 10: 77-82.

Kim, M. S., H. J. Kwon, Y. M. Lee, J. H. Baek, J. E. Jang, S. W. Lee, E. J. Moon, H. S. Kim, S. K. Lee, H. Y. Chung, C. W. Kim, and K. W. Kim. 2001. 'Histone deacetylases induce angiogenesis by negative regulation of tumor suppressor genes', *Nat Med*, 7: 437-43.

Kim, S. L., M. T. La, M. W. Shin, S. W. Kim, and H. K. Kim. 2020. 'A novel HDAC1 inhibitor, CBUD1001, exerts anticancer effects by modulating the apoptosis and EMT of colorectal cancer cells', *Int J Oncol*, 57: 1027-38.

Kittaneh, M., and C. Berkelhammer. 2018. 'Detecting germline BAP1 mutations in patients with peritoneal mesothelioma: benefits to patient and family members', *J Transl Med*, 16: 194.

Krantz, B. A., N. Dave, K. M. Komatsubara, B. P. Marr, and R. D. Carvajal. 2017. 'Uveal melanoma: epidemiology, etiology, and treatment of primary disease', *Clin Ophthalmol*, 11: 279-89.

Krencz, I., A. Sebestyen, J. Papay, A. Jeney, Z. Hujber, C. D. Burger, C. A. Keller, and A. Khoor. 2018. 'In situ analysis of mTORC1/2 and cellular metabolism-related proteins in human Lymphangioleiomyomatosis', *Hum Pathol*, 79: 199-207.

Krug, Lee M., Hedy L. Kindler, Hilary Calvert, Christian Manegold, Anne S. Tsao, Dean Fennell, Ronny Öhman, Ruth Plummer, Wilfried E. E. Eberhardt, Kazuya Fukuoka, Rabab M. Gaafar, Jean-Jacques Lafitte, Gunnar Hillerdal, Quincy Chu, Wieneke A. Buikhuisen, Gregory M. Lubiniecki, Xing Sun, Margaret Smith, and Paul Baas. 2015. 'Vorinostat in patients with advanced malignant pleural mesothelioma who have progressed on previous chemotherapy (VANTAGE-014): a phase 3, double-blind, randomised, placebo-controlled trial', *The Lancet Oncology*, 16: 447-56.

Kujala, Emma, Teemu Makitie, and Tero Kivela. 2003. 'Very Long-Term Prognosis of Patients with Malignant Uveal Melanoma', *Investigative Opthalmology & Visual Science*, 44.

Kuznetsoff, J. N., D. A. Owens, A. Lopez, D. A. Rodriguez, N. T. Chee, S. Kurtenbach, D. Bilbao, E. R. Roberts, C. H. Volmar, C. Wahlestedt, S. P. Brothers, and J. W. Harbour. 2021. 'Dual Screen for Efficacy and Toxicity Identifies HDAC Inhibitor with Distinctive Activity Spectrum for BAP1-Mutant Uveal Melanoma', *Mol Cancer Res*, 19: 215-22.

Kuznetsov, J. N., T. H. Aguero, D. A. Owens, S. Kurtenbach, M. G. Field, M. A. Durante, D. A. Rodriguez, M. L. King, and J. W. Harbour. 2019. 'BAP1 regulates epigenetic switch from pluripotency to differentiation in developmental lineages giving rise to BAP1-mutant cancers', *Sci Adv*, 5: eaax1738.

Ladanyi, M., M. G. Zauderer, L. M. Krug, T. Ito, R. McMillan, M. Bott, and F. Giancotti. 2012. 'New strategies in pleural mesothelioma: BAP1 and NF2 as novel targets for therapeutic development and risk assessment', *Clin Cancer Res*, 18: 4485-90.

LaFave, L. M., W. Beguelin, R. Koche, M. Teater, B. Spitzer, A. Chramiec, E. Papalexi, M. D. Keller, T. Hricik, K. Konstantinoff, J. B. Micol, B. Durham, S. K. Knutson, J. E. Campbell, G. Blum, X. Shi, E. H. Doud, A. V. Krivtsov, Y. R. Chung, I. Khodos, E. de Stanchina, O. Ouerfelli, P. S. Adusumilli, P. M. Thomas, N. L. Kelleher, M. Luo, H. Keilhack, O. Abdel-Wahab, A. Melnick, S. A. Armstrong, and R. L. Levine. 2015. 'Loss of BAP1 function leads to EZH2-dependent transformation', *Nat Med*, 21: 1344-9.

Lagger, G., D. O'Carroll, M. Rembold, H. Khier, J. Tischler, G. Weitzer, B. Schuettengruber, C. Hauser, R. Brunmeir, T. Jenuwein, and C. Seiser. 2002. 'Essential function of histone deacetylase 1 in proliferation control and CDK inhibitor repression', *EMBO J*, 21: 2672-81.

Landreville, S., O. A. Agapova, K. A. Matatall, Z. T. Kneass, M. D. Onken, R. S. Lee, A. M. Bowcock, and J. W. Harbour. 2012. 'Histone deacetylase inhibitors induce growth arrest and differentiation in uveal melanoma', *Clin Cancer Res*, 18: 408-16.

Lee, H. 2017. 'Phosphorylated mTOR Expression Profiles in Human Normal and Carcinoma Tissues', *Dis Markers*, 2017: 1397063.

Li, G., Y. Tian, and W. G. Zhu. 2020. 'The Roles of Histone Deacetylases and Their Inhibitors in Cancer Therapy', *Front Cell Dev Biol*, 8: 576946.

Linehan, W. M. 2012. 'Genetic basis of kidney cancer: role of genomics for the development of disease-based therapeutics', *Genome Res*, 22: 2089-100.

Lo Cascio, Costanza, Tigran Margaryan, Ernesto Luna Melendez, James McNamara, William Knight, Sarah Himes, Nader Sanai, Artak Tovmasyan, and Shwetal Mehta. 2021. 'Exth-24. Tumor Pharmacokinetics, Pharmacodynamics and Radiation Sensitization in Patient-Derived Xenograft Models of Glioblastoma Treated with the Second-Generation Hdac Inhibitor, Quisinostat', *Neuro-Oncology*, 23: vi168-vi68.

Louie, B. H., and R. Kurzrock. 2020. 'BAP1: Not just a BRCA1-associated protein', *Cancer Treat Rev*, 90: 102091.

Luchini, C., N. Veronese, S. Yachida, L. Cheng, A. Nottegar, B. Stubbs, M. Solmi, P. Capelli, A. Pea, M. Barbareschi, M. Fassan, L. D. Wood, and A. Scarpa. 2016. 'Different prognostic roles of tumor suppressor gene BAP1 in cancer: A

systematic review with meta-analysis', *Genes Chromosomes Cancer*, 55: 741-9.

Machida, Y. J., Y. Machida, A. A. Vashisht, J. A. Wohlschlegel, and A. Dutta. 2009. 'The deubiquitinating enzyme BAP1 regulates cell growth via interaction with HCF-1', *J Biol Chem*, 284: 34179-88.

Mancini, M., M. Righetto, and G. Baggio. 2020. 'Gender-Related Approach to Kidney Cancer Management: Moving Forward', *Int J Mol Sci*, 21.

Marks, P. A., T. Miller, and V. M. Richon. 2003. 'Histone deacetylases', *Curr Opin Pharmacol*, 3: 344-51.

Marschner, N., M. Staehler, L. Muller, A. Nusch, J. Harde, M. Koska, M. Janicke, P. J. Goebell, and R. C. C. Registry Group. 2017. 'Survival of Patients With Advanced or Metastatic Renal Cell Carcinoma in Routine Practice Differs From That in Clinical Trials-Analyses From the German Clinical RCC Registry', *Clin Genitourin Cancer*, 15: e209-e15.

Masson, N., and P. J. Ratcliffe. 2014. 'Hypoxia signaling pathways in cancer metabolism: the importance of co-selecting interconnected physiological pathways', *Cancer Metab*, 2: 3.

Miao, D., C. A. Margolis, W. Gao, M. H. Voss, W. Li, D. J. Martini, C. Norton, D. Bosse, S. M. Wankowicz, D. Cullen, C. Horak, M. Wind-Rotolo, A. Tracy, M. Giannakis, F. S. Hodi, C. G. Drake, M. W. Ball, M. E. Allaf, A. Snyder, M. D. Hellmann, T. Ho, R. J. Motzer, S. Signoretti, W. G. Kaelin, Jr., T. K. Choueiri, and E. M. Van Allen. 2018. 'Genomic correlates of response to immune checkpoint therapies in clear cell renal cell carcinoma', *Science*, 359: 801-06.

Micelli, C., and G. Rastelli. 2015. 'Histone deacetylases: structural determinants of inhibitor selectivity', *Drug Discov Today*, 20: 718-35.

Morales Torres, C., M. Y. Wu, S. Hobor, E. N. Wainwright, M. J. Martin, H. Patel, W. Grey, E. Gronroos, S. Howell, J. Carvalho, A. P. Snijders, M. Bustin, D. Bonnet, P. D. Smith, C. Swanton, M. Howell, and P. Scaffidi. 2020. 'Selective inhibition of cancer cell self-renewal through a Quisinostat-histone H1.0 axis', *Nat Commun*, 11: 1792.

Mosbeh, A., K. Halfawy, W. S. Abdel-Mageed, D. Sweed, and M. H. A. Rahman. 2018. 'Nuclear BAP1 loss is common in intrahepatic cholangiocarcinoma and a subtype of hepatocellular carcinoma but rare in pancreatic ductal adenocarcinoma', *Cancer Genet*, 224-225: 21-28.

Moschos, M. M., M. Dettoraki, S. Androudi, D. Kalogeropoulos, A. Lavaris, N. Garmpis, C. Damaskos, A. Garmpi, and M. Tsatsos. 2018. 'The Role of Histone Deacetylase Inhibitors in Uveal Melanoma: Current Evidence', *Anticancer Res*, 38: 3817-24.

Motzer, R. J., and R. M. Bukowski. 2006. 'Targeted therapy for metastatic renal cell carcinoma', *J Clin Oncol*, 24: 5601-8.

Motzer, R. J., E. Jonasch, S. Boyle, M. I. Carlo, B. Manley, N. Agarwal, A. Alva, K. Beckermann, T. K. Choueiri, B. A. Costello, I. H. Derweesh, A. Desai, S. George, J. L. Gore, N. Haas, S. L. Hancock, C. Kyriakopoulos, E. T. Lam, C. Lau, B. Lewis, D. C. Madoff, B. McCreery, M. D. Michaelson, A. Mortazavi, L.

Nandagopal, P. M. Pierorazio, E. R. Plimack, L. Ponsky, S. Ramalingam, B. Shuch, Z. L. Smith, B. Somer, J. Sosman, M. A. Dwyer, and A. D. Motter. 2020. 'NCCN Guidelines Insights: Kidney Cancer, Version 1.2021', *J Natl Compr Canc Netw*, 18: 1160-70.

Murali, R., T. Wiesner, and R. A. Scolyer. 2013. 'Tumours associated with BAP1 mutations', *Pathology*, 45: 116-26.

Nickerson, M. L., E. Jaeger, Y. Shi, J. A. Durocher, S. Mahurkar, D. Zaridze, V. Matveev, V. Janout, H. Kollarova, V. Bencko, M. Navratilova, N. Szeszenia-Dabrowska, D. Mates, A. Mukeria, I. Holcatova, L. S. Schmidt, J. R. Toro, S. Karami, R. Hung, G. F. Gerard, W. M. Linehan, M. Merino, B. Zbar, P. Boffetta, P. Brennan, N. Rothman, W. H. Chow, F. M. Waldman, and L. E. Moore. 2008. 'Improved identification of von Hippel-Lindau gene alterations in clear cell renal tumors', *Clin Cancer Res*, 14: 4726-34.

Nishikawa, H., W. Wu, A. Koike, R. Kojima, H. Gomi, M. Fukuda, and T. Ohta. 2009. 'BRCA1-associated protein 1 interferes with BRCA1/BARD1 RING heterodimer activity', *Cancer Res*, 69: 111-9.

Oehme, I., H. E. Deubzer, D. Wegener, D. Pickert, J. P. Linke, B. Hero, A. Kopp-Schneider, F. Westermann, S. M. Ulrich, A. von Deimling, M. Fischer, and O. Witt. 2009. 'Histone deacetylase 8 in neuroblastoma tumorigenesis', *Clin Cancer Res*, 15: 91-9.

Okino, Y., Y. Machida, S. Frankland-Searby, and Y. J. Machida. 2015. 'BRCA1-associated protein 1 (BAP1) deubiquitinase antagonizes the ubiquitin-mediated activation of FoxK2 target genes', *J Biol Chem*, 290: 1580-91.

Pan, H., R. Jia, L. Zhang, S. Xu, Q. Wu, X. Song, H. Zhang, S. Ge, X. L. Xu, and X. Fan. 2015. 'BAP1 regulates cell cycle progression through E2F1 target genes and mediates transcriptional silencing via H2A monoubiquitination in uveal melanoma cells', *Int J Biochem Cell Biol*, 60: 176-84.

Papastefanou, V. P., and V. M. Cohen. 2011. 'Uveal melanoma', *J Skin Cancer*, 2011: 573974.

Parish, A. J., V. Nguyen, A. M. Goodman, K. Murugesan, G. M. Frampton, and R. Kurzrock. 2018. 'GNAS, GNAQ, and GNA11 alterations in patients with diverse cancers', *Cancer*, 124: 4080-89.

Park, S. Y., J. A. Jun, K. J. Jeong, H. J. Heo, J. S. Sohn, H. Y. Lee, C. G. Park, and J. Kang. 2011. 'Histone deacetylases 1, 6 and 8 are critical for invasion in breast cancer', *Oncol Rep*, 25: 1677-81.

Peña-Llopis, S., A. Christie, X. J. Xie, and J. Brugarolas. 2013. 'Cooperation and antagonism among cancer genes: the renal cancer paradigm', *Cancer Res*, 73: 4173-9.

Peña-Llopis, S., S. Vega-Rubin-de-Celis, A. Liao, N. Leng, A. Pavia-Jimenez, S. Wang, T. Yamasaki, L. Zhrebker, S. Sivanand, P. Spence, L. Kinch, T. Hambuch, S. Jain, Y. Lotan, V. Margulis, A. I. Sagalowsky, P. B. Summerour, W. Kabbani, S. W. Wong, N. Grishin, M. Laurent, X. J. Xie, C. D. Haudenschild, M. T. Ross, D. R. Bentley, P. Kapur, and J. Brugarolas. 2012. 'BAP1 loss defines a new class of renal cell carcinoma'.

Perez-Garcia, V., G. Lea, P. Lopez-Jimenez, H. Okkenhaug, G. J. Burton, A. Moffett, M. Y. Turco, and M. Hemberger. 2021. 'BAP1/ASXL complex modulation regulates epithelial-mesenchymal transition during trophoblast differentiation and invasion', *Elife*, 10.

Prasad, P., M. Ronnerblad, E. Arner, M. Itoh, H. Kawaji, T. Lassmann, C. O. Daub, A. R. Forrest, A. Lennartsson, K. Ekwall, and Fantom consortium. 2014. 'High-throughput transcription profiling identifies putative epigenetic regulators of hematopoiesis', *Blood*, 123: e46-57.

Qin, J., Z. Zhou, W. Chen, C. Wang, H. Zhang, G. Ge, M. Shao, D. You, Z. Fan, H. Xia, R. Liu, and C. Chen. 2015. 'BAP1 promotes breast cancer cell proliferation and metastasis by deubiquitinating KLF5', *Nat Commun*, 6: 8471.

Rai, K., R. Pilarski, C. M. Cebulla, and M. H. Abdel-Rahman. 2016. 'Comprehensive review of BAP1 tumor predisposition syndrome with report of two new cases', *Clin Genet*, 89: 285-94.

Ramakrishnan, Swathi, ShengYu Ku, Eric Ciamporcero, Kiersten Marie Miles, Kris Attwood, Sreenivasulu Chintala, Li Shen, Leigh Ellis, Paula Sotomayor, Wendy Swetzig, Ray Huang, Dylan Conroy, Ashley Orillion, Gokul Das, and Roberto Pili. 2016. 'HDAC 1 and 6 modulate cell invasion and migration in clear cell renal cell carcinoma', *BMC Cancer*, 16.

Randall, J. M., F. Millard, and R. Kurzrock. 2014. 'Molecular aberrations, targeted therapy, and renal cell carcinoma: current state-of-the-art', *Cancer Metastasis Rev*, 33: 1109-24.

Rednam, K. R., L. M. Jampol, R. A. Levine, and M. F. Goldberg. 1981. 'Uveal melanoma in association with multiple malignancies. A case report and review', *Retina*, 1: 100-6.

Robertson, A. G., J. Shih, C. Yau, E. A. Gibb, J. Oba, K. L. Mungall, J. M. Hess, V. Uzunangelov, V. Walter, L. Danilova, T. M. Lichtenberg, M. Kucherlapati, P. K. Kimes, M. Tang, A. Penson, O. Babur, R. Akbani, C. A. Bristow, K. A. Hoadley, L. Iype, M. T. Chang, Tcga Research Network, A. D. Cherniack, C. Benz, G. B. Mills, R. G. W. Verhaak, K. G. Griewank, I. Felau, J. C. Zenklusen, J. E. Gershenwald, L. Schoenfield, A. J. Lazar, M. H. Abdel-Rahman, S. Roman-Roman, M. H. Stern, C. M. Cebulla, M. D. Williams, M. J. Jager, S. E. Coupland, B. Esmaeli, C. Kandoth, and S. E. Woodman. 2017. 'Integrative Analysis Identifies Four Molecular and Clinical Subsets in Uveal Melanoma', *Cancer Cell*, 32: 204-20 e15.

Rouleau, M., A. Patel, M. J. Hendzel, S. H. Kaufmann, and G. G. Poirier. 2010. 'PARP inhibition: PARP1 and beyond', *Nat Rev Cancer*, 10: 293-301.

Sabbatino, F., L. Liguori, U. Malapelle, F. Schiavi, V. Tortora, V. Conti, A. Filippelli, G. Tortora, C. R. Ferrone, and S. Pepe. 2020. 'Case Report: BAP1 Mutation and RAD21 Amplification as Predictive Biomarkers to PARP Inhibitor in Metastatic Intrahepatic Cholangiocarcinoma', *Front Oncol*, 10: 567289.

Sacco, J. J., J. Kenyani, Z. Butt, R. Carter, H. Y. Chew, L. P. Cheeseman, S. Darling, M. Denny, S. Urbe, M. J. Clague, and J. M. Coulson. 2015. 'Loss of the deubiquitylase BAP1 alters class I histone deacetylase expression and sensitivity of mesothelioma cells to HDAC inhibitors', *Oncotarget*, 6: 13757-71.

Sankala, H. M., N. C. Hait, S. W. Paugh, D. Shida, S. Lepine, L. W. Elmore, P. Dent, S. Milstien, and S. Spiegel. 2007. 'Involvement of sphingosine kinase 2 in p53-independent induction of p21 by the chemotherapeutic drug doxorubicin', *Cancer Res*, 67: 10466-74.

Scheuermann, J. C., A. G. de Ayala Alonso, K. Oktaba, N. Ly-Hartig, R. K. McGinty, S. Fraterman, M. Wilm, T. W. Muir, and J. Muller. 2010. 'Histone H2A deubiquitinase activity of the Polycomb repressive complex PR-DUB', *Nature*, 465: 243-7.

Schmidt, O., N. Nehls, C. Prexler, K. von Heyking, T. Groll, K. Pardon, H. D. Garcia, T. Hensel, D. Gurgen, A. G. Henssen, A. Eggert, K. Steiger, S. Burdach, and G. H. S. Richter. 2021. 'Class I histone deacetylases (HDAC) critically contribute to Ewing sarcoma pathogenesis', *J Exp Clin Cancer Res*, 40: 322.

Shaib, Y., and H. B. El-Serag. 2004. 'The epidemiology of cholangiocarcinoma', *Semin Liver Dis*, 24: 115-25.

Shaib, Y. H., H. B. El-Serag, J. A. Davila, R. Morgan, and K. A. McGlynn. 2005. 'Risk factors of intrahepatic cholangiocarcinoma in the United States: a case-control study', *Gastroenterology*, 128: 620-6.

Singh, A. D., and A. Topham. 2003. 'Incidence of uveal melanoma in the United States: 1973-1997', *Ophthalmology*, 110: 956-61.

Souri, Z., A. G. Jochemsen, A. P. A. Wierenga, W. G. M. Kroes, R. M. Verdijk, P. A. van der Velden, G. P. M. Luyten, and M. J. Jager. 2021. 'Expression of HDACs 1, 3 and 8 Is Upregulated in the Presence of Infiltrating Lymphocytes in Uveal Melanoma', *Cancers (Basel)*, 13.

Sun, C., C. Zhao, S. Li, J. Wang, Q. Zhou, J. Sun, Q. Ding, M. Liu, and G. Ding. 2018. 'EZH2 Expression is increased in BAP1-mutant renal clear cell carcinoma and is related to poor prognosis', *J Cancer*, 9: 3787-96.

Thorstenson, A., U. Harmenberg, P. Lindblad, B. Holmstrom, S. Lundstam, and B. Ljungberg. 2015. 'Cancer Characteristics and Current Treatments of Patients with Renal Cell Carcinoma in Sweden', *Biomed Res Int*, 2015: 456040.

Tian, T., X. Li, and J. Zhang. 2019. 'mTOR Signaling in Cancer and mTOR Inhibitors in Solid Tumor Targeting Therapy', *Int J Mol Sci*, 20.

Tyagi, S., A. L. Chabes, J. Wysocka, and W. Herr. 2007. 'E2F activation of S phase promoters via association with HCF-1 and the MLL family of histone H3K4 methyltransferases', *Mol Cell*, 27: 107-19.

Uner, O. E., T. R. O. See, E. Szalai, H. E. Grossniklaus, and G. Stalhammar. 2021. 'Author Correction: Estimation of the timing of BAP1 mutation in uveal melanoma progression', *Sci Rep*, 11: 17036.

Ungerstedt, J. S., Y. Sowa, W. S. Xu, Y. Shao, M. Dokmanovic, G. Perez, L. Ngo, A. Holmgren, X. Jiang, and P. A. Marks. 2005. 'Role of thioredoxin in the response of normal and transformed cells to histone deacetylase inhibitors', *Proc Natl Acad Sci U S A*, 102: 673-8.

van Essen, T. H., S. I. van Pelt, M. Versluis, I. H. Bronkhorst, S. G. van Duinen, M. Marinkovic, W. G. Kroes, C. A. Ruivenkamp, S. Shukla, A. de Klein, E. Kilic, J. W. Harbour, G. P. Luyten, P. A. van der Velden, R. M. Verdijk, and M. J. Jager.

2014. 'Prognostic parameters in uveal melanoma and their association with BAP1 expression', *Br J Ophthalmol*, 98: 1738-43.

Vanaja, G. R., H. G. Ramulu, and A. M. Kalle. 2018. 'Overexpressed HDAC8 in cervical cancer cells shows functional redundancy of tubulin deacetylation with HDAC6', *Cell Commun Signal*, 16: 20.

Varela, I., P. Tarpey, K. Raine, D. Huang, C. K. Ong, P. Stephens, H. Davies, D. Jones, M. L. Lin, J. Teague, G. Bignell, A. Butler, J. Cho, G. L. Dalgliesh, D. Galappaththige, C. Greenman, C. Hardy, M. Jia, C. Latimer, K. W. Lau, J. Marshall, S. McLaren, A. Menzies, L. Mudie, L. Stebbings, D. A. Largaespada, L. F. Wessels, S. Richard, R. J. Kahnoski, J. Anema, D. A. Tuveson, P. A. Perez-Mancera, V. Mustonen, A. Fischer, D. J. Adams, A. Rust, W. Chan-on, C. Subimerb, K. Dykema, K. Furge, P. J. Campbell, B. T. Teh, M. R. Stratton, and P. A. Futreal. 2011. 'Exome sequencing identifies frequent mutation of the SWI/SNF complex gene PBRM1 in renal carcinoma', *Nature*, 469: 539-42.

Varricchio, L., C. Dell'Aversana, A. Nebbioso, G. Migliaccio, L. Altucci, A. Mai, G. Grazzini, J. J. Bieker, and A. R. Migliaccio. 2014. 'Identification of NuRSERY, a new functional HDAC complex composed by HDAC5, GATA1, EKLF and pERK present in human erythroid cells', *Int J Biochem Cell Biol*, 50: 112-22.

Ventii, K. H., N. S. Devi, K. L. Friedrich, T. A. Chernova, M. Tighiouart, E. G. Van Meir, and K. D. Wilkinson. 2008. 'BRCA1-associated protein-1 is a tumor suppressor that requires deubiquitinating activity and nuclear localization', *Cancer Res*, 68: 6953-62.

Venugopal, B., R. Baird, R. S. Kristeleit, R. Plummer, R. Cowan, A. Stewart, N. Fourneau, P. Hellemans, Y. Elsayed, S. McClue, J. W. Smit, A. Forslund, C. Phelps, J. Camm, T. R. Evans, J. S. de Bono, and U. Banerji. 2013. 'A phase I study of quisinostat (JNJ-26481585), an oral hydroxamate histone deacetylase inhibitor with evidence of target modulation and antitumor activity, in patients with advanced solid tumors', *Clin Cancer Res*, 19: 4262-72.

Verdin, E., and M. Ott. 2015. '50 years of protein acetylation: from gene regulation to epigenetics, metabolism and beyond', *Nat Rev Mol Cell Biol*, 16: 258-64.

Verma, V., and M. P. Mehta. 2016. 'Clinical Outcomes of Proton Radiotherapy for Uveal Melanoma', *Clin Oncol (R Coll Radiol)*, 28: e17-27.

Wada, T., J. Kikuchi, N. Nishimura, R. Shimizu, T. Kitamura, and Y. Furukawa. 2009. 'Expression levels of histone deacetylases determine the cell fate of hematopoietic progenitors', *J Biol Chem*, 284: 30673-83.

Wang, A. H., and X. J. Yang. 2001. 'Histone deacetylase 4 possesses intrinsic nuclear import and export signals', *Mol Cell Biol*, 21: 5992-6005.

Wang, A., A. Papneja, M. Hyrcza, A. Al-Habeeb, and D. Ghazarian. 2016. 'Gene of the month: BAP1', *J Clin Pathol*, 69: 750-3.

Watamoto, K., M. Towatari, Y. Ozawa, Y. Miyata, M. Okamoto, A. Abe, T. Naoe, and H. Saito. 2003. 'Altered interaction of HDAC5 with GATA-1 during MEL cell differentiation', *Oncogene*, 22: 9176-84.

Watanabe, Y., K. Khodosevich, and H. Monyer. 2014. 'Dendrite development regulated by the schizophrenia-associated gene FEZ1 involves the ubiquitin proteasome system', *Cell Rep*, 7: 552-64.

Weichert, W., C. Denkert, A. Noske, S. Darb-Esfahani, M. Dietel, S. E. Kalloger, D. G. Huntsman, and M. Kobel. 2008. 'Expression of class I histone deacetylases indicates poor prognosis in endometrioid subtypes of ovarian and endometrial carcinomas', *Neoplasia*, 10: 1021-7.

Weichert, W., A. Roske, V. Gekeler, T. Beckers, M. P. Ebert, M. Pross, M. Dietel, C. Denkert, and C. Rocken. 2008. 'Association of patterns of class I histone deacetylase expression with patient prognosis in gastric cancer: a retrospective analysis', *Lancet Oncol*, 9: 139-48.

Welchman, R. L., C. Gordon, and R. J. Mayer. 2005. 'Ubiquitin and ubiquitin-like proteins as multifunctional signals', *Nat Rev Mol Cell Biol*, 6: 599-609.

White, A. E., and J. W. Harper. 2012. 'Cancer. Emerging anatomy of the BAP1 tumor suppressor system', *Science*, 337: 1463-4.

Wilson, A. J., D. S. Byun, N. Popova, L. B. Murray, K. L'Italien, Y. Sowa, D. Arango, A. Velcich, L. H. Augenlicht, and J. M. Mariadason. 2006. 'Histone deacetylase 3 (HDAC3) and other class I HDACs regulate colon cell maturation and p21 expression and are deregulated in human colon cancer', *J Biol Chem*, 281: 13548-58.

Wilting, R. H., E. Yanover, M. R. Heideman, H. Jacobs, J. Horner, J. van der Torre, R. A. DePinho, and J. H. Dannenberg. 2010. 'Overlapping functions of Hdac1 and Hdac2 in cell cycle regulation and haematopoiesis', *EMBO J*, 29: 2586-97.

Winter, M., M. A. Moser, D. Meunier, C. Fischer, G. Machat, K. Mattes, B. M. Lichtenberger, R. Brunmeir, S. Weissmann, C. Murko, C. Humer, T. Meischel, G. Brosch, P. Matthias, M. Sibilia, and C. Seiser. 2013. 'Divergent roles of HDAC1 and HDAC2 in the regulation of epidermal development and tumorigenesis', *EMBO J*, 32: 3176-91.

Wu-Baer, F., K. Lagrazon, W. Yuan, and R. Baer. 2003. 'The BRCA1/BARD1 heterodimer assembles polyubiquitin chains through an unconventional linkage involving lysine residue K6 of ubiquitin', *J Biol Chem*, 278: 34743-6.

Wu, J., L. Y. Lu, and X. Yu. 2010. 'The role of BRCA1 in DNA damage response', *Protein Cell*, 1: 117-23.

Xie, H. J., J. H. Noh, J. K. Kim, K. H. Jung, J. W. Eun, H. J. Bae, M. G. Kim, Y. G. Chang, J. Y. Lee, H. Park, and S. W. Nam. 2012. 'HDAC1 inactivation induces mitotic defect and caspase-independent autophagic cell death in liver cancer', *PLoS One*, 7: e34265.

Yamaguchi, T., F. Cubizolles, Y. Zhang, N. Reichert, H. Kohler, C. Seiser, and P. Matthias. 2010. 'Histone deacetylases 1 and 2 act in concert to promote the G1-to-S progression', *Genes Dev*, 24: 455-69.

Yang, J., D. K. Manson, B. P. Marr, and R. D. Carvajal. 2018. 'Treatment of uveal melanoma: where are we now?', *Ther Adv Med Oncol*, 10: 1758834018757175.

Yoo, Y. G., G. Kong, and M. O. Lee. 2006. 'Metastasis-associated protein 1 enhances stability of hypoxia-inducible factor-1alpha protein by recruiting histone deacetylase 1', *EMBO J*, 25: 1231-41.

Yoshikawa, Y., A. Sato, T. Tsujimura, M. Emi, T. Morinaga, K. Fukuoka, S. Yamada, A. Murakami, N. Kondo, S. Matsumoto, Y. Okumura, F. Tanaka, S. Hasegawa, T. Nakano, and T. Hashimoto-Tamaoki. 2012. 'Frequent inactivation of the BAP1 gene in epithelioid-type malignant mesothelioma', *Cancer Sci*, 103: 868-74.

Yu, H., N. Mashtalir, S. Daou, I. Hammond-Martel, J. Ross, G. Sui, G. W. Hart, F. J. Rauscher, 3rd, E. Drobetsky, E. Milot, Y. Shi, and B. Affar el. 2010. 'The ubiquitin carboxyl hydrolase BAP1 forms a ternary complex with YY1 and HCF-1 and is a critical regulator of gene expression', *Mol Cell Biol*, 30: 5071-85.

Zauderer, Marjorie Glass, Peter Szlosarek, Sylvestre Le Moulec, Sanjay Popat, Paul Taylor, David Planchard, Arnaud Scherpereel, Thierry Jahan, Marianna Koczywas, Martin Forster, Robert B. Cameron, Tobias Peikert, Carly Campbell, Inbal Sapir, Alice McDonald, Coreen Oei, Alicia Clawson, Maria Roche, and Dean A. Fennell. 2018. 'Phase 2, multicenter study of the EZH2 inhibitor tazemetostat as monotherapy in adults with relapsed or refractory (R/R) malignant mesothelioma (MM) with BAP1 inactivation', *Journal of Clinical Oncology*, 36: 8515-15.

Zbar, B., H. Brauch, C. Talmadge, and M. Linehan. 1987. 'Loss of alleles of loci on the short arm of chromosome 3 in renal cell carcinoma', *Nature*, 327: 721-4.

Zeng, L. S., X. Z. Yang, Y. F. Wen, S. J. Mail, M. H. Wang, M. Y. Zhang, X. F. Zheng, and H. Y. Wang. 2016. 'Overexpressed HDAC4 is associated with poor survival and promotes tumor progression in esophageal carcinoma', *Aging (Albany NY)*, 8: 1236-49.

Zhang, J., and Q. Zhong. 2014. 'Histone deacetylase inhibitors and cell death', *Cell Mol Life Sci*, 71: 3885-901.

Zhou, H., Y. Cai, D. Liu, M. Li, Y. Sha, W. Zhang, K. Wang, J. Gong, N. Tang, A. Huang, and J. Xia. 2018. 'Pharmacological or transcriptional inhibition of both HDAC1 and 2 leads to cell cycle blockage and apoptosis via p21(Waf1/Cip1) and p19(INK4d) upregulation in hepatocellular carcinoma', *Cell Prolif*, 51: e12447.

Zhou, L., X. Xu, H. Liu, X. Hu, W. Zhang, M. Ye, and X. Zhu. 2018. 'Prognosis Analysis of Histone Deacetylases mRNA Expression in Ovarian Cancer Patients', *J Cancer*, 9: 4547-55.

Znaor, A., J. Lortet-Tieulent, M. Laversanne, A. Jemal, and F. Bray. 2015. 'International variations and trends in renal cell carcinoma incidence and mortality', *Eur Urol*, 67: 519-30.

7. Appendix

7.1 First synthetic lethal screen

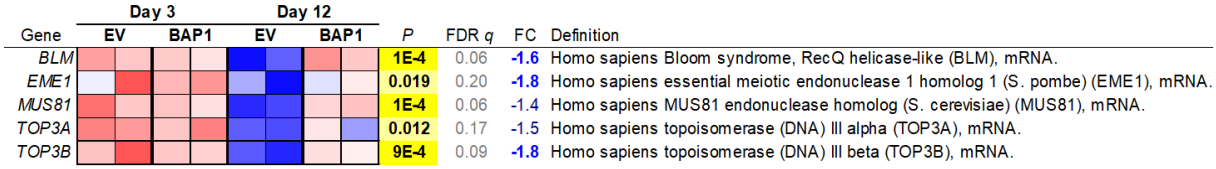

Gene	Day 3 EV	Day 3 BAP1	Day 12 EV	Day 12 BAP1	*P*	FDR *q*	FC	Definition
BLM					1E-4	0.06	-1.6	Homo sapiens Bloom syndrome, RecQ helicase-like (BLM), mRNA.
EME1					0.019	0.20	-1.8	Homo sapiens essential meiotic endonuclease 1 homolog 1 (S. pombe) (EME1), mRNA.
MUS81					1E-4	0.06	-1.4	Homo sapiens MUS81 endonuclease homolog (S. cerevisiae) (MUS81), mRNA.
TOP3A					0.012	0.17	-1.5	Homo sapiens topoisomerase (DNA) III alpha (TOP3A), mRNA.
TOP3B					9E-4	0.09	-1.8	Homo sapiens topoisomerase (DNA) III beta (TOP3B), mRNA.

Supplementary Figure 1: Genes associated with DNA double-strand break repair machinery appeared as top candidates of the first shRNA screen
The figure is showing a heatmap of top candidates of the synthetic lethality screen. For the shRNA screen UMRC-6 EV (BAP1-deficient) and UMRC-6 BAP1-wt (BAP1 expressed) cell lines were transduced in duplicates with module 1 and module 2 of a pooled DECIPHER shRNA library using lentiviral transfer. On day 3 after transduction, samples of both cell lines were harvested as baseline control. After selection of infected cells with puromycin, again samples of both cell lines were harvested on day 12 post-infection. Harvested samples were determined by high-throughput (HT) sequencing of vector barcodes and analyzed with RIGER. Blue highlighting indicates down-regulation of the gene expression and red highlighting shows upregulation of the gene expression. *p*= *p*-value, FDR *q*= *q*-values of false discovery rate and FC= fold change, positive and negative FC indicates increased and decreased expression values. *N* = 2, Performed by Dr. Samuel Peña-Llopis.

7.2 Effect of *RECQL* and *TOP3A* knockdown on BAP1-deficient cells

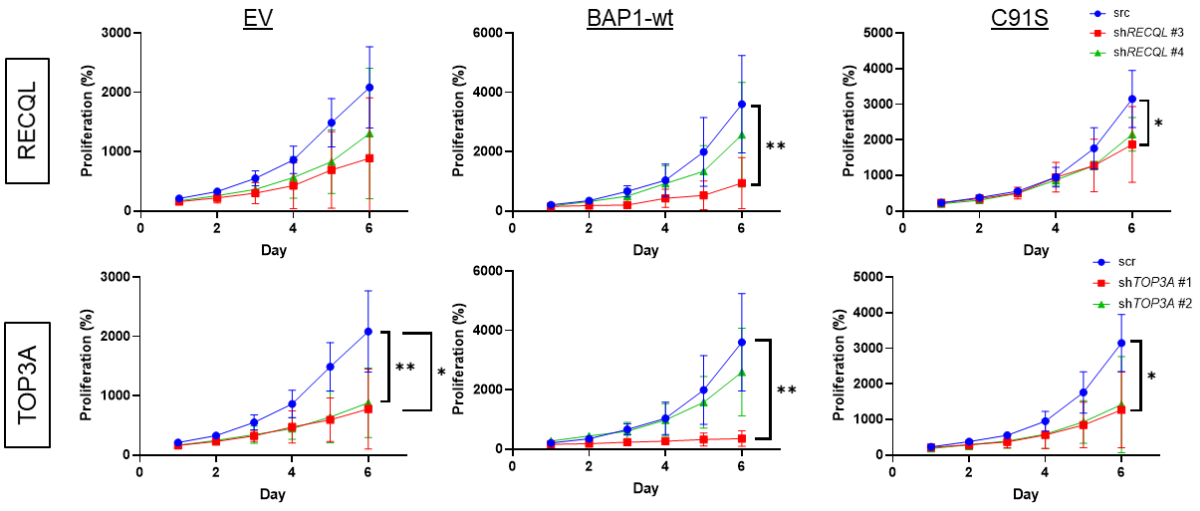

Supplementary Figure 2: Effect of a *RECQL* and *TOP3A* knockdown on the proliferation of ccRCC UMRC-6 cell lines
Proliferation curves for UMRC-6 cell lines expressing EV, *BAP1*-wt or BAP1 p.C91S mutant plasmid transduced with Scr control or two different shRNAs against *RECQL* or *TOP3A*, normalized to data of day one. *N* = 3 for all experiments. Significance was assessed using nonparametric Kruskal-Wallis test. *p*-values: $p<0.05$ (*) and $p<0.01$ (**).

7.3 Expression levels of HDACs after *HDAC1* knockdown in BAP1-expressing and *BAP1* knockout 786-O cell lines

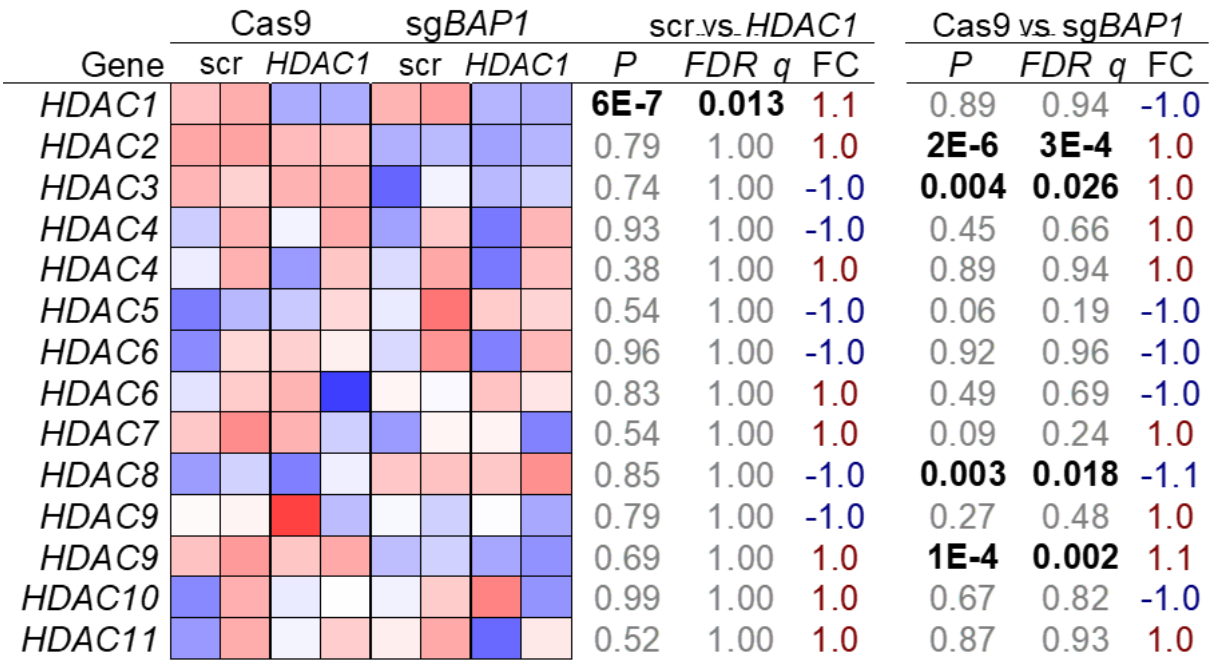

	Cas9		sg*BAP1*		scr vs. *HDAC1*			Cas9 vs. sg*BAP1*		
Gene	scr	*HDAC1*	scr	*HDAC1*	*P*	*FDR q*	FC	*P*	*FDR q*	FC
HDAC1					**6E-7**	**0.013**	1.1	0.89	0.94	-1.0
HDAC2					0.79	1.00	1.0	**2E-6**	**3E-4**	1.0
HDAC3					0.74	1.00	-1.0	**0.004**	**0.026**	1.0
HDAC4					0.93	1.00	-1.0	0.45	0.66	1.0
HDAC4					0.38	1.00	1.0	0.89	0.94	1.0
HDAC5					0.54	1.00	-1.0	0.06	0.19	-1.0
HDAC6					0.96	1.00	-1.0	0.92	0.96	-1.0
HDAC6					0.83	1.00	1.0	0.49	0.69	-1.0
HDAC7					0.54	1.00	1.0	0.09	0.24	1.0
HDAC8					0.85	1.00	-1.0	**0.003**	**0.018**	-1.1
HDAC9					0.79	1.00	-1.0	0.27	0.48	1.0
HDAC9					0.69	1.00	1.0	**1E-4**	**0.002**	1.1
HDAC10					0.99	1.00	1.0	0.67	0.82	-1.0
HDAC11					0.52	1.00	1.0	0.87	0.93	1.0

Supplementary Figure 3: Effect on mRNA expression of all HDACs after *HDAC1* knockdown
Analysis of microarray data from 786-O control (Cas9) and *BAP1* knockout cells (sg*BAP1*) (Cas9 vs. sg*BAP1*). The effect of a *HDAC1* knockdown on the expression of other *HDACs* genes was compared between the 786-O Cas9 and 786-O sgBAP1 cell line. Heatmap of the expression rates of HDACs was performed. Blue highlighting indicates down-regulation of the gene expression and red highlighting shows upregulation of the gene expression. *p*= *p*-value, FDR *q*= *q*-values of false discovery rate and FC= fold change, positive and negative FC indicates increased and decreased expression values. *N* = 2, Performed by the Microarray Core Facility of DKFZ Heidelberg.

8. Acknowledgements

First of all, I want to thank Prof. Dr. Jens Siveke to take over the role as my first supervisor of my PhD project. I am very grateful for all his advices and his broad knowledge in cancer research. I also want to thank Prof. Dr. Verena Jendrossek for kindly agreeing to take on the task of second proof reader.

My special thanks are to Dr. Samuel Peña-Llopis for letting me join his lab and his interesting research project and for his guidance throughout the entire project. Moreover, I am thankful for all his suggestions, constructive discussions and many nice conversations.

At this point, I would also like to thank all “old” and “new” members of the Peña-Llopis, Siveke and Grüner groups for their great helpfulness, friendly atmosphere and great time, which contributed significantly to the success of this work.

I want to express my sincerest gratitude to my partner for his patience and understanding, his professional and emotional support and his special ability to always make me laugh.

9. Curriculum Vitae

The curriculum vitae is not included in the online version for data protection reasons.

The curriculum vitae is not included in the online version for data protection reasons.

The curriculum vitae is not included in the online version for data protection reasons.

10. Declarations

Erklärung:

Hiermit erkläre ich, gem. § 6 Abs. (2) g) der Promotionsordnung der Fakultät für Biologie zur Erlangung der Dr. rer. nat., dass ich das Arbeitsgebiet, dem das Thema „Exploiting genetic vulnerabilities for BAP1 loss by synthetic lethality“ zuzuordnen ist, in Forschung und Lehre vertrete und den Antrag von Anna Bazarna befürworte und die Betreuung auch im Falle eines Weggangs, wenn nicht wichtige Gründe dem entgegenstehen, weiterführen werde.

Essen, den _____ _____ _____

Name des Betreuers an der Universität Duisburg-Essen | Unterschrift

Erklärung:

Hiermit erkläre ich, gem. § 7 Abs. (2) d) + f) der Promotionsordnung der Fakultät für Biologie zur Erlangung des Dr. rer. nat., dass ich die vorliegende Dissertation selbständig verfasst und mich keiner anderen als der angegebenen Hilfsmittel bedient, bei der Abfassung der Dissertation nur die angegeben Hilfsmittel benutzt und alle wörtlich oder inhaltlich übernommenen Stellen als solche gekennzeichnet habe.

Essen, den _____ _____

Unterschrift des Doktoranden

Erklärung:

Hiermit erkläre ich, gem. § 7 Abs. (2) e) + g) der Promotionsordnung der Fakultät für Biologie zur Erlangung des Dr. rer. nat., dass ich keine anderen Promotionen bzw. Promotionsversuche in der Vergangenheit durchgeführt habe und dass diese Arbeit von keiner anderen Fakultät/Fachbereich abgelehnt worden ist.

Essen, den _____ _____

Unterschrift des Doktoranden